ABSTRACT

Climate-Driven Variability and Potential Land Use Change Effect on Sources of Water from Mountain Headwater Systems

Ram P. Neupane, Ph.D.

Mentor: Joseph D. White, Ph.D.

This study estimated the climate and land use change effects on hydrological processes of major Nepalese watersheds including Kali Gandaki, Tamor and Seti using the Soil and Water Assessment Tool. Future climate change effect was modeled using the outputs of temperature and precipitation changes derived from Special Report on Emission Scenarios (B1, A1B & A2) of 16 global circulation models for 2080s. The discharge of the Kali Gandaki River was approximately 39% higher than current values for the maximum temperature and precipitation changes of the A2 scenario and 22% less for minimum changes of the same scenario. With 7% of original forested land removed, sediment yield for the Tamor basin was estimated to be 65% higher, but increased to 124% for the SRES-B1 scenario. For the Seti basin, 4% deforestation yielded 33% more sediment for the SRES-A1B scenario. The effect appears to be geographically important with higher influence in the eastern Tamor basin potentially due to longer and stronger monsoonal period of that area. To better understand the potential groundwater dynamics in mountain stream system and also to better assess the model simulation outputs, I used

$\delta^{18}O$ and $\delta^{2}H$ of water, solute concentrations, and ^{222}Rn to determine which of these may best characterizes water derived from sub-surface sources present in the stream during summer recession flow in McDonald Creek watershed. This study was important since higher groundwater contribution to the stream discharge was assessed in the Himalaya Mountain systems. In main channel of the McDonald Creek, I measured peak ^{222}Rn activity of 2,646 Bq/m^3 at 7.9 km distance downstream located in middle of the watershed associated with streamflow constriction that corresponded to changes in local orientation of underlying rocks. Based on ^{222}Rn mass balance calculations, I estimated that groundwater contributed between 0.3 and 29% of total flow. However, 60% of the total groundwater input was likely to have been produced from hyporheic zone of the stream channel. Finally, I estimated a 5.9% of groundwater contribution integrated for stream reach measured at McDonald Creek during recession flow period.

Climate-Driven Variability and Potential Land Use Change Effect on Sources of Water from Mountain Headwater Systems

by

Ram P. Neupane, B.S., M.S.

A Dissertation

Approved by the Institute of Ecological, Earth, and Environmental Science

_____
Joe C. Yelderman Jr., Ph.D., Director

Submitted to the Graduate Faculty of
Baylor University in Partial Fulfillment of the
Requirements for the Degree
of
Doctor of Philosophy

Approved by the Dissertation Committee

_____
Joseph D.White, Ph.D., Chairperson

_____
Peter M. Allen, Ph.D.

_____
John Dunbar, Ph.D.

_____
Stephen I. Dworkin, Ph.D.

_____
Sara E. Alexander, Ph.D.

Accepted by the Graduate School
December 2014

_____
J. Larry Lyon, Ph.D., Dean

Page bearing signatures is kept on file in the Graduate School

TABLE OF CONTENTS

LIST OF FIGURES

LIST OF TABLES

ACKNOWLEDGMENTS

I would like to thank my mentor, Dr. Joseph D. White for his guidance in my journey of pursuing PhD. I would also like to thank my other committee members, Dr. Peter M. Allen, Dr. John Dunbar, Dr. Sara Alexander, and Dr. Stephen I. Dworkin for their support and scientific opinions on this project. I thank my colleagues at the Baylor Spatial Ecology Lab: Jian Yao, Arjun Adhikari, and Darrel B. Murray.

This research was financially supported by the C. Gus Glasscock, Jr. endowed fund for excellence in Environmental Science from Baylor University. I thank to Mr. Phul P. Subedi for his valuable time in providing hydro-meteorological data from the department of hydrology and meteorology (DHM), Nepal. I also thank to Dr. Daniel Fagre of the USGS Northern Rocky Mountain Science Center at Glacier National Park for his support facilitating this research.

I would also like to thank my family for supporting me to study aboard. I thank all my friends who helped me during this time. Finally, I thank my wife, Prema Neupane, for supporting me through this entire process

CHAPTER ONE

Introduction

Water is an important natural resource covering 71% of the earth's surface. Out of this water, 97% is saline present in the ocean and only 3% is considered fresh. The majority of fresh water, which is about 69%, is stored in glaciers and ice caps, mainly in Antarctica, Greenland and high mountains (Gleick, 1996). While freshwater may be abundant on the planet's surface, its availability for human consumption is low due to geographic, temporal, and quality issues. Efficient utilization and sustainable management of water resources is an urgent need for the existence of a rapidly increasing human population, specifically for the people who mainly depend on energy and water resources obtained from mountain watersheds.

Mountains are important for humans as they store huge amount of water in solid forms that supply water during dry periods to the downstream areas. Large mountain systems also referred to as the "third pole", occupy 24% of the total global surface area, and are an important source of fresh water, sustaining 12% of the world's population (ICIMOD, 2008). Storage and release of water from glaciers are potential to influence generation of hydro-electricity, sea level fluctuations, sediment transportation, and formation of landforms (Jansson et al., 2003). The process of snow and glacial ice deposition and melt are closely related to the quality and quantity of river waters that affect human appropriation of this water on ecological sustainability of mountain streams. One-sixth of the world's population depend on glaciers and seasonal snow and ice for water resources derived from mountain regions (Barnett et al., 2005). Reduction in

mountain snowpack and change in timing of river discharge are of great concern in arid regions where growing population water use exceeds supply. Since mountains are the repositories of fresh water in the form of snow and ice, it is important to assess changing climate effects on future hydrological processes of these mountain basins.

Watershed hydrology is highly sensitive to climate change due to orographic effects where small changes in temperature influence the balance of precipitation falling as snow and rain (Barnet et al., 2005). Potential climate change influences the hydrologic systems in mountain environments, associated with reduced snow and glacier cover (White et al., 1998). Climate change can also affect the sediment transportation in mountain basins, primarily due to varying meltwater contribution associated with changing mountain glaciers and snowpack. This includes increased variation in hydrologic output such as reduced water flows during dry periods and high flows with flood problems during wet periods (Akhtar et al., 2008).

Global climate change and associated impacts are already observed in the Himalaya Mountains (Beniston 2003; Cruz et al., 2007). However, few studies have examined the effect of snowpack in glacier-fed river systems in South Asia with the current changing climate (Monirul and Mirza, 1997). Snow and glacier accumulation and melt processes are associated with monsoonal precipitation in headwaters of the south Asian Himalayas. These processes influence the hydrologic discharge by temporary storing and releasing of water at different time scales (Jansson et al., 2003). Singh and Kumar (1997) on their study of the Spiti River of western Himalayan region found an earlier peak streamflow due to advanced snowpack and glacier melt associated with a potentially warmer climate. Most mountain glaciers are changing due to global climate

change with subsequent intensification of the water cycle (Dyurgerov, 2003). Regions dominated by snowmelt hydrology are expected to be more susceptible to climate change due to alteration in seasonality of river flow regimes (Adam et al., 2009). Climate change in mountains is affected by the complex geography of these systems where differences in precipitation and temperature occur across small spatial scales. Anthropogenic-induced climate change is therefore challenging due to interactions of geography, precipitation, temperature, and snowpack and glacier ice accumulation and loss (eg. Mote et al., 2008).

In contrast to most other mountain glacier systems, ice accumulation and ablation occur during the same summer melting season in the Himalaya Mountain systems (Fujita et al., 2006). The mountain hydrology is highly affected by the behavior of glaciers as they determine the discharge during dry summer months and they also act as natural regulator (Stenborg, 1969). Himalayan glaciers receive snow from both winter westerlies and some summer monsoon. Most of the eastern Himalayan glaciers have both maximum advance and ablation during summer months which may have large contribution to make the maximum discharge in rivers. This process is highly controlled by the Indian summer monsoonal precipitation that weakens towards western part of the Himalayan regions. However, in western part of the Nepalese Himalayas, glacier advance occurs during winter season and ablation occurs during summer season.

The Himalaya Mountains are also important in terms of originating many largest and most sediment-loaded rivers in the world. However, there is lack of sufficient research works to address the potential changes in sediment loads under a changing climate (Knight and Harrison, 2009). About 35% of the discharge in mouth of the Indus and 60% of sediment loads of rivers in the Karakoram are glacier-derived (Collins and

Hasnain, 1995) that emphasize the importance of precipitation and glacial melting processes responsible for sediment yield in Himalaya mountain basins. Sediment in Himalaya Mountains is mainly contributed by glacial melt water that causes channel erosion due to high relief and velocity of water. In addition, summer monsoonal rain also causes heavy sediment transport due to flash flooding. The intensity of this flooding is increased due to deforestation and road construction which affect overland flow of precipitation.

Anthropogenic-induced impacts on hydrological processes include land degradation, and water pollution that change the utilization of water resources in the mountain basins (Sharma et al., 1991; Rawat and Rawat, 1994; Yue et al., 2004; Lu, 2005; Vanacker et al., 2007). The land use changes, primarily caused by overgrazing, mining, fuel wood collection, and road construction have affected quality and quantity of water derived from the mountain basins that have caused changes in the economy and ecological functions among the Indo-Gangetic plains (Tiwari, 2000; Awasthi et al., 2002). The future climate change also alters the hydrological processes in mountain basins potentially caused by less snowfall and earlier melting (White et al., 1998). Therefore, the overall objective of this study was to assess the effects of both climate change and land use modification on future water availability and sediment yield of mountain basins that might be crucial for future national and transnational water management implications.

CHAPTER TWO

Estimating the Effects of Climate Change on the Intensification of Monsoonal-driven Stream Discharge in a Himalayan Watershed

This chapter published as: Neupane RP, Yao J, White JD. 2013. Estimating the effects of climate change on the intensification of monsoonal-driven stream discharge in a Himalayan watershed. Hydrological Processes DOI: 10.1002/hyp.10115.

Introduction

The mountain systems such as the Himalayas occupy 24% of the total global surface area and may provide a source of fresh water, sustaining 12% of the world's population (ICIMOD, 2008). Mountain systems with snowmelt-dominated hydrology constrain water supply for human appropriation by maintaining stream discharge during dry periods where snowpack accumulation is sufficient and snowmelt is low. Snow and glacial melt are important for mountain hydrological processes (Immerzeel *et al*., 2009); and therefore potential changes in temperature and precipitation are predicted to adversely impact the melt characteristics (Barnett *et al*., 2005). With continued climate change coupled with increasing human population in the Himalayas, hydrologic changes in these regions are serious for water quantity and quality issues (Kundzewicz *et al*., 2007).

In the Himalayas, climate change has already been observed with temperature increasing faster than the global average with the increase mostly during winter season amplified at higher elevations (Beniston, 2003). Most mountain glaciers are receding due to continued warming at higher altitudes with subsequent intensification of the hydrologic cycle (Dyurgerov, 2003). Regions dominated by snowmelt hydrology are

expected to be more susceptible to climate change due to alteration in seasonality and intensity of river flow regimes (Adam *et al*., 2009). Some of the previous studies have emphasized the importance of meltwater contribution to the stream discharge and also assessed the potential effects of continued climate change on downstream hydrological processes (Barnett *et al*., 2005; Cyranoski, 2005). Continued climate change potentially impacts mountainous headwater systems by changing hydrologic discharge timing and amount associated with altered seasonal snowmelt patterns and reduced glacier cover (White *et al*., 1998; Kiffney *et al*., 2006). However, the meltwater contribution to water availability may be minor in Himalayan catchments having monsoon dominated climate system (Kaser *et al*., 2010).

The climate of the Himalaya Mountains is mainly influenced by the summer monsoon that originates from the Bay of Bengal. Peak melting season of these mountains coincides with the summer monsoon and therefore any intensification of monsoon or accelerated melting would contribute to increased summer runoff that would result in severe changes in mountain hydrology such as flood disasters (Shrestha, 2005). For example, the annual runoff of the Alkananda River (in western Himalaya) has increased by 2.8% annually during 1980-2000, whereas that of Kali Gandaki River in central Nepal Himalaya has increased by about 1.0% annually during 1964-2000. However, discharge in the Kosi Basin in eastern Nepal has decreased, particularly during the low-flow season (Sharma *et al*., 2000). Determination of trends in stream discharge across Himalayas is hindered by the lack of consistent long-term hydro-meteorological information from high elevation of the regions (Grabs and Pokhrel, 1993).

Estimation of hydrological response to continued climate change in the Himalaya catchment is complicated due to climatic heterogeneity, lack of sufficient hydro-meteorological information, and uncertainty in snow and glacier characteristics (Beniston, 2003). However, hydrological models have been widely used to study the effects of continued climate changes on the hydrological cycle (Guo *et al*., 2008; Ma *et al*., 2009). The Soil and Water Assessment Tool (SWAT), a quasi-distributed hydrological model, has been used to assess climate change impacts on watershed hydrology of mountain basins (Eckhardt and Ulbrich, 2003; Song and Zhang, 2012). The SWAT was originally developed for simulation of large sized ungauged basins with minimal calibration (Arnold *et al*., 1998). This study is one of the first to simulate climate change effects on hydrological processes on the monsoon dominated Himalaya Mountain basin of Nepal. The major objectives of this study are: (1) to determine if the SWAT model can be calibrated and confirmed for projecting stream discharge of a relatively isolated Himalaya Mountain catchment; (2) to identify sensitive hydrological SWAT parameters for the basin; (3) to project climate change impacts on key hydrological processes related to water availability over time; and (4) to assess the effect of climate change impacts on future water yield.

Materials and Methods

Description of the Study Watershed

The Kali Gandaki Watershed (KGW) located in central part of Nepal (Figure 1) covers an area of 7,261 km^2 as a subset basin of the Narayani River Watershed (NRW) and is one of the main tributaries of Ganges River. The watershed's elevation ranges from 548 m to over 8000 m above mean sea level. The highest elevation occurs at the

peaks of Annapurna and Dhaulagiri which are two large Himalaya Mountain peaks with elevations > 8000 m, potentially influencing orographic precipitation patterns. Dominant soils of the basin include Cambisols and Leptosols.

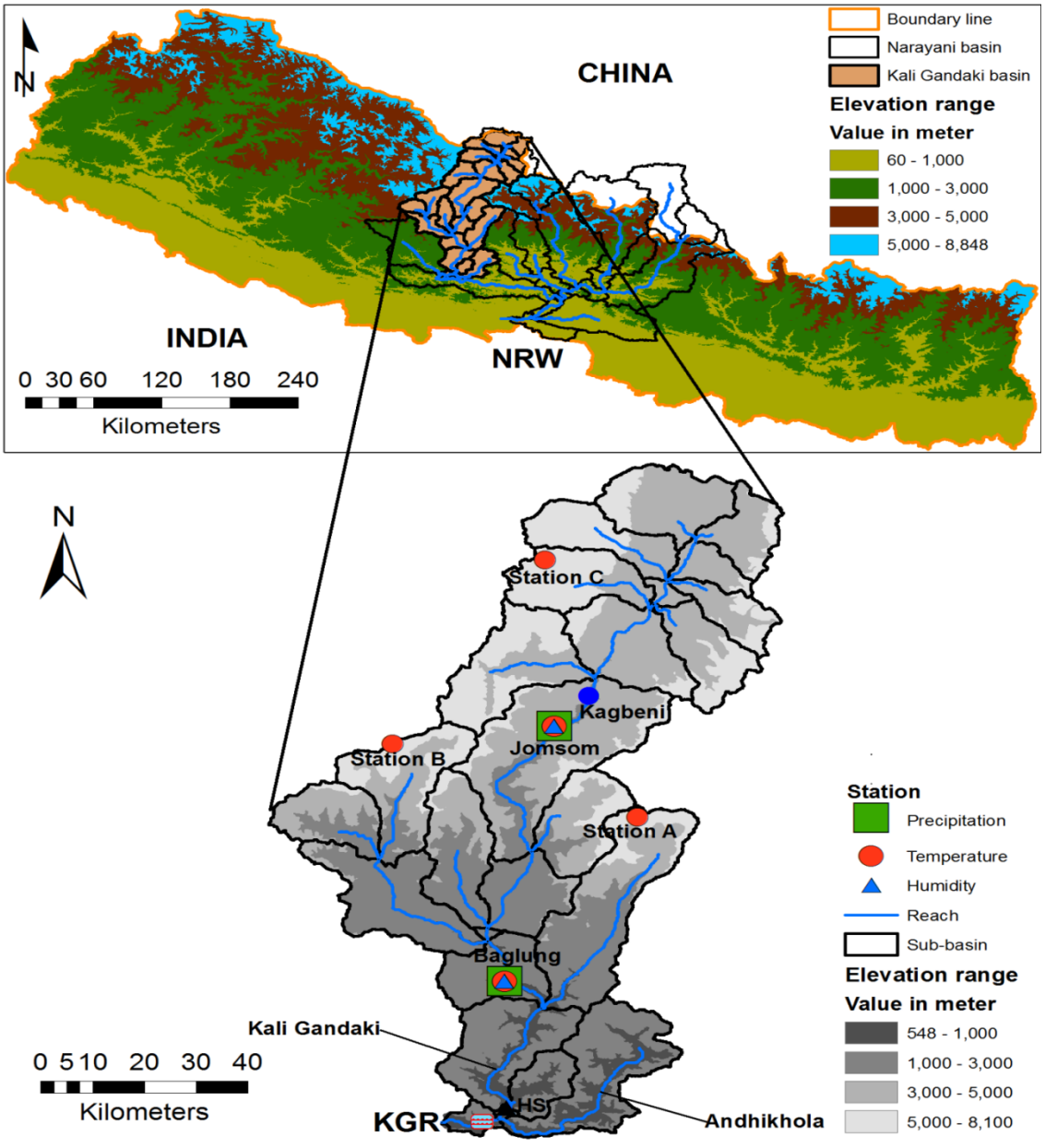

Figure 1. The KGW is shown as a subset of the Narayani Basin located in central Nepal with the hydro-meteorological stations used in this study.

The KGW varies climatically corresponding to elevation changes. The basin has three distinct climatic zones: sub-tropical zone (<1800 m); temperate zone (1800 to 4000 m); and alpine zone (> 4000 m) (Polunin and Stainton, 2000). The lower elevation is characterized with maximum temperature of 40^{o} C during summer months and total annual rainfall of 1500 to 2000 mm (Ichiyanagi *et al*., 2007). At higher elevations, cold and dry conditions persist with the average temperature of 11^{o} C and average annual precipitation of 257 mm (Pohle, 1991). Analysis of 40 years (1970-2009) of precipitation and 32 years (1964-1995) of stream discharge data derived from the Department of Hydrology and Meteorology (DHM), Nepal, indicated that more than 75% of the total precipitation occurred during monsoon season (similar to Sharma, 1993), comprising approximately 77% of the total stream discharge of the basin in the same season (Figure 2). During winter season, the watershed is affected by westerly winds which can influence snowfall at higher elevations.

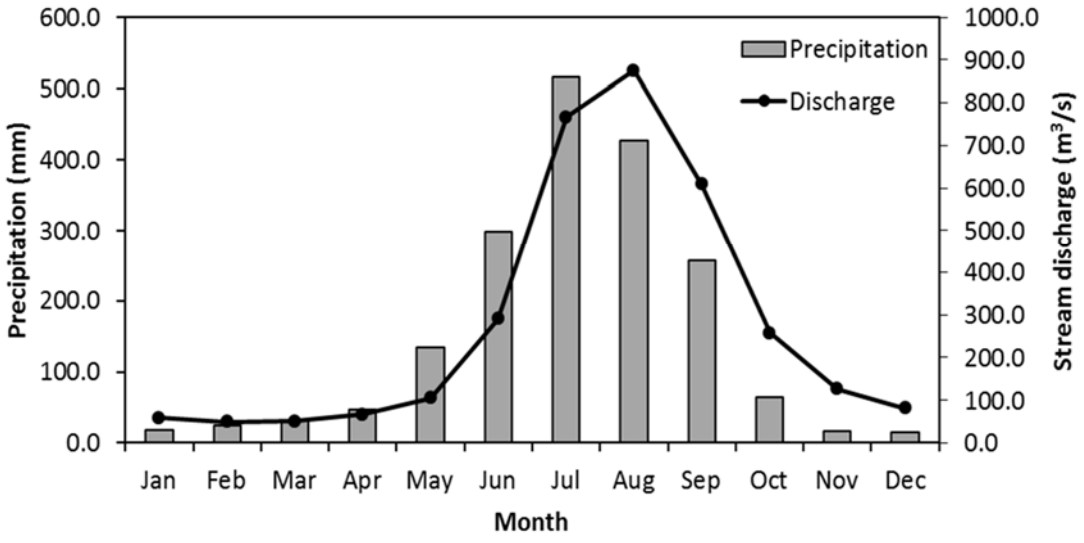

Figure 2. Mean monthly precipitation and stream discharge of the Kali Gandaki basin.

Hydrological Model

For this study, I used the Arc GIS interface of the SWAT (version 2009) (http://swatmodel.tamu.edu/software/swat-model). The hydrologic cycle in SWAT is based on the water balance equation (1) as follows, all expressed in mm.

$$SW_t = SW_0 + \sum(R_{day} - Q_{surf} - E_a - W_{seep} - Q_{gw}) \quad (1)$$

where SW_t is the final soil water content, SW_0 is the initial soil water content, t is time in days, R_{day} is the amount of precipitation, Q_{surf} is the amount of surface runoff, E_a is the amount of evapotranspiration, W_{seep} is the amount of water entering the vadose zone from the soil profile, and Q_{gw} is the amount of return flow. To estimate the surface runoff, I used the curve number method (USDA, 1986). Actual evapotranspiration (ET) was estimated from the method developed by Ritchie (1972) which considers a wide variety of soil types and climatic conditions. The Penman-Monteith procedure (Monteith, 1965), based on energy balance, was used to estimate potential evapotranspiration (PET).

Generally, it is expected that the inflows equal the outflows in a basin with limited storage. However, models such as SWAT include storage in the shallow aquifer (ΔGW Storage in mm) or the soil profile (ΔSW Storage in mm), and is represented by the following Equation 2.

$$P = ET + WYLD + \Delta SW\ Storage + \Delta GW\ Storage + Losses \quad (2)$$

where P is the precipitation (mm), ET is the evapotranspiration (mm), and WYLD is the water yield to the stream channels (mm). The WYLD in the model is computed by the following relation, all expressed in mm.

$$WYLD = SURQ + LATQ + GWQ - TLOSS - Pond\ Abstractions \quad (3)$$

where SURQ is the surface runoff, LATQ is the lateral flow contribution to stream discharge, GWQ is the groundwater contribution to the stream discharge, and TLOSS is the transmission losses from the system.

Snowmelt in the model is estimated through temperature-index or degree-day approach. The amount of water stored in the snowpack is represented as snow water equivalent (SWE). Increase or decrease of the snowpack depends on additional snowfall or release of meltwater in the basin, respectively. The mass balance for snowpack in the model is represented by the following Equation 4.

$$SNO = SNO + R_{day} - E_{sub} - SNO_{mlt} \quad (4)$$

where SNO is the total amount of water in snowpack on a given day (mm H_2O), R_{day} is the amount of precipitation (mm H_2O), E_{sub} is the amount of sublimation (mm H_2O), and SNO_{mlt} is the amount of snowmelt (mm H_2O). Despite the model's deficiency of representing glacier processes, a classical degree-day model (Singh *et al*., 2006) which relates ice or snowmelt to air temperature, was used and is represented by the following equation.

$$M = \begin{cases} D.\ (T_{av} - T_{gmlt}), when\ T_{av} > T_{gmlt} \\ 0, \qquad\qquad otherwise \end{cases} \quad (5)$$

where M is the depth of melt water (mm/day), D is the degree-day factor for ice melt (mm/day^{o}C), T_{av} is daily air temperature (^{o}C), and T_{gmlt} is the threshold value for ice melt (^{o}C). The D factor for snowmelt in the SWAT model is estimated by a sinusoidal function to represent the seasonal changes (Neitsch *et al*., 2005). However, the factor value for glacial melt estimation was taken from the study conducted in Langtang glaciers of the Himalaya Mountain system (Immerzeel *et al*., 2012). The ice volume estimation which is an important aspect of glacial melt was calculated as explained in Liu *et al*. (2003). In

this study, glacial accumulation, ablation, and contribution to the basin's water balance components were assessed for 1981 to 1990.

Input Spatial Data

Data required for SWAT includes elevation, land-use, soil properties, weather and climate, and measured stream discharge data. The Global Digital Elevation Model (GDEM) with a 30 m×30 m resolution (http://gdem.ersdac.jspacesystems.or.jp/search.jsp) was obtained and used for delineating sub-watersheds and defining stream networks. The watershed defined 27 sub-watersheds based on the minimum drainage area threshold value of 130 km^2. To account for the extreme topographic gradient on hydrological processes within the basin, I defined elevation bands in each sub-basin for every 510 m change in elevation. These bands were expected to be important in representing snow accumulation and melt processes in complex mountain systems (Fontaine *et al*., 2002). Details of elevation gradient of each sub-basin with the number of elevation band in the watershed are as shown in Figure 3.

Land-use for the KGW was derived through spectral classification of Landsat 5 Thematic Mapper (TM) satellite images (http://glovis.usgs.gov/). To classify the land-use of the basin, I performed an unsupervised classification using the Imagine software (ERDAS Inc. 2010). Our final classification was comprised of 11 different land-use classes including forest-evergreen, forest-deciduous, forest-mixed, grassland, rice, corn, snow/ice, tundra, water, urban, and others (pasture, bare rock, meadow and wetland) (Table 1) (Figure 4).

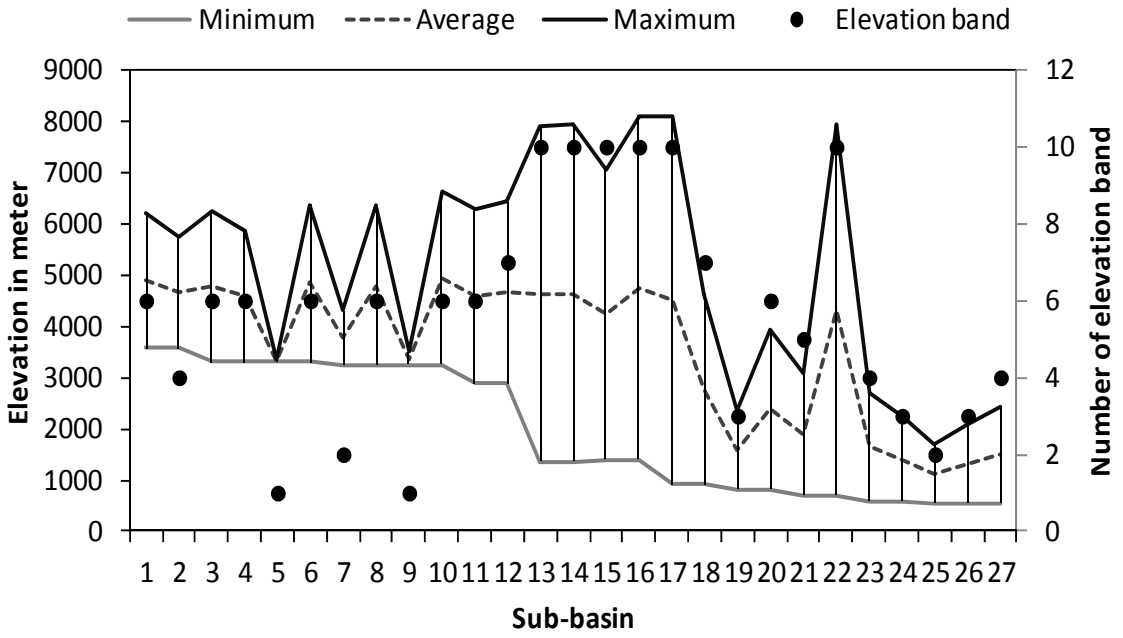

Figure 3. Total sub-basins with elevation gradients and number of elevation band developed for the simulation of snow processes in the basin.

Table 1. Percent cover of land-use in the KGW obtained using Landsat 5 (TM) satellite data.

Land-use class	Percent cover
Forest-evergreen	23.33
Forest-deciduous	1.69
Forest-mixed	3.66
Grassland	24.51
Rice	0.75
Corn	2.40
Snow/Ice	6.91
Tundra	11.35
Water	0.21
Urban	0.44
Others	24.75

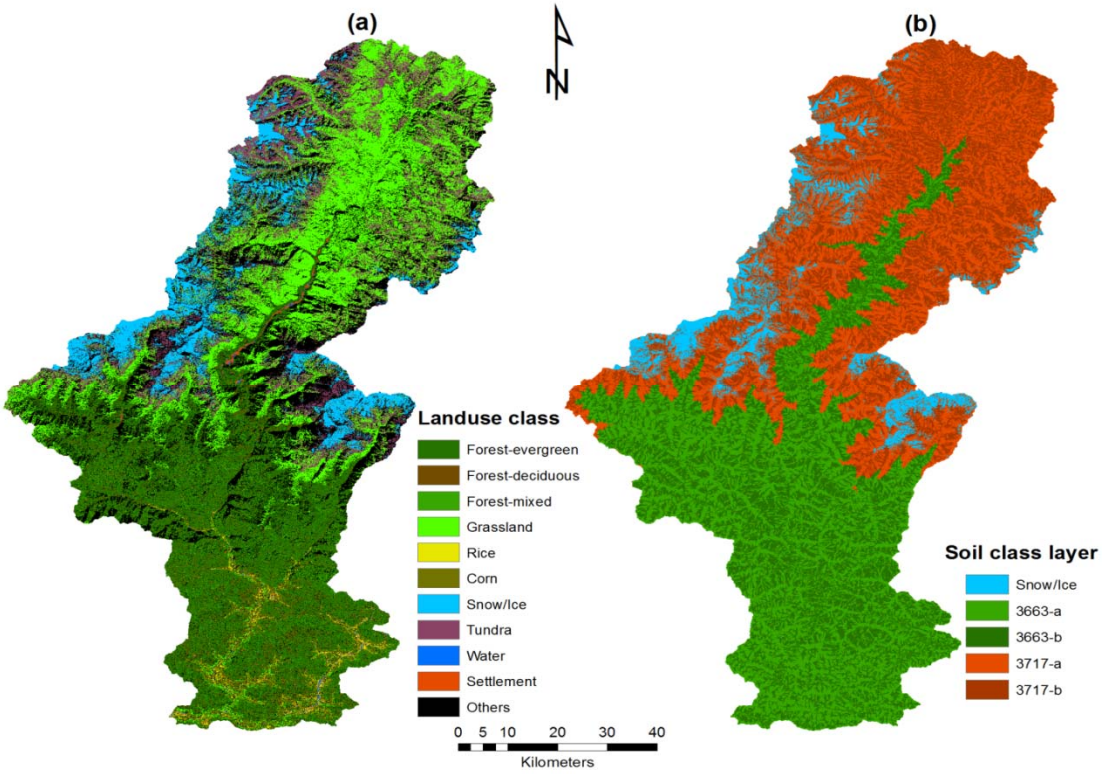

Figure 4. Different land-use and soil distribution of the KGW: (a) land-use and (b) soil distribution. The soil is shown with two different depth classes (a-for shallow soil layer and b-for deep soil layer).

Soil data with a 400 m spatial resolution were obtained from the Waterbase project (http://waterbase.org/download_data.html). I reclassified soil categories according to the Food and Agriculture Organization/United Nations Educational, Scientific and Cultural Organization (FAO/UNESCO, 2003). User's soil database was developed based on the FAO/UNESCO Soil Map of the World at an original scale of 1:5 million (Batjes, 1997). The digital datasets were linked to the units shown on the digital Soil Map of the World through legend code using ArcGIS software and they were categorized into different groups primarily based on the soil characteristics including pH, organic carbon content, cation exchange capacity, bulk density, available water capacity, soil texture and soil albedo for both topsoil (0-30 cm) and subsoil (30-100 cm). The point specific soil

depths were calculated using topographic integration (Zheng *et al*., 1996). Based on the information obtained from FAO/UNESCO soil data, soils were categorized in two different layers: shallow layer (<650 mm from surface) and deep layer (>650 mm from surface) (Figure 4). Finally, resolution of all of the datasets was made uniform and the required spatial datasets were co-registered to the projection of WGS-1984 UTM Zone 44N using the Arc GIS. Each of the 27 sub-basins of the KGW was further divided into one or more hydrologic response units (HRUs) based on the unique combination of topographic slope, land-use, and soil type. I defined 479 HRUs using the thresholds of 5, 5, and 20% to land-use, soil, and slope classes respectively. Based on the inclusion of land-use data, 33 HRUs from 8 different sub-basins have permanent glaciers with the total area of 397 km^2 and the total volume of 43 km^3.

Meteorological Data

The required meteorological inputs for SWAT include daily precipitation, maximum and minimum temperatures, net radiation, wind speed and relative humidity. For our simulations, I used 31 years (1979-2009) of meteorological data (except solar radiation and wind speed) obtained from DHM for two weather stations: Jomsom (28.78^o N, 83.71^o E, elevation: 2744 m) and Baglung (28.26^o N, 83.60^o E, elevation: 984 m). For solar radiation, I used the mountain climate simulator (MT-CLIM) (http://www.ntsg.umt.edu/project/mtclim) to estimate shortwave radiation from daily input temperature and precipitation data for these two weather stations. Wind data were taken from Kagbeni station (28.84^o N, 83.78^o E, elevation: 2838 m) from 2001 to 2005 and Surkhet station (28.88^o N, 81.25^o E, elevation: 950 m) from 1994 to 2008 as representative winds for the Jomsom and Baglung stations respectively. Due to large

number of glaciers in the basin, it was not possible to estimate the air temperature for individual glaciers, however, I considered 3 stations (A: 28.59º N, 83.87º E, elevation: 5,657 m, slope: 28.35º, aspect: 214.3º from Annapurna mountain region; B: 28.75º N, 83.39º E, elevation: 6,546 m, slope: 45.49º, aspect: 142.98º from Dhaulagiri mountain region; and C: 29.12º N, 83.70º E, elevation: 5,857 m, slope: 4.85º, aspect: 78.69º from northern part of the basin) and simulated mean daily air temperature using MT-CLIM for the period of 1981 to 1990 using measured data from Jomsom station to incorporate with the degree-day model for estimating glacier melt in the basin.

The temperature and precipitation lapse rates required by SWAT were estimated by using meteorological data from two stations: Lumle (28.30º N, 83.80º E, elevation: 1740 m) and Pokhara (28.12º N, 84.12ºE, elevation: 856 m), both of which are located in windward side of the basin. The Lumle station indicates the highest precipitation in Nepal (>5000 mm/year). The Pokhara station is situated approximately at 37 kilometers southeast of Lumle station. The ranges of local temperature and precipitation lapse rate were derived from 31 years (1979-2009) with mean annual data which is presented in the following Table 2.

Management Operations

For our simulations, corn was designated as the major crop type cultivated in the basin (pers. obsv.). For crop management operations, land units were considered to be terraced, which is a common land management practice in the region (Carson, 1990). Cattle-based fresh manure was used as the primary fertilizer for growing corn with application rate of 42 kg/ha (Pandey *et al*., 2009) and tillage operation was used to redistribute nutrients to the upper soil layers using traditional plough. The management

operations including fertilization, tillage, planting, and harvesting were adopted based on the potential heat unit value (representing the number of heat units required to bring a plant to maturity) for the corn farming in the region (Table 3).

Table 2. Mean annual temperature (TMP), and precipitation (PCP) of all the meteorological stations used for this study including the range of temperature and precipitation lapse rates (TLAPS and PLAPS, respectively) estimated from two recording sites which provided climate forcing data for the model simulations.

Climate station	Elevation (m)	TMP (^oC)	PCP (mm)	TLAPS (^oC/km)	PLAPS (mm/km)
[a]Pokhara	856	20.80	3674	(-6.12) - (-4.58)	368 - 2937
[a]Lumle	1740	16.06	5440	-	-
[b]Jomsom	2744	11.61	264	-	-
[b]Baglung	984	21.49	1928	-	-
[c]Syangja	868	20.89	2858	-	-

[a]Stations used for estimating TLAPS and PLAPS for this study.
[b]Stations used for incorporation of meteorological data for the model simulations.
[c]Station used for calculating potential heat units required for corn cultivation in the basin.

Table 3. Management operations adopted in KGW for corn cultivation including the total heat units required for plant maturity (PHU) and the total base zero heat units (PHU_0). The data were generated using 17 years (1979-1995) daily measured air temperature data from Syangja station (28.10^o N, 83.88^o E, elevation: 868 m) as described in SWAT documentation.

Date	Operation	Base Zero Heat Units Accumulated	Plant Heat Units Accumulated	Fraction of PHU_0 (PHU_0 = 7587)	Fraction of PHU (PHU = 2066)
May 1, 1979	Terracing	-	-	-	-
May 3	Fertilizer application	2151	-	0.28	-
May 5	Tillage operation	2197	-	0.29	-
May 10	Planting corn (PHU = 2066)	2314	0	0.31	-
October 10	Harvest & Kill	6173	2342	-	1.2

Model Calibration and Confirmation

Before calibration, the model was first run with SWAT default parameter values to compare with measured data for the period of 1981 to 1990; and referred as the pre-calibration simulation. I then simulated the basin for separate model runs used for calibration (1979-1990) and confirmation (1991-1995) at daily time step. I compared these simulations to 17 years (1979-1995) of daily stream discharge data taken from the gauging station at Seti Beni (28.00º N, 83.60º E, elevation: 546 m) obtained from DHM. For calibration, the initial two years were not included in the analysis and used as a spin-up period for simulations. To assess the effects of orographic precipitation and glacier processes in the basin, calibration and confirmation simulations were run in two different scenarios: 1) band-no glac: elevation bands were used and glacier melt data were not used, and 2) band-glac: elevation bands were used and glacier melt data were used. Calibration outputs were then taken as the baseline data to compare with further climate change simulations. Calibration and confirmation success was judged by the percent bias (PBIAS) (Equation 6).

$$PBIAS = \frac{\sum(Y^{obs} - Y^{sim})}{\sum Y^{obs}} \times 100 \qquad (6)$$

where Y^{obs} is the measured data and Y^{sim} is the model output. Both calibration and confirmation studies consider satisfactory PBIAS values to be < 25% (Van Liew *et al*., 2007).

The model calibration and confirmation simulations were also evaluated using goodness of fit statistics including Nash-Sutcliffe efficiency (NSE) (Equation 7) and coefficient of determination (r^2).

$$NSE = 1 - \frac{\sum(Y^{obs} - Y^{sim})^2}{\sum(Y^{obs} - Y^{mean})^2} \quad (7)$$

where Y^{mean} is the mean of measured data. I adopted the rating of NSE value with Moriasi *et al*. (2007). The correlation coefficient of determination (r^2) was calculated using Microsoft Excel. The higher the r^2 value, the lesser the error variance, and typically the values > 0.5 are considered acceptable (Santhi *et al*., 2001). For our analysis, I assessed these measures for both daily and monthly model outputs of stream discharge. However, monthly simulations were used to estimate climate change impacts on hydrological processes of the watershed.

Sensitivity of SWAT Parameters

In this study, model parameters potentially influencing hydrological processes of the mountain basin were identified through a detailed review of literature sources which apply the SWAT model (e.g., Fontaine *et al*., 2002; Muleta and Nicklow, 2005; Rostamian *et al*., 2008). During calibration, optimal parameter values were derived from a trial and error process in which one parameter was adjusted at a time; however, this does not account for the interactions among parameters (Gardner et al., 1980; Downing et al., 1985). Only one parameter was changed in each run so the changes in output can be unequivocally attributed to the input parameter changed. Despite some shortcomings of computational effort and output changes through selection of other parameters, this process has become very useful for SWAT modeling as it is able to analyze sensitivity of a large number of hydrologic parameters (Lenhart et al., 2002; Francos et al., 2003). To assess the sensitivity of modeled stream discharge, 10 years (1981-1990) daily stream discharge data were compared with individual simulations in which selected parameters

were altered ±20% from a base value leaving all others constant. The relative sensitivity was evaluated as follows:

$$S_r \cong \frac{O_{p+\Delta p} - O_{p-\Delta p}}{O_p} / (\frac{2\Delta P}{P}) \quad (8)$$

where S_r is the relative sensitivity, $O_{p+\Delta p}$ and $O_{p-\Delta p}$ are the model outputs of mean stream discharge from the simulations with input parameter changes of ±20% respectively, O_p is the model output of mean stream discharge with base input parameter, ΔP is the absolute change in the value of input parameter, and P is the initial value of input parameter. The S_r value of the parameters was rated based on the methods described by Lenhart *et al*. (2002). In addition, standardized residual error analysis (White and Running, 1994) was done to estimate the uncertainties of model predicted stream discharge values.

Climate Change Scenarios

To assess climate change impacts on watershed hydrology, SWAT simulations were run for the period of 2080 to 2089 at a monthly time step. However, only eight years (2082-2089) of simulated data were used for the analyses as I ignored the initial two years as model spin-up period. For this study, I derived the average, minimum, and maximum outputs of temperature and precipitation changes projected for the Special Report on Emission Scenarios (SRES) including the low (B1), medium (A1B), and high (A2) emission scenarios from16 global circulation models (GCMs) (http://www.climatewizard.org/) for 2080s. Monthly changes of temperature and precipitation data derived from the GCMs were incorporated with the baseline SWAT database.

Mean annual changes of the basin precipitation, stream discharge, snowfall, snowmelt, water percolation, groundwater discharge to stream flow, evapotranspiration,

and soil water content were estimated to compare with the simulated baseline data. I analyzed the potential seasonal changes in stream discharge of the basin. I also estimated the trend of glacier melt over the calibration and confirmation periods. Analyses of climate change effects on modeled hydrologic elements were compared with the baseline simulation using the following Equation 9.

$$\%\, Change = \left(\frac{Y^{sim} - Y^{base}}{Y^{base}}\right) \times 100 \quad (9)$$

where Y^{base} is the baseline output.

Results and Discussion

Model Calibration and Confirmation Analysis

The results of pre-calibrated simulation showed low correspondence for PBIAS and NSE with values of 56 and 0.21, respectively with daily measured stream discharge values (Table 4). The r^2 also showed low correspondence with the value of 0.46. For monthly simulations, the PBIAS, NSE and r^2 values were 56, 0.40, and 0.88, respectively. Following the addition of elevation bands coupled with corn cropping, correlation between modeled and measured stream discharge were moderate to high as indicated by the PBIAS = 3, NSE = 0.79 and $r^2 = 0.79$ for daily simulation during the calibration period. For monthly simulations, the PBIAS, NSE and r^2 values were 3, 0.85, and 0.85 respectively. The increase in correlation between simulated and measured stream discharge with the inclusion of elevation bands showed the importance of orographic precipitation in the basin. While adding the glaciermelt data with elevation band, the PBIAS, NSE and r^2 values were -0.73, 0.79 and 0.79 respectively for daily simulation. The model showed better performance in monthly simulations with the values of -0.76,

0.86 and 0.86, respectively indicating the importance of glacier melt contribution for predicting stream discharge of the basin.

During confirmation period, the PBIAS value was higher in band-no glac scenario in both daily and monthly simulations indicating the large average difference between measured and model simulated values. However, similar to the calibration, the model showed moderate to high correlation with the NSE = 0.76 and $r^2 = 0.79$ for daily simulations. For monthly simulations, the NSE, and r^2 values were 0.84, and 0.88 respectively. With the addition of glacier melt data, the PBIAS and NSE values were 14 and 0.78 respectively for daily simulations. I found the highest accuracy for simulating stream discharge during the confirmation period at monthly scale. Finally, simulated mean daily stream discharge with a value of 273 m^3/s corresponded well with the measured value of 271 m^3/s. Based on the water balance equation, I calculated a total loss of 79 mm (about 4%) of water from the total inflows during the period of 1981 to 1990 potentially indicating water flux into deep groundwater reservoirs. The shallow-aquifer baseflow which was properly reproduced by SWAT (Arnold et al., 2000) is a major component of hydrologic modeling in mountainous basins (Luo et al., 2012). I separated the baseflow component during pre-calibration period (Figure 5) that showed the contribution of 24% to the total annual flow volume with major contribution during low-flow seasons.

The hydrographs (Figure 6) obtained from pre-calibrated simulations showed that the stream discharge during winter months was consistently underestimated by the model for both daily and monthly simulations. For summer months, simulated monthly stream discharge values were also lower than the measured values. For daily simulation, peak

Table 4. Model performance statistics for pre-calibration, calibration and confirmation simulations in both daily and monthly time periods (no band-no glac: elevation bands were not used and glacier melt data were not used; band-no glac: elevation bands were used and glacier melt data were not used; band-glac: elevation bands were used and glacier melt data were used).

Statistics	Pre-calibration		Calibration				Confirmation			
	no band-no glac		band-no glac		band-glac		band-no glac		band-glac	
	Daily	Monthly	Daily	Monthly	Daily	Monthly	Daily	Monthly	Daily	Monthly
PBIAS	56	56	3	3	-0.73	-0.76	18	18	14	14
NSE	0.21	0.40	0.79	0.85	0.79	0.86	0.76	0.84	0.78	0.86
r^2	0.46	0.88	0.79	0.85	0.79	0.86	0.79	0.88	0.79	0.89

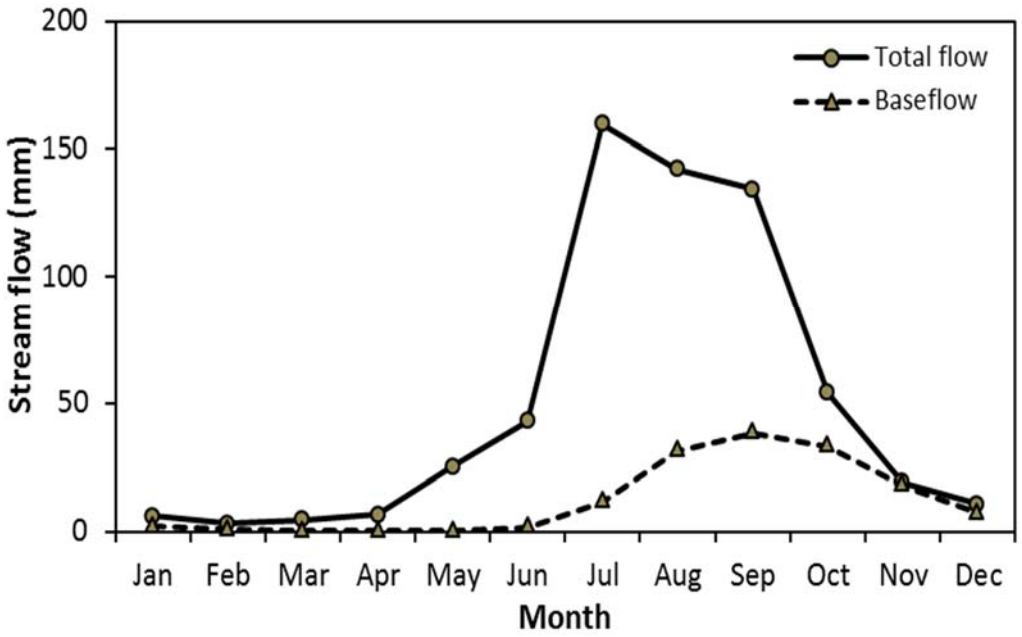

Figure 5. Comparison of total stream flow with the baseflow component (The data is averaged over the period from 1981 to 1990).

flows were overestimated, particularly during summer months. Correspondence of model simulated stream discharge with the measured values in both daily and monthly

simulations increased for calibration and confirmation periods (Figure 7) with the inclusion of elevation bands and glacier melt data. In most of the years, the best fit was observed in the spring runoff period, particularly on the rising limb of the hydrographs. However, the model overestimated the summer recession values and underestimated the winter and early spring base flow components.

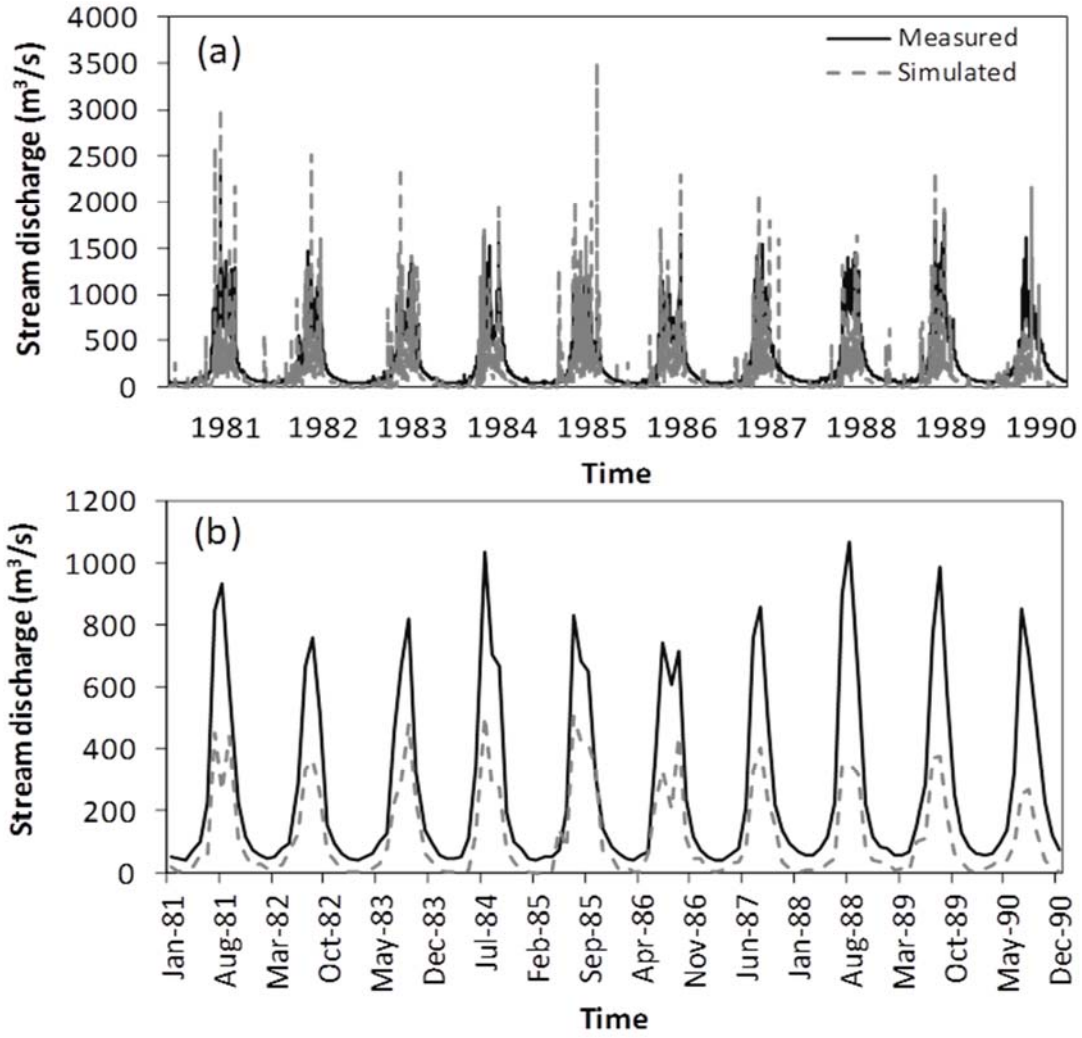

Figure 6. Pre-calibration hydrographs obtained from model simulations: (a) for daily, and (b) for monthly time periods.

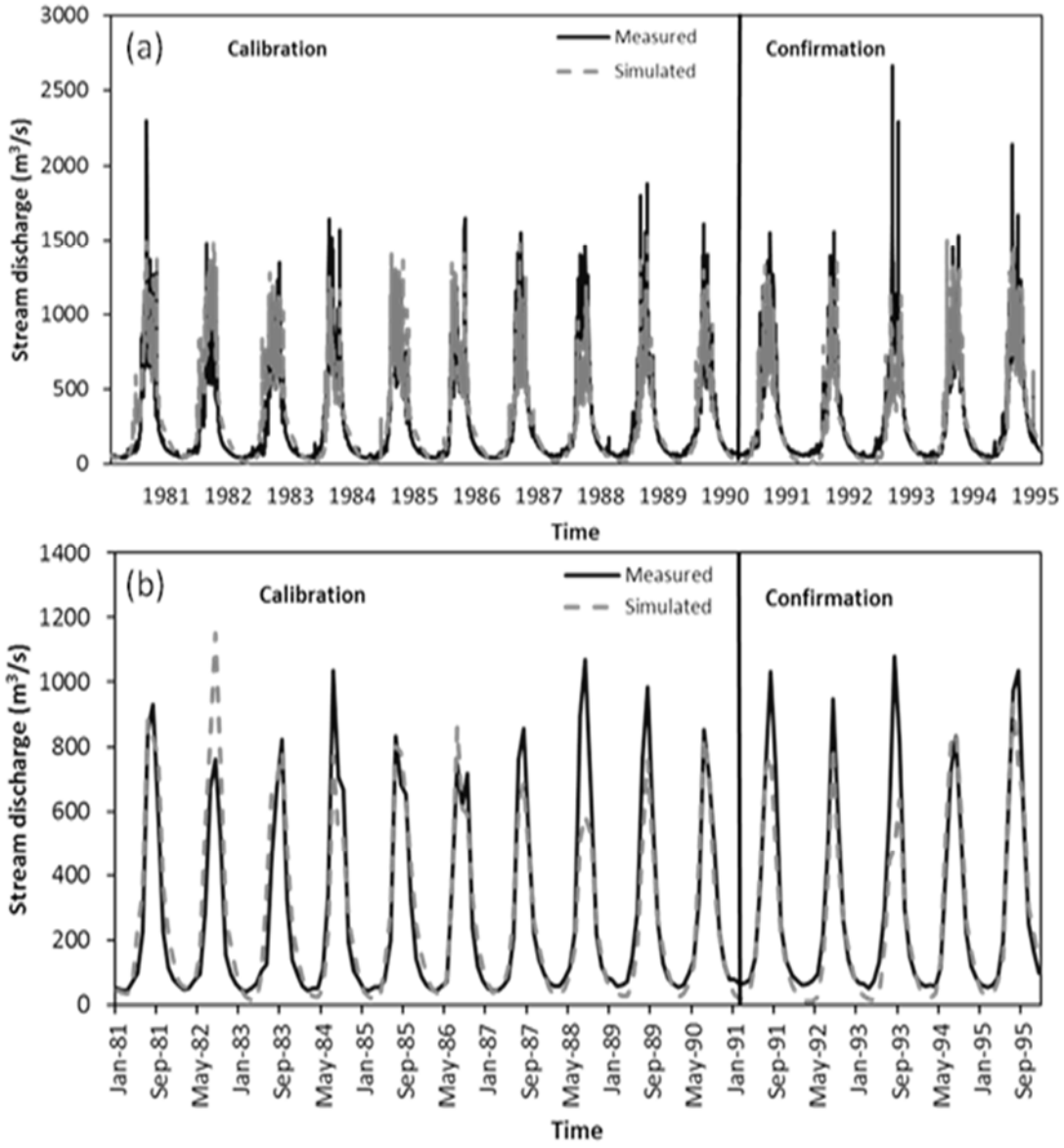

Figure 7. Hydrographs obtained during model calibration and confirmation periods: (a) for daily, and (b) for monthly time periods.

Simulation outputs showed that about 48% of the total annual stream discharge was contributed mostly by rain (Figure 8) indicating the importance of monsoonal precipitation in the basin. Snowmelt, groundwater, and glacier melt contribution were estimated as 9, 14 and 29% respectively. These assessments were supported by the findings of Bookhagen and Burbank (2010) who estimated 10% of the stream discharge

was derived from snowmelt in the Kali Gandaki basin. Similar modest role of meltwater to the stream discharge with substantial role of rainfall contribution was estimated to the Ganges basin (Immerzeel *et al*., 2010). Our estimation was higher than 10% meltwater contribution to the annual stream discharge from the three (Koshi, Narayani and Karnali) major Nepalese Himalayan watersheds (Anderman *et al*., 2012). However, our estimated value was less than the 59% estimated for the western Himalayan regions (Singh and Jain, 2002). I attribute these differences to higher influence of monsoonal precipitation to the stream discharge in the central and eastern Himalayas.

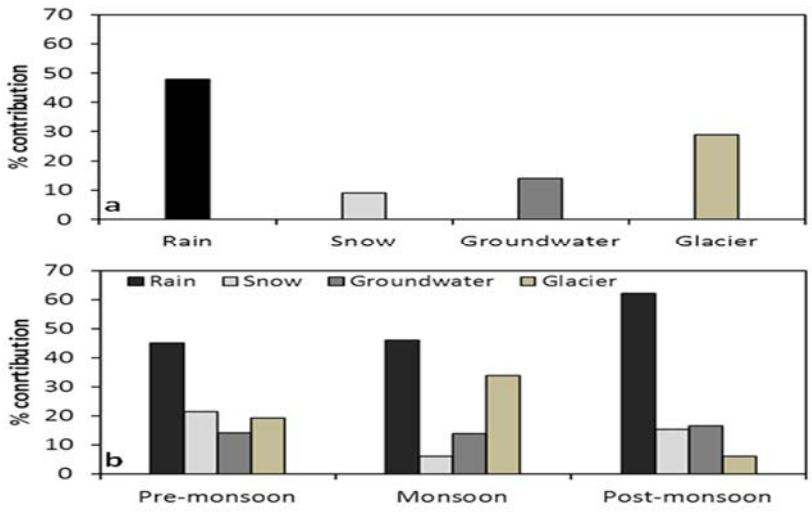

Figure 8. Stream discharge contribution of the KGW by different source waters obtained from model simulations: (a) for yearly, and (b) for seasonal basis.

Seasonal analysis of the model outputs showed that rain dominates the stream discharge in all the seasons with a maximum contribution of 62% during post-monsoon season (Figure 8). Groundwater contribution to the stream discharge was also highest during post-monsoon season with an estimate of 17% of surface water derived from groundwater reservoirs. Snowmelt contribution was found to be at its highest value of 21%

during pre-monsoon season which might be indicating the importance of seasonal snowmelt in the basin. However, maximum meltwater from the glaciers may contribute 34% of the stream discharge during monsoon season. Our results that include SWAT stream discharge with estimated glacier melt data are similar to Sharma (1993) who showed that snow and glacier meltwater from high elevations contributes substantially (> 30%) to the stream discharge, mainly during the pre-monsoon period with groundwater resources playing an important role during the post-monsoon season. I also estimated a trend of glacier melt in the basin with the average rate of 4.4 mm/year during the period of 1981 to 1990. Variations in stream discharge are only partially related to changing glacier melt of the Himalayan catchments (Thayyen & Gergan, 2010) and therefore long-term field observations on glacier mass balance might be crucial for projecting hydrologic processes of these catchments and for the Ganges River.

Sensitivity Analysis

The results of our sensitivity analysis are shown and ranked in Table 5. From the 19 parameters I tested, 16 were found to affect the stream discharge. Three of these, snowmelt base temperature (SMTMP), snowfall temperature (SFTMP), and surface runoff lag time (SURLAG) were not found sensitive to influence stream discharge of the KGW. I found the PLAPS and TLAPS, ranked as 1 and 2 respectively in the table, as the most sensitive with potentially higher influence on the accuracy of simulated stream discharge. This assessment confirmed that temperature lapse rates are affected by the extreme orographic effect of the Himalayas where air is lifted vertical rapidly over short distances (Minder *et al*., 2010) affecting the amount of rainfall and snowfall ultimately influencing amount and timing of stream discharge of the basin.

Table 5. Sensitivity results with the ranking of key SWAT parameters for stream discharge in the KGW including the range of parameter values adopted from Muleta & Nicklow (2005) and Rostamian et al. (2008).

Parameter	Description	Range	Optimal value	S_r	Rank
[a]PLAPS	Precipitation lapse rate (mm H_2O/Km)	368 - 2629	700	0.626861	1
[a]TLAPS	Temperature lapse rate (^oC/Km)	(-5.8) - (-4)	-5.5	0.603202	2
SMFMX	Maximum melt rate for snow during the year (mm/^oC-day)	1.4 - 7.5	7.24	0.039837	3
REVAPMN	Threshold depth of water in the shallow aquifer for revap (mm H_2O)	0 - 100	50	0.004127	4
RCHRG_DP	Deep aquifer percolation fraction	0.01 - 0.75	0.01	0.003703	5
[b]TIMP	Snow pack temperature lag factor	0.5 - 1	0.25	0.003224	6
SMFMN	Minimum melt rate for snow during the year (mm/^oC-day)	1.4 - 7.5	4.31	0.003114	7
ALPHA_BNK	Baseflow alpha factor for bank storage (Days)	0.05 - 1	0.07	0.001509	8
ESCO	Soil evaporation compensation factor	0.001 - 1	0.15	0.001479	9
GWQMN	Threshold depth of water in the shallow aquifer required for return flow to occur (mm H_2O)	0 - 100	25	0.001473	10
CH_K2	Effective hydaulic conductivity in main channel alluvium (mm/hr)	0 - 150	150	0.001321	11
ALPHA_BF	Baseflow alpha factor (Days)	0.001 - 1	0.60	0.001061	12
GW_REVAP	Groundwater "revap" coefficient	0.02 - 0.2	0.14	0.000827	13
GW_DELAY	Groundwater delay time (Days)	0.001 - 100	5	0.000281	14
CH_N2	Manning's n value for the main channel	0.01 - 0.15	0.11	0.000241	15
EPCO	Plant uptake compensation factor	0.001 - 1	0.01	0.000037	16
SMTMP	Snow melt base temperature (^oC)	(-2) - 20	5	0.000000	NS
SFTMP	Snowfall temperature (^oC)	(-10) - 5	1	0.000000	NS
SURLAG	Surface runoff lag time (days)	0.001 - 15	13.38	0.000000	NS

[a] Range of these parameters were estimated using temperature and precipitation data from local stations as given in Table 2.
[b]Calibrated baseline value of this parameter is out of the given range.
NS indicates as not sensitive.

The maximum melt rate for snow (SMFMX) and the snowpack temperature lag factor (TIMP) were also found to affect stream discharge of the basin. This is also supported by the findings of Wang and Melesse (2005). The higher SMFMX value indicated that faster snow melt was required for higher correspondence between modeled and measured stream discharge values. Because higher snowmelt rates tend to be

associated with increased absorbed radiation (Bengtsson and Westerstrom, 1992), this might indicate that snow and ice of the basin may have lower albedos. Recently, satellite-detected dust plumes from the Arabian Peninsula have also been found to affect snow albedo in the Himalayas, particularly during pre-monsoon season (Gautam *et al*., 2013). I estimated the TIMP value lower than the minimum value of 0.5 suggested by Muleta and Nicklow (2005). Snowpack depth is a primary factor affecting the snowpack temperature of the mountain system (Fontaine *et al*., 2002) such that our lower TIMP value might be the reflection of extreme cold environment particular to the Himalayas.

The higher value of 150 mm/hr for channel conductivity (CH_K2) may be related to the deep alluvium composed of large sized gravel and sand of the stream channels which rapidly transmit water to deeper groundwater (Scanlon *et al*., 2002). This was also related to the lower baseflow alpha factor for bank storage (ALPHA_BNK) with the value of 0.07 days which is associated with highly transmissive material of the river systems. I obtained a larger channel roughness coefficient (CH_N2) value which might be associated with large sized riverbed materials, typical of the Himalayan mountain rivers (Soto and Madrid-Aris, 1994). However, the deep aquifer percolation fraction (RCHRG_DP) was calibrated with a minimum value of 0.01. I performed an uncertainty analysis of one year model predicted data from the calibration period and it is presented in Figure 9. It demonstrated that the model predictions showed significant over and underestimation values only during monsoon period with better performance during low-flow (pre-monsoon and post-monsoon) seasons.

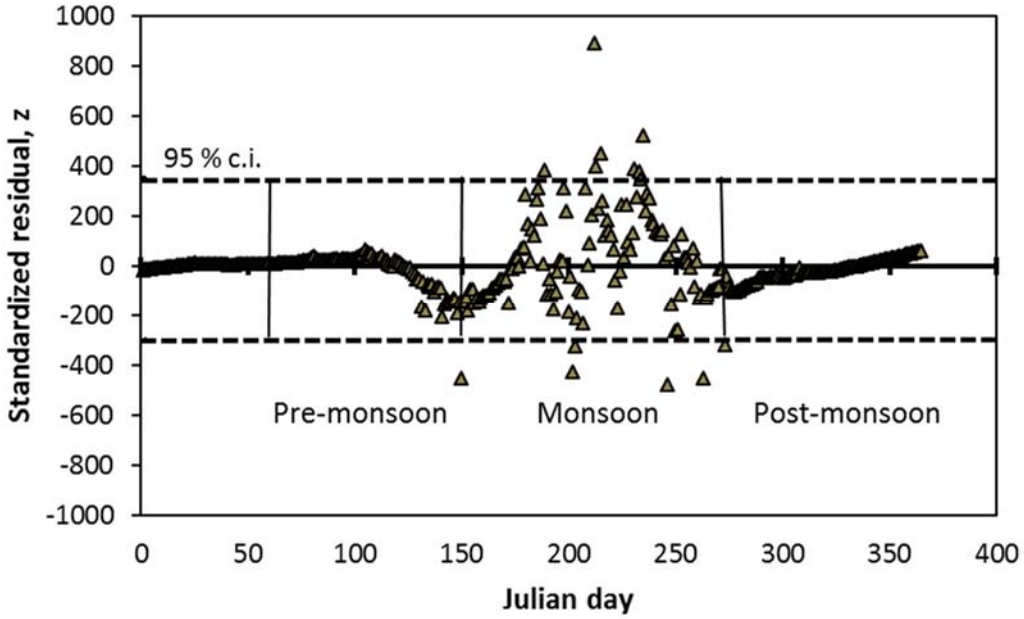

Figure 9. Standardized residual error (z-scores) for the SWAT model simulations of stream discharge (m^3/s) versus measured stream discharge from the KGW.

Effects of Climate Change

Projected changes of temperature and precipitation based on GCM-derived scenarios for the Jomsom and Baglung meteorological stations are shown in Table 6. These data showed that mean annual temperatures were higher than current values ranging from 1.3° C to 6° C for the Jomsom station. This was slightly higher than the projected values of 1.2° C to 5.7° C for the Baglung station. Temperature varied monthly ranging from 0.5° C to 6.7° C for both of the stations. These data confirm the general expectation of warming of the basin under all of the scenarios, with highest temperature values for the maximum GCM projection of the A2 scenario and smallest increases for the minimum GCM projection of the B1 scenario.

Simulation outputs showed the changes of projected annual precipitation from -46.8 % to +62.5 % in Jomsom and -42.5 % to +63.3 % in Baglung stations. Large variation in monthly precipitation was found which ranges from -62 % to +177 % for

Table 6. Various scenarios for Jomsom and Baglung meteorological stations obtained from GCM outputs to use for future hydrologic assessment of the basin: (a) annual and monthly average temperature changes (° C), and (b) annual and monthly cumulative precipitation changes (in %).

(a)	**Jomsom station**												
Scenario	Month												
	1	2	3	4	5	6	7	8	9	10	11	12	Annual
B1 maximum	4.4	5.2	4.5	4.8	4.2	4.6	3.1	3.6	3.3	3.4	3.5	4.5	4.1
B1 minimum	1.8	2.3	1.9	1.7	1.0	0.9	0.5	0.9	0.9	1.3	1.2	1.3	1.3
B1 average	3.1	3.1	3.0	2.9	2.7	2.6	2.2	2.2	2.3	2.4	2.5	3.0	2.7
A1B maximum	6.4	6.6	5.9	6.1	5.7	6.6	4.7	4.8	4.6	4.9	5.2	6.2	5.7
A1B minimum	2.9	2.7	2.6	2.4	1.9	1.4	1.5	1.5	1.6	2.1	2.7	2.8	2.2
A1B average	4.6	4.6	4.3	4.3	4.1	3.7	3.3	3.2	3.4	3.6	3.9	4.3	3.9
A2 maximum	6.5	6.6	6.7	6.5	5.8	6.7	5.2	5.1	5.0	5.3	5.5	6.5	6.0
A2 minimum	3.6	3.9	3.3	3.0	2.3	1.8	1.8	1.6	1.7	2.3	2.8	3.3	2.6
A2 average	5.2	5.1	5.1	5.0	4.7	4.2	3.6	3.7	3.8	4.1	4.4	5.1	4.5
	Baglung station												
B1 maximum	4.3	4.9	4.5	4.6	3.7	3.7	3.2	3.5	3.4	3.1	3.5	4.4	3.9
B1 minimum	1.8	1.9	1.8	1.5	0.9	0.8	0.5	0.9	1.1	1.3	1.2	1.5	1.2
B1 average	3.0	3.0	3.0	2.8	2.5	2.3	2.1	2.1	2.2	2.3	2.4	2.8	2.5
A1B maximum	5.9	6.2	5.4	5.6	5.2	5.5	4.8	5.1	4.7	4.7	5.0	5.8	5.3
A1B minimum	2.7	2.7	2.7	2.5	2.0	1.2	1.3	1.8	1.7	2.2	2.4	2.7	2.1
A1B average	4.3	4.4	4.1	4.1	3.8	3.4	3.0	3.1	3.2	3.4	3.6	4.0	3.7
A2 maximum	6.4	6.3	6.7	6.4	5.6	5.5	4.8	4.9	4.8	4.9	5.3	6.2	5.7
A2 minimum	3.5	3.3	3.3	2.8	2.3	1.6	1.9	1.8	1.8	2.4	2.5	3.1	2.5
A2 average	4.9	4.8	4.9	4.7	4.3	3.7	3.3	3.5	3.6	3.8	4.1	4.7	4.2

(b)	**Jomsom station**												
Scenario	Month												
	1	2	3	4	5	6	7	8	9	10	11	12	Annual
B1 maximum	20	32	25	33	42	51	72	68	81	104	28	24	48.3
B1 minimum	-45	-28	-33	-46	-33	-38	-39	-34	-19	-47	-46	-38	-37.2
B1 average	-9.6	-7.5	-13.5	-7.9	0.1	6.8	8.1	12.2	16.8	8.8	-8.3	-8.6	-0.2
A1B maximum	8	31	16	23	50	81	76	59	102	177	60	67	62.5
A1B minimum	-43	-34	-39	-48	-62	-48	-53	-47	-32	-53	-53	-49	-46.8
A1B average	-14.8	-9.4	-12.3	-16.6	0.8	19.3	13.5	14.4	26.2	27.7	-4.9	-5.8	3.2
A2 maximum	43	4	8	20	46	90	88	70	87	128	92	46	60.2
A2 minimum	-50	-38	-45	-51	-53	-54	-52	-41	-32	-46	-57	-35	-46.2
A2 average	-12.4	-16.7	-16.6	-13.6	2.4	22.3	16	14.7	24.8	19.6	-1.9	-6.8	2.7
	Baglung station												
B1 maximum	18	31	26	37	48	42	59	52	69	101	28	35	45.5
B1 minimum	-50	-32	-37	-49	-36	-27	-28	-18	-16	-39	-51	-46	-35.8
B1 average	-13.2	-8.4	-13.6	-5.8	3.9	5.4	7.4	12.3	17.1	11.1	-8.4	-11.5	-0.3
A1B maximum	20	23	49	41	65	55	59	51	77	151	62	107	63.3
A1B minimum	-49	-37	-41	-53	-59	-33	-26	-19	-24	-48	-57	-64	-42.5
A1B average	-17.7	-11.7	-10.1	-15.6	7.2	14.4	13	14.3	26.4	29.3	-3.6	-6.1	3.3
A2 maximum	42	5	9	48	61	64	67	69	68	141	97	53	60.3
A2 minimum	-54	-43	-47	-57	-50	-34	-24	-23	-27	-49	-55	-44	-42.3
A2 average	-16.4	-17.3	-16.6	-9.1	8.9	16.9	15.4	15.6	25.1	25.1	2.1	-9.8	3.3

Jomsom station and from -64 % to +151 % for Baglung station. Generally, precipitation amount was projected by all the GCM models to be higher during summer months, presumably associated with monsoonal intensification; and lower during winter months. The magnitude of changes in projected precipitation was surprisingly large indicating some difficulty in predicting meteorology in the Himalayas with such high topographic relief. This is due to the extreme topographic variation in the Himalaya Mountains for which orographic effect on seasonal climatology is characterized (Beniston, 2003).

Our simulations showed that the precipitation distributed across the basin was higher for the average and maximum and lower for the minimum of all SRES types compared to the baseline simulation (Figure 10a). These precipitation differences corresponded with similar differences in the stream discharge in the same scenarios, respectively (Figure 10b). The range of mean annual stream discharge changes were from -21.90 % in the minimum of A2 scenario to +39.42 % in the maximum of A2 scenario corresponding with relative changes of precipitation from -18.22 % to +36.92 % in the same scenarios respectively.

Model simulations indicated that both snowfall and snowmelt decreased for all climate change scenarios (Figure 10c & 10d). Snowfall decreased by an average of 10.12 % in the minimum of B1 scenario and 30.43 % in the maximum of A2 scenario which might affect the volume of glaciers at higher peaks of the mountain regions. Similar snowmelt changes of -9.26 % and -29.33 % was estimated in the same scenarios, respectively. The Himalaya Mountains are the repositories of fresh water resources in the form of permanent ice and snow sustaining the 10 largest rivers in Asia. However, the substantial decrease in snowfall and glacier mass coupled with continued climate change can have

long-term effects on stream discharge of the Himalayan headwaters that may reduce water availability mainly during dry seasons (Xu *et al*., 2009).

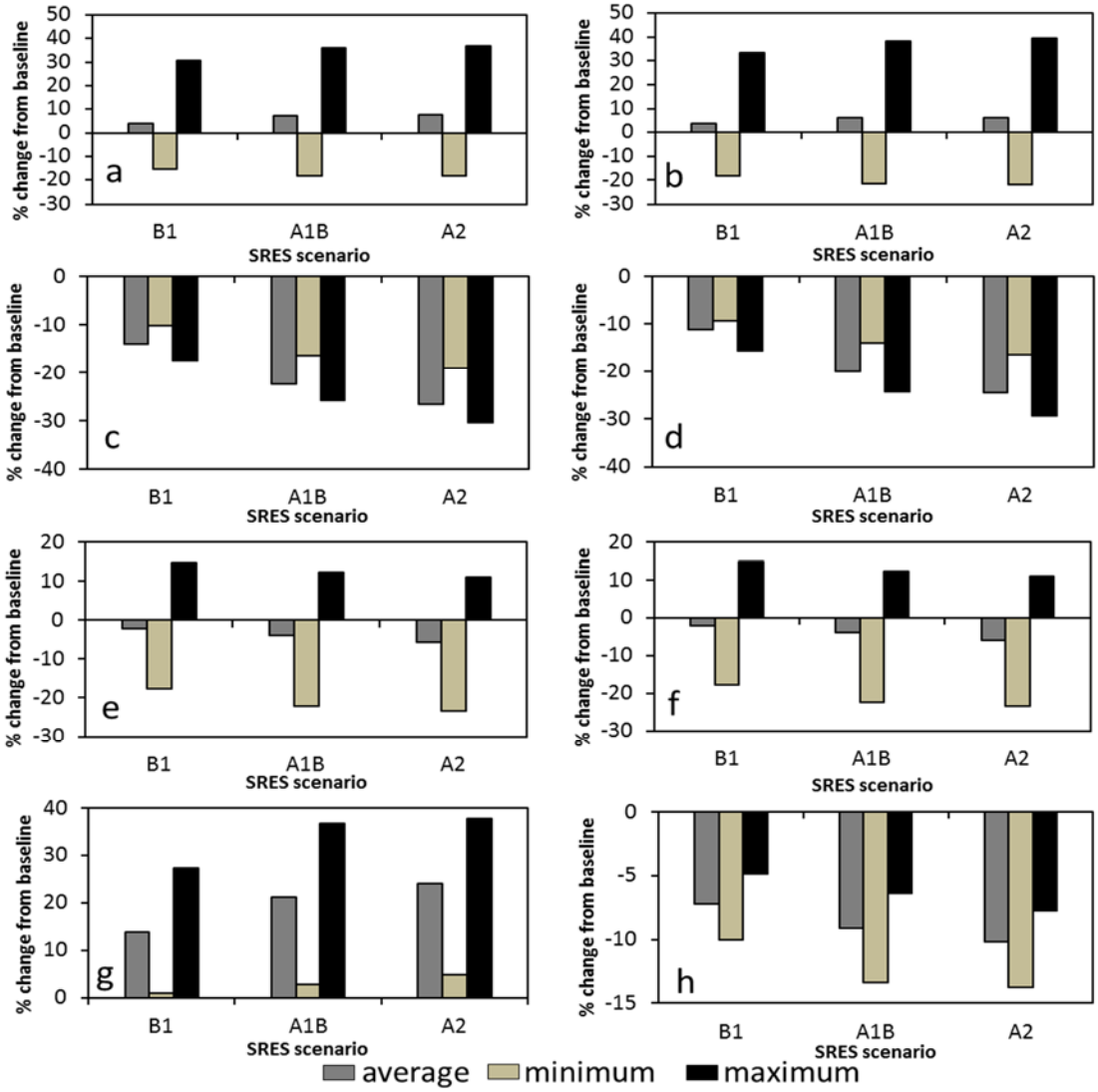

Figure 10. Mean annual changes of (a) precipitation, (b) stream discharge, (c) snowfall, (d) snowmelt, (e) water percolation, (f) groundwater contribution to stream discharge, (g) evapotranspiration, and (h) soil water content in the basin from the baseline in different GCM scenarios.

Water percolation controls the infiltration rate and groundwater recharge. Our modeled data (Figure 10e) showed that the range of soil water percolation changes was from -23 % in the minimum of A2 scenario to +15 % in the maximum of B1 scenario.

This process was likely higher in the maximum scenarios due to higher precipitation predicted under these scenarios. Estimated ranges of groundwater contribution to the stream discharge was from -23 % in the minimum of A2 scenario to +15 % in the maximum of B1 scenario (Figure 10f). On average, the projected groundwater contribution was found lower indicating a reduction in future sustainability of *in situ* mountain groundwater resources. These data confirm that the maximum soil water percolation and groundwater contribution to the stream discharge corresponded with the increased precipitation of 31% in the same scenario.

Due to warmer projected temperature, evapotranspiration (ET) rates were higher for all the scenarios (Figure 10g). The range of changes in ET was from +1% in the minimum of B1 scenario to +38% in the maximum of A2 scenario corresponding with similar temperature increase scenarios of the basin. Due to higher temperature and evapotranspiration, soil water availability in the basin was estimated to be lower in all the scenarios (Figure 10h). The range of changes in soil water was from -5% in the maximum of B1 scenario to -14% in the minimum of A2 scenario. These estimates might indicate reduced future soil water availability as a function of a future climate with higher PET which may lower agricultural production of the region (Thomas, 2000).

The ranges of projected seasonal stream discharge change in the basin were from -6.2 % to -5.3 % during pre-monsoon; +5.4 % to +8.7% during monsoon; and +1.7% to +3.9 % during post-monsoon seasons (Figure 11). These simulates indicated that most influence occurred during summer months. Maximum decrease of the stream discharge was predicted in A2 scenario during pre-monsoon season and maximum increase was estimated in the same scenario during monsoon season. This indicated for the A2

scenario, potential hydrological-related disasters (e.g. flood, landslide) that currently occur during the monsoon season in the basin would be enhanced by higher flows. Similar to the prominent impact of continued climate change on seasonal waters reported by Singh and Bengtsson (2004), our simulations also indicated seasonal influences to the stream discharge which might affect water availability for irrigation and hydropower generation downstream of the watershed.

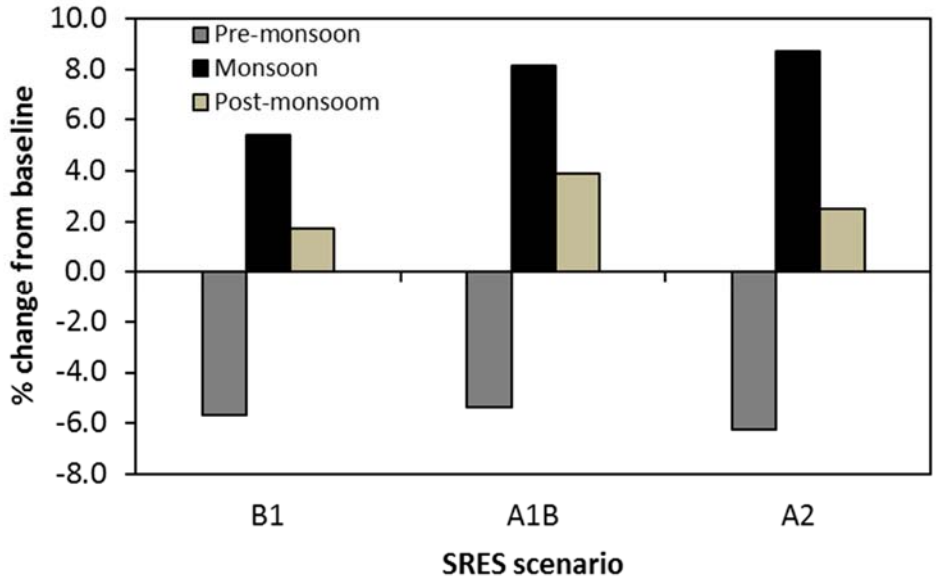

Figure 11. Potential seasonal stream discharge changes of KGW for different GCM scenarios (Pre-monsoon: March-May, Monsoon: June-September, and Post-monsoon: October-February).

CHAPTER THREE

A Snapshot Comparison of Environmental Tracers for Estimating Sub-surface Water Contribution to Recession Flow in a Mountain Stream

Introduction

Groundwater contribution to streams is important as management of limited water resources must account for all yield and potential storage sources that affect socioeconomic planning (FAO, 1998; Brodie et al., 2007). In mountainous watersheds, the amount of groundwater composition of streamflow is difficult to determine as complex geologic and geomorphic factors influence vertical and horizontal groundwater transmission. Groundwater contribution to streams has been traditionally estimated by analytical methods based on calibrated well and stream flow data (Winter et al., 1998). Environmental tracers such as isotopic composition of water ($\delta^{18}O$ and $\delta^{2}H$) and radon (^{222}Rn) have been used to assess sources, timing, and quantity of groundwater exfiltration into streams (Cook et al., 2003, 2006, 2012; Stellato et al., 2008; Unland et al., 2013). Estimation of groundwater addition to mountain headwater streams from hydrogeologic data (e.g., Winter, 2001), coupled with geochemical tracers, is potentially a powerful method for refining sources, flux, and transmission path analyses (e.g., Manning and Solomon, 2003; Smerdon et al., 2009; Kuras et al., 2008; Winter et al., 2008).

Field measurements such as water temperature, pH and electrical conductivity have been used to determine groundwater contribution to stream water (Cook et al., 2003; Rodgers et al., 2004; Song et al., 2006; Stellato et al., 2008; Rautio and Korkka-Niemi, 2011; Unland et al., 2013) as groundwater with different temperature is added to the

surface waters (Loheide II and Gorelick, 2006). The $\delta^{18}O$ and $\delta^{2}H$ values of water are also widely used to study exchange between ground and surface waters (McCarthy et al., 1992; Ojiambo et al., 2001). These isotope ratios can be ideal tracers since they comprise the water molecule and may provide insights on hydrological processes of a region (Gibson et al., 2005; Lambs et al., 2005; Song et al., 2006; Kattan, 2008). Similar to stable isotope technique, solute concentration of the water is also used to assess the interaction between ground and surface waters (Stellato et al., 2008; Yang et al., 2012) due to higher concentration of solutes in groundwater, such as Na^{+} and Cl^{-}, present as a function of dissolution (Genereux and Pringle, 1997; Cook et al., 2003; Genereux, 2004; Cartwright et al., 2011). Combined analysis of solute concentration with water temperature also have been used to distinguish ground and surface water sources as varying concentrations are affected by rock mineralogy and exposure time (Stellato et al., 2008).

^{222}Rn is an intermediate daughter product in the decay series of ^{238}U with a half-life of 3.8 days. Elevated ^{222}Rn concentration, referred to as activity, in streams is indicative of recent groundwater inputs (Cook et al., 2003, 2006, 2012; Mullinger et al., 2007; Burnett et al., 2010). Because ^{222}Rn concentration in groundwater is substantially higher than in stream water (Corbett et al., 1997), measured concentration differences in these two sources can be used to estimate the location and amount of groundwater contribution to a stream (Guida et al., 2013). Because streams may be both gaining and losing within a reach, incomplete representation of stream hydrology may complicate assessment of groundwater exfiltration (Covino and McGlynn, 2007). However, once the groundwater containing ^{222}Rn discharges to the stream water, there is a known and

consistent decrease of ^{222}Rn downstream due to degassing and radioactive decay that helps reduce uncertainty in sub-surface hydrologic connectivity (Mullinger et al., 2007; Cook, 2012; Knee and Jordan, 2013).

In addition to groundwater from basin deep-flow return, hyporheic water contributes to the total groundwater contribution to streams that is derived from the alluvial aquifer directly connected to the streams both vertically and laterally (Gooseff, 2010). Hyporheic water can significantly contribute to stream discharge though with low ^{222}Rn activity values due to the assumed shorter time of storage in the hyporheic zone (Cook et al., 2006; Lamontagne and Cook, 2007). Most previous studies have not considered the interpretation of environmental tracers data with regard to possible exchange between stream and hyporheic water associated with alluvial streambeds. However, recent studies have focused on inclusion of hyporheic exchange with stream water using ^{222}Rn mass balance equations (Cook et al., 2006; Lamontagne and Cook, 2007).

In this study, I show that in a mountain headwater system the geologic setting for which a stream flows through may vary the amount of groundwater contribution to the stream. To assess this I used multiple tracers ($\delta^{18}O$, $\delta^{2}H$, Ca^{++}, Na^{+}, Mg^{++}, SO_4^{--}, Cl^{-}, NO_3 and ^{222}Rn) all of which had the potential to indicate point-source addition of groundwater to a flowing mountain stream. Finally, by analyzing patters of tracer concentrations within the stream, I estimated groundwater proportion and derivation of the total water discharge during recession flow influenced by geomorphology in a headwater basin.

Materials and Methods

Description of the Study Site

I studied the McDonald Creek watershed located in Glacier National Park, USA, with an area of 441 km^2 and an elevation range of 940 to 2,837 m (Figure 12). Most of the watershed's landscape is dominated by evergreen forests (about 69%) intermingled with grassland (10%), bare rock (10%), water (7%), and permanent snow and ice (1%) (http://nris.mt.gov/). The upslope bedrock includes stratum dominated by Proterozoic limestone, argillite, sandstone, and dolomite while the valley bottoms are comprised of Quaternary glacial till interbedded with recent alluvium and colluvium deposits (Whipple, 1992). The watershed is a steep, glaciated valley with 37% of the total area having greater than a 45^o slope. The upper portion of McDonald Creek is composed of a dominant meandering channel with numerous small waterfalls before entering to Lake McDonald.

The McDonald Creek watershed's average annual precipitation is 91 cm with 52% as rain and 48% as snow (Finklin, 1986; White and Running, 1994). The minimum January temperature of the watershed is -11.2^{o}C and maximum temperature reaches up to -3^{o}C whereas the July temperatures are 8 and 26^{o}C, respectively. Analysis of 32 years (1980-2011) of precipitation (http://daymet.ornl.gov/) and 72 years (1940-2011) of stream discharge data (http://waterdata.usgs.gov/nwis) indicated that 24, 22, 26, and 28% of total precipitation contributed during spring (March-May), summer (June-August), Fall (September-November), and winter (December-February) seasons, respectively that corresponded to 39, 45, 9, and 7% of total stream discharge contribution in the same seasons, respectively (Figure 13) (Thornton et al., 2012). Maximum annual discharge

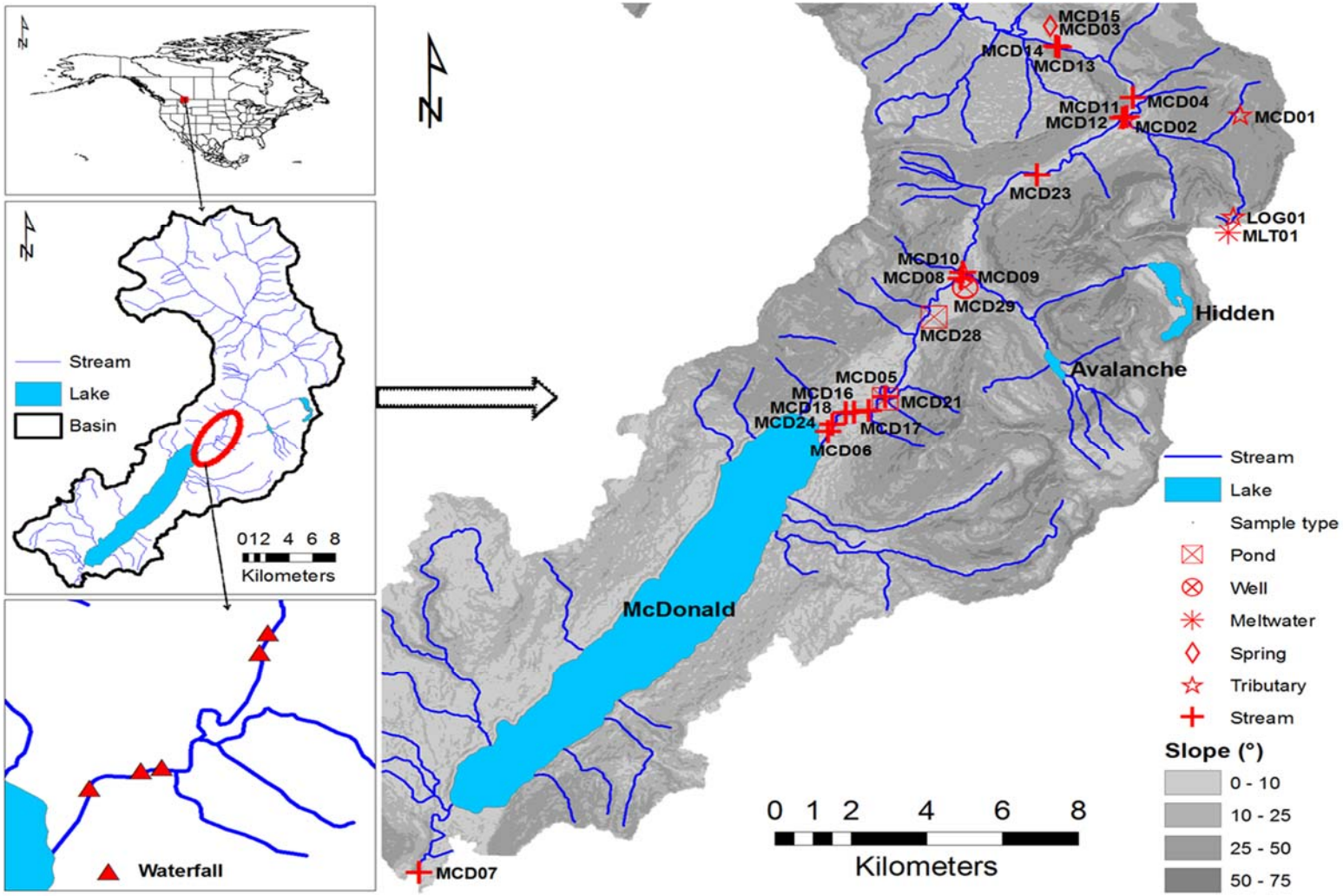

Figure 12. Map of the McDonald Creek watershed with the relative location within North America including dominant streams, lakes, waterfalls and water sampling locations. The topographic slope is shown using the gray scale.

contribution value was analyzed during summer months with minimum precipitation potentially due to higher summer temperatures and rain-on-snow events that increase snowmelt. However wettest months, minimum stream discharge was analyzed during winter season that might be due to less meltwater contribution caused by freezing air temperatures (White and Running, 1994).

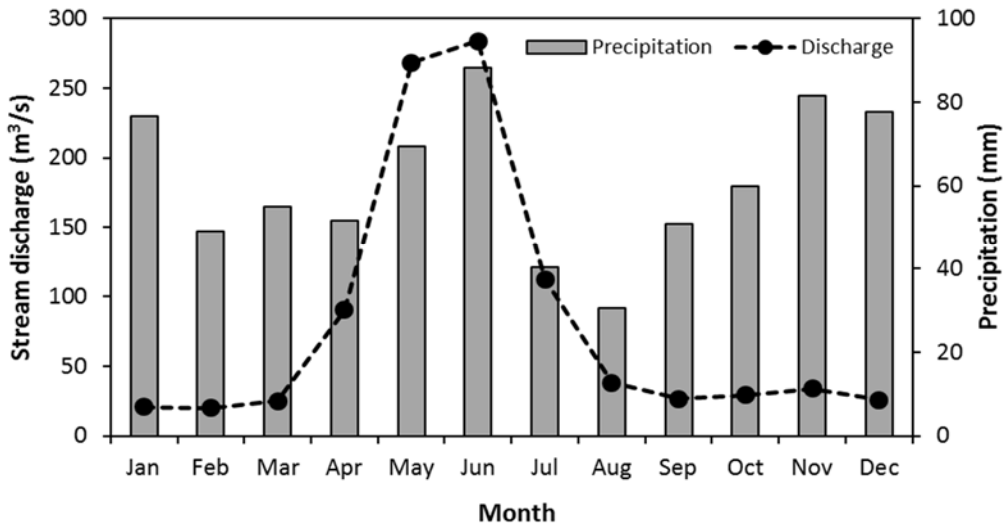

Figure 13. Hydrograph showing mean monthly precipitation, including snow and rain. Snow values are presented in water equivalent values of mm. The 32 years (1980-2011) of precipitation data are derived from West Glacier site (48.49° N, -114.01° E, elevation: 996 m) acquired online (http://daymet.ornl.gov) for tile #12453 and 72 years (1940-2011) stream discharge data have been taken from United States Geological Survey (USGS) gauging station #12358500 located at the confluence of McDonald Creek and Middle Fork of the Flathead River.

Water Sampling

Water samples were collected during August, 2013 with 31 samples collected from 25 locations within McDonald Creek watershed. The timing of this collection intentionally coincided with recession of stream discharge with assumed higher groundwater contribution to streamflow. Samples were taken from mountain divide to the

valley bottom. The focus of our sampling included the main stream channel that extended approximately 38 km from the upper most site referred to as MCD-14 to the outlet below Lake McDonald referred to as MCD-07 (Figure 12). Of the total samples collected, one water sample was taken from top of the mountain derived from fresh snowmelt (Meltwater), 21 from the main stream (SW), four from tributaries (TR), two from terrace-ponds (TP), one from a well (Well), and two from springs (Spring). The terrace ponds were assumed to have formed from past meander cutoffs of McDonald Creek with potential hydrological connection to the main stream channel through sub-surface alluvial material.

Field measurements included temperature (^{o}C), pH (HANNA 98127, Smithfield, RI) and electrical conductivity (EC) (μS/cm) (HANNA 9033, Smithfield, RI). Both the instruments were calibrated at the start of each day. Measurements were recorded from fresh water samples with values monitored *in situ* until the instrument showed no change in value over a minute of observation. At each stream location, width and depth of the channel were determined using a handheld laser, and water velocity estimated using the simple float method at the time of water sample collection.

Water samples that were later analyzed for isotope ratios ($\delta^{18}O$ and $\delta^{2}H$) and solute concentrations (Ca^{++}, Na^{+}, Mg^{++}, $SO4^{--}$, Cl^{-}, and $NO3^{-}$) were collected in 50 ml narrow necked glass bottles with Teflon lined caps and were returned to Baylor University for analysis. For ^{222}Rn measurements, water samples were collected by immersing empty 250 ml glass bottles 10 cm below the water surface to avoid exposure with air. Bottles were then sealed underwater using Teflon lined caps and insulated. All stream water samples were collected near the middle of the stream channel. The spring

samples were collected directly from discharge locations and the terrace-pond samples were taken 10 cm below the water surface in the approximate middle of each pond. A well water sample was collected after purging the well for five minutes. To assess potential diurnal variation in ^{222}Rn activity, additional water samples were collected at 9:40 am, 1:00 pm, and 6:00 pm during 6th of August, 2013 from MCD-12 and MCD-06 as sites representing the upper and lower ends of McDonald Creek above Lake McDonald, respectively.

Analytical Methods

Stable isotopes of oxygen and hydrogen were determined by the Stable Isotope Laboratory at Baylor University by continuous spectrometry (Finnigan GasBench II) using Delta V Advantage IRMS for isotopic measurements. Isotope ratios were reported as per mil (‰) (Equation 10) relative to Vienna Standard Mean Ocean Water (VSMOW) standard using the delta (δ) notation (Gonfiantini et al., 1995).

$$\delta(in\ ‰\ or\ per\ mil) = \left(\frac{R_x}{R_s} - 1\right) \times 1000 \qquad (10)$$

where R_x and R_s are the isotopic ratios of the sample and standard, respectively. Results were presented as parts per thousand deviation from the VSMOW standard with analytical precision of ±0.09‰ for oxygen and ±1.2‰ for hydrogen. The solute concentrations were measured using a Waters Quanta capillary electrophoresis instrument. The precision of our measurements was better than +/- 5% based on replicate analyses. The outputs of solute concentration measurements from each water sample were graphically represented in a distribution plot (not a Piper diagram since $NO3^-$ is used instead of $HCO3^-$).

For ^{222}Rn measurements, samples were analyzed within about 4 hours of collection to minimize the loss of radon due to radioactive decay. For each sample, the activity of dissolved ^{222}Rn was measured using the RAD7 (Durridge Inc. Billerica), equipped with a water probe and a RAD7H2O radon-in-water grab sample accessory. To reduce contamination of the samples from ambient radon, the RAD7 instrument was purged for a minimum of 30 minutes before each test. In addition, a blank sample composed of distilled water without radon was tested before each sample run.

^{222}Rn Mass Balance Calculations

For this study, I used a simple mass balance model (Equation 11) to calculate groundwater discharge for stream sections using ^{222}Rn, similar to those of Genereux and Hemond (1992), Cook et al. (2006), and Mullinger et al. (2007).

$$Q\frac{dC_r}{dx} = I(C_{gw} - C_r) + wEC_r + F_h - k_v HwC_r - \lambda HwC_r \qquad (11)$$

where Q is the stream discharge (m^3/day), C_r is the concentration of ^{222}Rn in the stream (Bq/m^3), x is the distance downstream (m), I is the groundwater inflow rate (m^3/m/day), C_{gw} is the groundwater radon concentration (Bq/m^3), w is the stream width (m), E is the evaporation rate (m/day), F_h is the flux of ^{222}Rn from the hyporheic zone (Bq/m/day), k_v is the degassing coefficient (day^{-1}), H is the stream depth (m), and λ is the radon decay constant (0.181/day). This model is assumed if concentration of ^{222}Rn in the atmosphere and suspended sediments of streams is negligible (Cook et al., 2006; Mullinger et al. 2007). Due to very limited samples from the study site, I considered the average ^{222}Rn value from the springs and well water samples as a representative groundwater ^{222}Rn activity for this study. Groundwater inflow rate (I) for stream segment was calculated by rearranging the Equation 11.

To assess potential ^{222}Rn loss from the McDonald Creek watershed stream water, I used a stagnant film model (Lewis and Whitman, 1924; Broecker and Peng 1982; Elsinger and Moore, 1983; Cook et al., 2003) that assumes the gas transfer through water-atmosphere boundary layers occur by molecular diffusion throughout the depth and therefore degassing rate constant (k_v) is defined as

$$k_v = \frac{D}{zH} \quad (12)$$

where D is the molecular diffusivity of ^{222}Rn (m^2/s) for the temperature of stream water and z is the thickness of boundary layer (m). The molecular diffusivity of ^{222}Rn depends mainly on water temperature (T in K) and was estimated by an empirical relation as in Equation 13 (Peng et al., 1974).

$$-\text{LogD} = \left(\frac{980}{T}\right) + 1.59 \quad (13)$$

For this study, I assumed cascading reaches of the stream to have minimal contribution of groundwater to the stream sections due to high stream flow velocities. Background ^{222}Rn activity (all expressed in Bq/m^3) of streambed sediment flux of the cascade sections was estimated using Equation 14 (Ellins et al., 1990) as follows.

$$C_b = C_a - C_p \quad (14)$$

where C_b is the background ^{222}Rn activity in stream water, C_a is the actual radon activity downstream and C_p is the predicted radon activity downstream. Assuming no groundwater contribution to the stream water, the decrease in ^{222}Rn activity downstream is caused by molecular diffusion to the atmosphere (Danckwerts, 1951). Therefore, any differences in observed and predicted values should be due to ^{222}Rn flux between stream water and the air.

The stagnant film model represents the water and atmosphere as well-mixed reservoirs with ^{222}Rn transfer occurring by molecular diffusion across a stagnant film of air located above the water surface. The ^{222}Rn flux density depends on the activity gradient and conductance of the stagnant boundary layer. The thicker the stagnant layer, the smaller the flux of ^{222}Rn from stream water to the atmosphere. The stagnant film thickness was predicted based on Equation 15 (Wu et al., 2004).

$$z = \frac{LD}{Hv\ Ln(\frac{C_u}{C_d})} \quad (15)$$

where z is the thickness of the stagnant layer between stream water and atmosphere (m), L is the distance between sampling stations (m), v is the velocity of stream water (m/s), C_u and C_d are the activity values of ^{222}Rn (Bq/m^3) at upstream and downstream measurement sites, respectively. The derived value of z was then used to estimate ^{222}Rn activity at points downstream based on reference value of C_u where turbulent stream water losses of ^{222}Rn were accounted for using the Equation 16.

$$C_d = C_u . e^{-LD/ZHv} \quad (16)$$

The ^{222}Rn mass balance is hard to constrain for the hyporheic zone exchange. Some studies have not considered the ^{222}Rn production in the hyporheic zone but it can be of significance in streams with low groundwater inflows (Cook et al., 2006; Lamontagne and Cook, 2007) or where groundwater ^{222}Rn concentration is generally low (Cook et al., 2006). ^{222}Rn fluxes in stream reaches that have no groundwater contribution must derive from the hyporheic zone if the contribution from suspended matter is negligible. Re-arranging Equation 11 and assuming that the terms I and dC_r/dx are 0, flux from the hyporheic zone can be estimated from Equation 17.

$$F_h = k_v H w C_r + \lambda H w C_r - w E C_r \quad (17)$$

Due to potential hydrological connection of terrace-ponds to the stream channel through sub-surface alluvial materials, the average ^{222}Rn activity value analyzed from these pond samples was considered as the representative hyporheic sample for our calculations. Stream water infiltrating into the hyporheic zone will increase in ^{222}Rn concentration until equilibrium is reached, however depending on the residence time, concentration may vary. As concentration of ^{222}Rn in the hyporheic zone is generally unknown, it is commonly assumed that minimum concentrations measured in stream water reflect potential additions from F_h (Cook et al., 2006; Cartwright et al., 2011). However, increase in stream ^{222}Rn concentration due to evaporation and hyporheic exchange is much smaller than groundwater flux (Ellins et al., 1990).

Results

Temperature, pH and Electrical Conductivity

Overall water temperatures were lower with increasing distance downstream in the watershed (Figure 14). The temperature of main stream water samples varied widely from 9.8 to 21.9ºC with an average of 15.2ºC (Table 7). Average water temperature of the tributaries (11.4ºC), and springs (9.0ºC) were lower than the average stream temperature. The average temperature values of terrace-pond and well water samples were 15.5 and 15.4ºC, respectively, similar to the stream water temperature. Diurnal stream water temperatures differed between two measured locations (MCD-12 and MCD-06; Table 8). Maximum temperature of 16.7ºC was measured for MCD-12 at 6:00 pm compared to 18.9ºC for MCD-06 at 1:00 pm during sampling period. Both sites had minimum water temperature values of 9.8 and 11.7ºC, respectively at 9:40 am. The pH

value of the water samples increased downstream in the watershed (Figure 14). For stream samples, the pH value ranged from 8.2 to 8.7 with an average of 8.3. The average pH of the water from spring, terrace-pond and well samples had slightly lower values of 8.0, 7.9, and 8.2, respectively. The EC values of the stream water decreased downstream that ranged between 101 and 121 µS/cm, with an average of 108 µS/cm. The average EC values from tributaries and terrace-ponds were 85 and 66 µS/cm, respectively. However, the maximum EC value, 145 µS/cm, was measured from the spring samples.

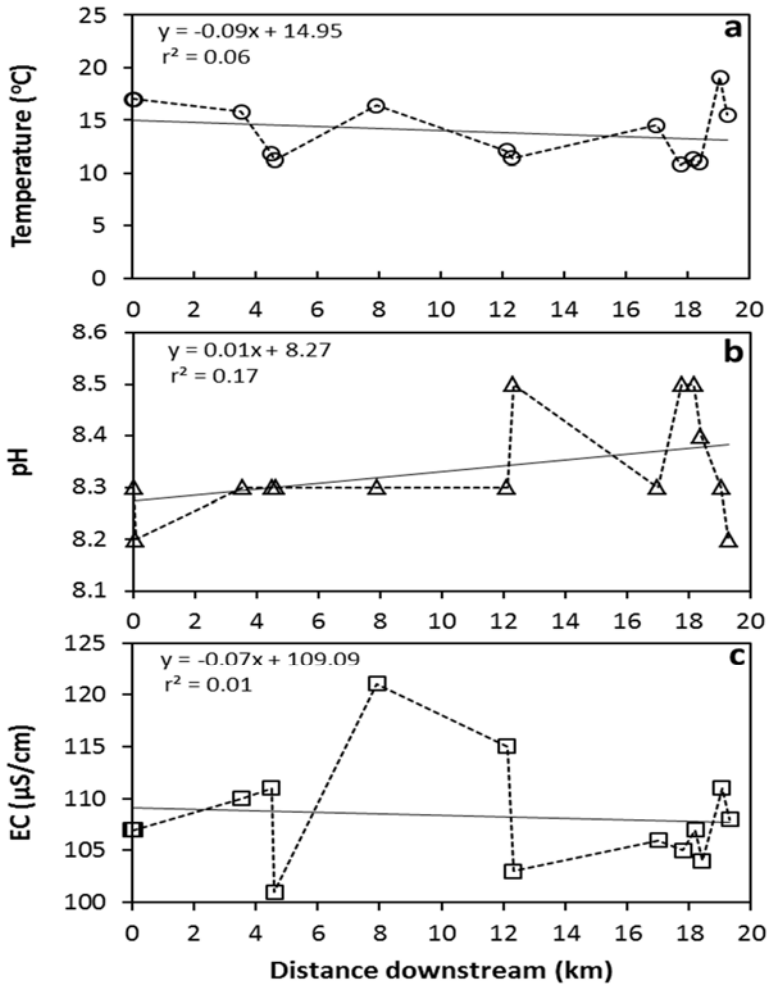

Figure 14. Water sample temperature, pH, and electrical conductivity values collected from main channel of the McDonald Creek watershed are shown with distance where (a) Temperature (°C), (b) pH, and (c) Electrical conductivity (µS/cm).

Table 7. Mean measurements of temperature (ºC), pH, electrical conductivity (µs/cm), $\delta^{18}O_{water}$ (‰), $\delta^{2}H_{water}$ (‰), Ca^{++} (mg/L), Na^{+} (mg/L), Mg^{++} (mg/L), SO_4^{--}(mg/L), Cl^{-} (mg/L), NO_3^{-} (mg/L) and ^{222}Rn (Bq/m^3) of the main stream, tributary, meltwater, spring, terrace-pond, and well water samples.

Sample	Type	Date	Temp (ºC)	pH	EC (µs/cm)	^{222}Rn (Bq/m^3)	$\delta^{18}O_{water}$ (‰)	$\delta^{2}H_{water}$ (‰)	Ca (mg/L)	Na (mg/L)	Mg (mg/L)	Cl (mg/L)	SO_4 (mg/L)	NO_3 (mg/L)
MLT01	Melt	08/04/13	-	-	-	116	-17.42	-125.90	4.65	1.11	0.90	0.09	0.12	0.15
LOG01	TR	08/04/13	11.5	8.6	30	0	-17.57	-126.10	5.32	4.24	0.50	0.28	0.31	0.24
MCD01	TR	08/04/13	10.5	8.4	146	0	-17.62	-132.65	29.85	3.66	4.42	0.18	1.48	0.21
MCD02	TR	08/04/13	12.0	8.3	86	0	-17.42	-127.78	10.38	4.09	2.15	0.05	1.56	0.29
MCD03	Spring	08/04/13	7.0	7.9	144	1,713	-17.59	-128.50	23.64	4.54	3.71	0.14	2.88	0.28
MCD04	RW	08/04/13	15.8	8.3	110	581	-17.46	-127.55	17.07	3.70	3.84	0.27	2.77	0.28
MCD05	RW	08/04/13	14.5	8.3	106	581	-17.34	-127.28	22.07	4.96	4.29	0.20	1.84	0.29
MCD06	RW	08/04/13	15.5	8.2	108	78	-17.40	-126.46	17.87	1.54	4.22	0.24	1.91	0.31
MCD07	RW	08/04/13	21.9	8.7	103	194	-16.92	-125.93	12.82	3.13	2.89	0.29	1.61	0.44
MCD08	RW	08/05/13	11.4	8.5	103	659	-17.38	-126.75	20.69	1.35	4.03	0.10	1.86	0.34
MCD09	TR	08/05/13	11.6	8.3	78	0	-17.39	-128.35	11.13	4.19	2.56	0.05	1.07	0.17
MCD10	RW	08/05/13	12.1	8.3	115	659	-17.33	-126.80	20.13	1.96	4.39	0.09	2.18	0.46
MCD11	RW	08/05/13	11.8	8.3	111	1,243	-17.48	-126.54	22.45	1.45	4.59	0.11	2.54	0.22
MCD12	RW	08/05/13	11.2	8.3	101	2,220	-17.42	-125.89	18.74	4.38	3.88	0.09	1.96	0.52
MCD13	RW	08/05/13	17.0	8.2	107	233	-17.52	-127.50	16.68	2.65	3.69	0.11	2.75	0.17
MCD14	RW	08/05/13	17.0	8.3	107	194	-17.46	-126.05	18.82	1.39	3.89	0.07	2.57	0.15
MCD15	Spring	08/05/13	10.9	8.1	146	2,919	-17.62	-126.34	50.78	12.38	5.64	0.06	2.76	0.38
MCD16	RW	08/06/13	11.3	8.5	107	117	-17.35	-125.30	21.17	1.45	4.37	0.21	2.23	0.44
MCD17	RW	08/06/13	10.8	8.5	105	544	-17.33	-127.04	17.76	4.31	3.86	0.10	1.81	0.63
MCD18	RW	08/06/13	11.0	8.4	104	194	-17.32	-125.35	17.56	4.98	3.86	0.10	1.81	0.38
MCD21	TP	08/06/13	17.1	8.0	45	8,584	-16.94	-123.54	10.31	5.25	1.24	0.30	2.11	0.25
MCD23	RW	08/06/13	16.4	8.3	121	2,646	-17.50	-125.94	18.43	4.28	4.17	0.39	2.44	0.28
MCD24	RW	08/06/13	19.1	8.3	111	194	-17.37	-124.35	19.46	2.46	4.39	0.10	1.88	0.35
MCD28	TP	08/07/13	13.8	7.7	87	9,620	-16.46	-120.70	11.41	5.74	4.51	0.14	1.70	0.59
MCD29	Well	08/07/13	15.4	8.2	104	17,427	-17.55	-126.10	15.85	4.15	3.66	0.85	1.03	0.42

Table 8. Diurnal variation in measured parameters of the water samples collected from MCD-12 and MCD-06 sites (Figure 12) in the McDonald Creek watershed.

Description	**MCD-12**			**MCD-06**		
	9:40 am	1:00 pm	6:00 pm	9:40 am	1:00 pm	6:00 pm
Temperature (^{o}C)	9.8	15.4	16.7	11.7	18.9	16.4
pH	8.4	8.2	8.4	8.3	8.4	8.4
EC (µs/cm)	107	104	110	106	109	109
^{222}Rn (Bq/m^{3})	2,257	1,284	1,088	39	155	155

Stable Isotope Composition of Water

The $\delta^{18}O$ (VSMOW) values for all the water samples ranged from -17.6 to -16.5‰ and the $\delta^{2}H$ values ranged between -133 and -121‰ (Table 7). For stream water, $\delta^{18}O$ and $\delta^{2}H$ values ranged from -17.5 to -16.9‰ and -128 to -124‰, respectively. The spring water had average values of -17.6‰ and -127‰ for $\delta^{18}O$ and $\delta^{2}H$, respectively compared to -17.5‰ and -129‰ for tributary water samples, respectively. The well water sample had similar values of -17.6‰ and -126‰ for $\delta^{18}O$ and $\delta^{2}H$, respectively. Comparison of stable isotope ratios of water samples with the local meteoric water line (LMWL) is shown in Figure 15. Most water samples had $\delta^{18}O$ and $\delta^{2}H$ values located slightly above the LMWL. A notable outlier was the stream water sample taken from outlet of the Lake McDonald (MCD-07) which when plotted on the LMWL, was clearly separate from the other samples. The water sample from a tributary (MCD-01) had $\delta^{18}O$ and $\delta^{2}H$ values that was plotted on the LMWL. Most of the water samples grouped toward lower end of the LMWL indicating cool conditions associated with the water source. The terrace-pond samples had the values that were positioned above and right of the LMWL. The $\delta^{18}O$ and $\delta^{2}H$ values of the water samples from main stream channel of the watershed presented in Figure 16 showed increasing delta values with distance downstream. Minimum $\delta^{18}O$ value of -17.5‰ was measured from the sample at 0.1 km and minimum $\delta^{2}H$ value of -

128‰ at 3.5 km distance downstream of the main channel. Maximum stream $\delta^{18}O$ and $\delta^{2}H$ values of -17.3 and -124‰ were measured at 18.4 and 19.1 km distances downstream, respectively.

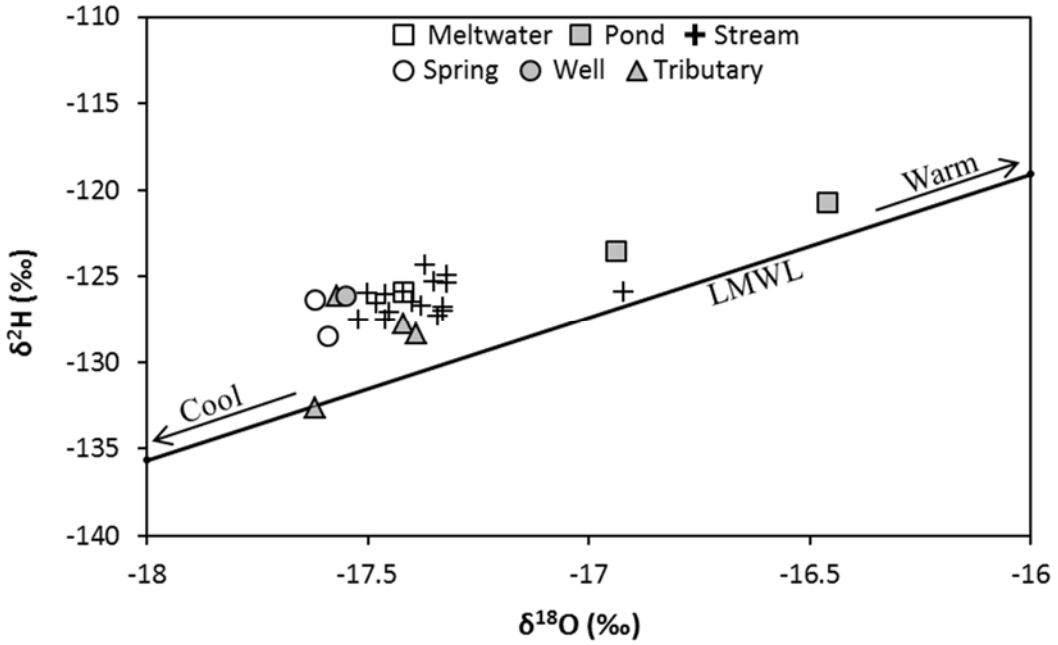

Figure 15. Values of $\delta^{18}O$ versus $\delta^{2}H$ activity for water samples taken from the McDonald Creek watershed [local meteoric water line; slope - 8.3, intercept - 13.7 and r^2 - 0.98 from 501 data points, Kendall and Coplen (2001)].

Solute Chemistry

Our analysis showed a relatively higher concentration of cations than anions in the water samples (Table 7). The dominant cation was Ca^{++} with smaller amounts of Na^{+} and Mg^{++} (Figure 17). The Ca^{++} measured in main stream water samples ranged from 12.8 to 22.5 mg/L with an average of 18.5 mg/L compared to 4.7 mg/L measured from meltwater. The average Ca^{++} concentrations were 14.2, 10.9, and 15.9 mg/L for tributary, terrace-pond, and well water samples, respectively. Maximum Ca^{++} concentration was measured in the spring water sample with an average of 37.2 mg/L. The range of Na^{+}

concentration for main stream water samples was from 1.4 to 5.0 mg/L with an average of 3.1 mg/L. The average Na^{+} values were 4.1, 5.5, and 4.2 mg/L for tributary, terrace-pond, and well water samples, respectively, with maximum value of 8.5 mg/L measured from the spring sample and minimum value of 1.1 mg/L measured from the meltwater sample. Similarly, the Mg^{++} concentration for main stream water samples ranged from 2.9 to 4.6 mg/L with an average of 4.0 mg/l compared to 0.9 mg/L from the meltwater sample. The tributary, terrace-pond and well water samples had average Mg^{++} values of 2.4, 2.9 and 3.7 mg/L, respectively, with maximum concentration value of 4.7 mg/L in the spring water sample. The SO_4^{--}concentration for stream water ranged from 1.6 to 2.8 mg/L with an average of 2.1 mg/L. The average SO_4^{--}concentrations for tributary, terrace-pond and well water samples were 1.1, 1.9 and 1.0 mg/L, respectively, with maximum and minimum values of 2.8 and 0.1 mg/L for spring and meltwater samples, respectively. The Cl^{-} measured in main stream water samples ranged from 0.1 to 0.4 mg/L with an average of 0.2 mg/L compared to 0.1 mg/L measured from the meltwater sample. The average Cl^{-} concentration values were 0.1, 0.2 and 0.9 mg/L for tributary, terrace-pond and well water samples, respectively, with the smaller value of 0.1 mg/L for spring water sample. Measured NO_3^{-} concentration for main stream water samples had a range between 0.2 and 0.6 mg/L with an average of 0.4 mg/L compared to 0.2 mg/L from meltwater sample. The tributary, terrace-pond and well water samples had average NO_3^{-} values of 0.2, 0.4 and 0.4 mg/L, respectively. The spring sample had an average of 0.3 mg/L. Solute concentrations (except SO_4^{--}) in water samples were slightly higher downstream of the main channel (Figure 18).

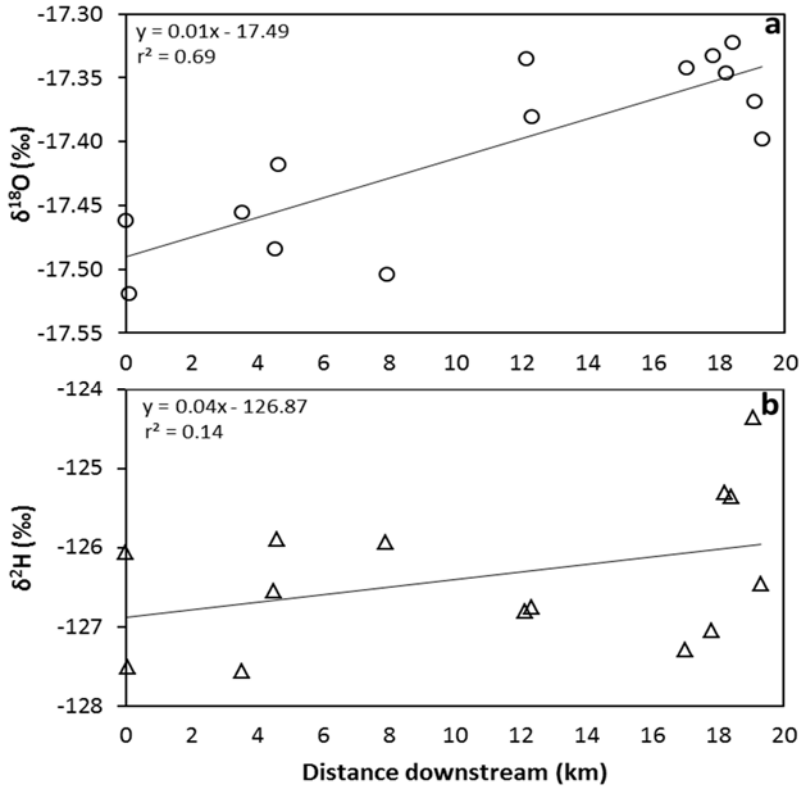

Figure 16. Isotopic composition of the water samples collected from main channel of the McDonald Creek watershed on August of 2013: (a) $\delta^{18}O$ and (b) $\delta^{2}H$.

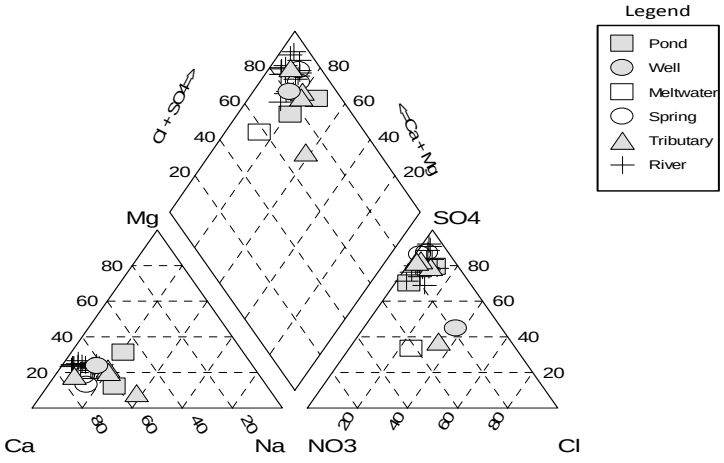

Figure 17. Distribution plot of solute compositions of meltwater, terrace-pond, main stream, tributary, spring and well water samples in the McDonald Creek watershed.

b.

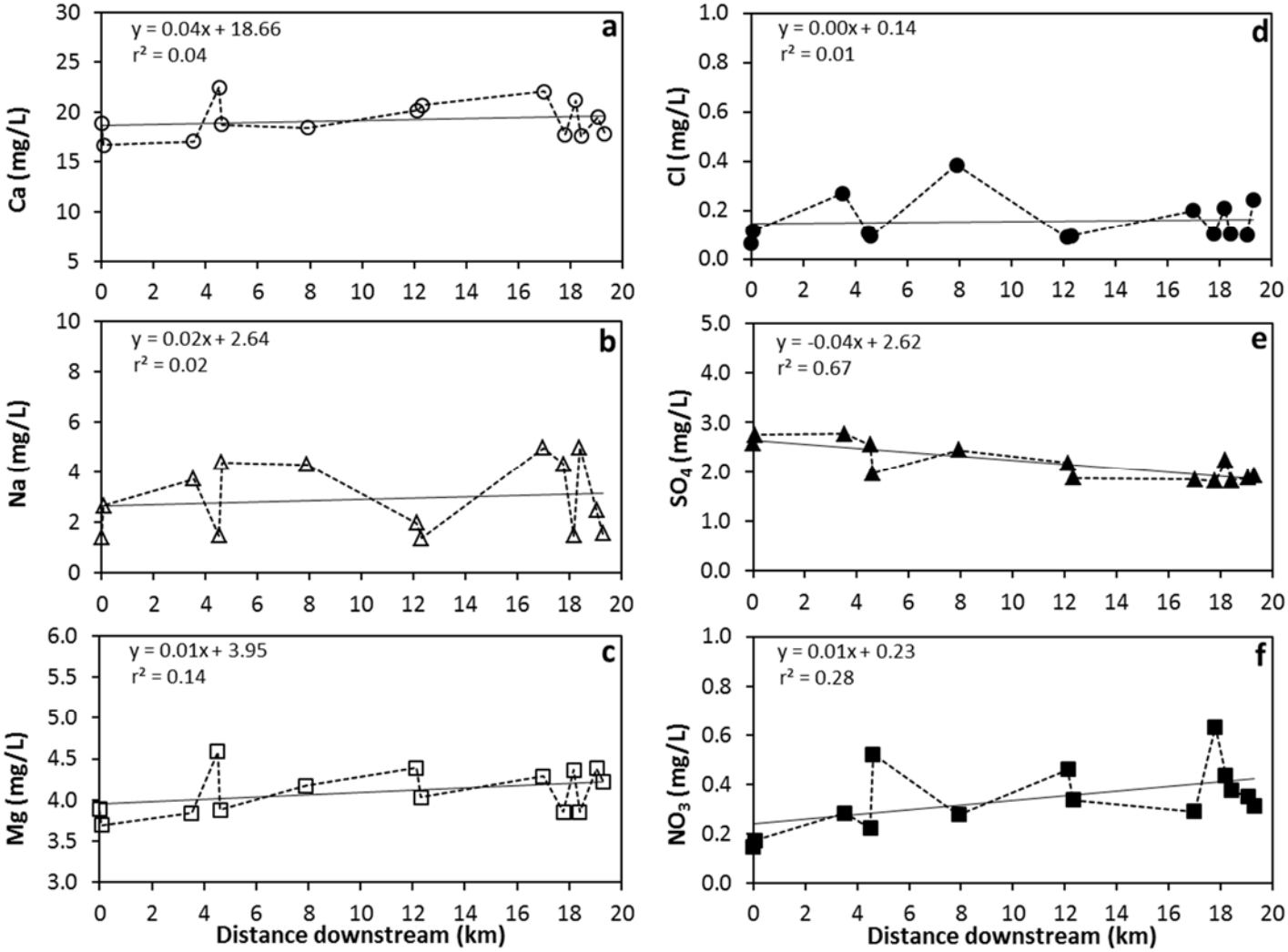

Figure 18. Analysis of solute concentrations measured for the water samples with distance downstream of main channel of the McDonald Creek: (a) Ca^{++}, (b) Na^{+}, (c) Mg^{++}, (d) Cl^{-}, (e) SO_4^{--}, and (f) NO_3^{-}.

^{222}Rn Activity

Water samples had variable ^{222}Rn activity values ranging from 39 to 17,427 Bq/m^3 (Tables 7 and 8). No ^{222}Rn activity was detected in the tributaries that were contributed directly from meltwater sources; however, a meltwater sample collected from top of the watershed (MLT01, Figure 12) had 116 Bq/m^3 of ^{222}Rn activity. In the main channel, ^{222}Rn activity of stream water samples ranged from 39 to 2,646 Bq/m^3, with an average of 729 Bq/m^3. The spring, terrace-pond and well water samples had higher average values of 2,316, 9,102 and 17,427 Bq/m^3, respectively. For water samples collected from the stream, ^{222}Rn activity was 194 Bq/m^3 at MCD-14, the uppermost point sample, to a peak value of 2,646 Bq/m^3 for MCD-23 located at 7.9 km downstream (Figure 19). The minimum ^{222}Rn activity value of 78 Bq/m^3 was measured for MCD-06 at 19.3 km distance downstream located at the inlet of Lake McDonald. Diurnal changes in ^{222}Rn activity measured from two observation sites (MCD-12 and MCD-06) showed opposite trends over time (Figure 20). For MCD-12, maximum ^{222}Rn activity value of 2,257 Bq/m^3 measured at about 9:40 am was reduced at 1:00 pm with a value 1,284 Bq/m^3 with the lowest value of 1,088 Bq/m^3 measured at 6:00 pm on 6th of August, 2013. Lower ^{222}Rn activity corresponded with higher water temperature. In contrast, for MCD-06, the ^{222}Rn activity increased in value from 39 to 155 Bq/m^3 with increase in temperature from 11.7 to 18.9^{o}C at 9:40 am and 1:00 pm, respectively. But, ^{222}Rn activity value remained same at 6:00 pm with a lower temperature value of 16.4^{o}C.

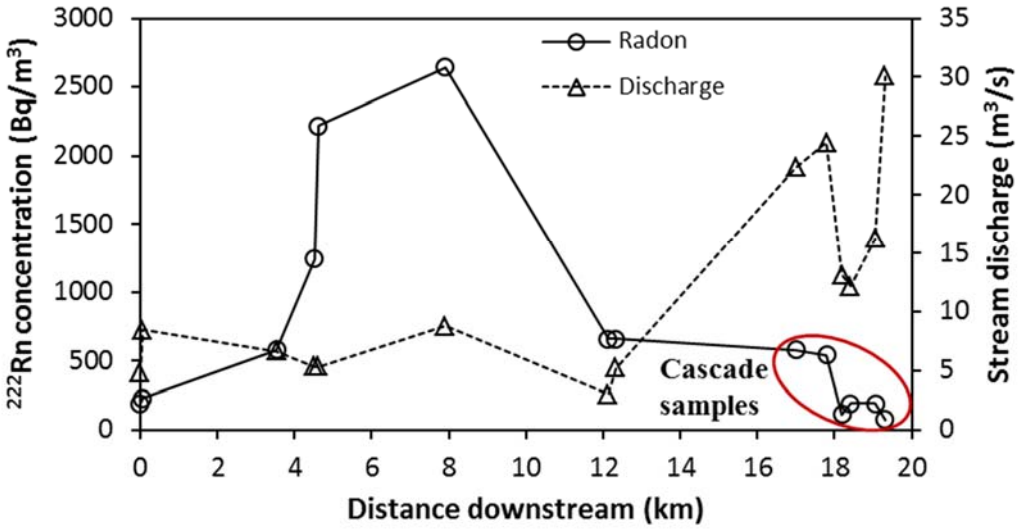

Figure 19. Radon activity (Bq/m^3) measured from stream water samples with estimated discharge values at increasing distance along main channel of the watershed. The upper sampling site, MCD-14 is used as the reference for distance with the total length of the channel beyond this point estimated to be 14 km to the top of the watershed.

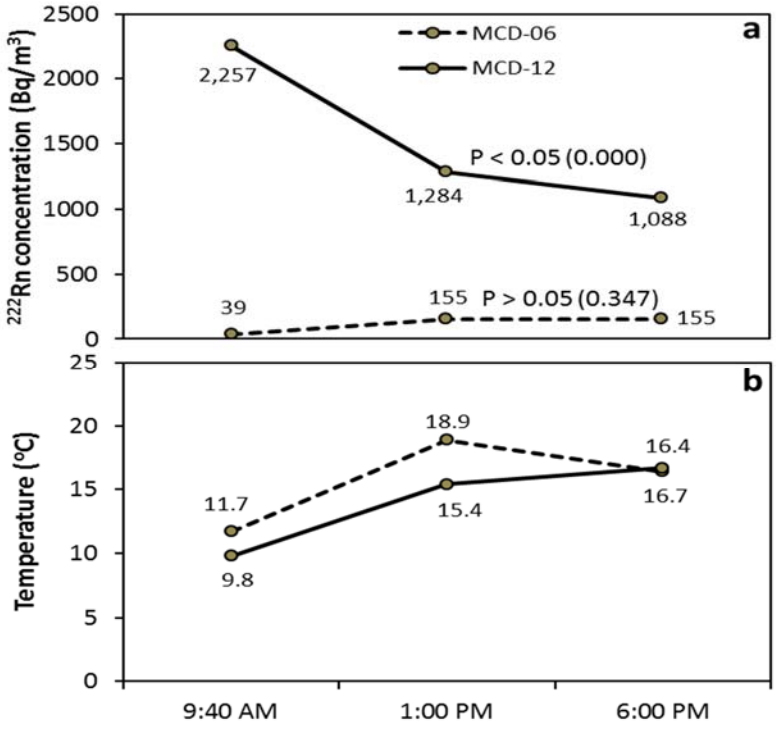

Figure 20. Diurnal changes of ^{222}Rn activities at two locations (MCD-12 and MCD-06) of the McDonald Creek watershed sampled on 6th of August 2013: (a) ^{222}Rn activity and (b) temperature.

^{222}Rn Mass Balance and Groundwater Fluxes

Predicted boundary layer thickness, ^{222}Rn molecular diffusivity, and loss of ^{222}Rn activity due to diffusion are presented in Table 9. Estimated thickness values of water-air boundary layers using the input data from MCD-08, MCD-05, MCD-17 and MCD-16 were 7.2×10^{-5}, 1.2×10^{-5} and 2.5×10^{-7} m, respectively. Modeled ^{222}Rn molecular diffusivity values for each of these locations were 9.2×10^{-10}, 1.0×10^{-9}, 9.1×10^{-10} and 9.2×10^{-10} m^2/s, respectively. Molecular diffusion of ^{222}Rn was found to be associated with ^{222}Rn decrease in cascade system of the stream channel. I estimated a change in ^{222}Rn activity from each location of the cascade region, with -37 Bq/m^3 between MCD-05 and MCD-17 along 790 m distance. Maximum change of -427 Bq/m^3 was modeled between MCD-17 and MCD-16 over the distance of 400 m. Similarly, the values of degassing coefficient (k_v) for main stream sections using Equation 12 ranged between 0.002 and 521 day^{-1}, with an average of 129 day^{-1}.

Table 9. Predicted loss of ^{222}Rn activities in cascade region of the watershed due to diffusion and stream sediment flux. The values were estimated based on thickness of boundary layer, ^{222}Rn molecular diffusion and channel characteristics.

Channel characteristics & ^{222}Rn modeling outputs	**Sampling sites**			
	MCD-08	MCD-05	MCD-17	MCD-16
Length (m)	0	4680	790	400
Width (m)	35	23	32	12
Average depth (m)	0.49	0.61	0.37	0.61
Flow velocity (m/s)	0.30	1.60	2.12	1.79
Discharge (m^3/s)	5.26	22.35	24.48	13.15
Thickness of boundary layer (m)	-	7.2×10^{-5}	1.2×10^{-5}	2.5×10^{-7}
^{222}Rn molecular diffusivity (m^2/s)	9.2×10^{-10}	1.0×10^{-9}	9.1×10^{-10}	9.2×10^{-10}
Loss of ^{222}Rn activity due to diffusion (Bq/m^3)	-	77.7	37.0	427.4
Loss of background ^{222}Rn activity (Bq/m^3)	-	0	0	0

Groundwater fluxes at different stream sections were calculated using Equation 11. From 14 sampling sections of the main channel, three sections (MCD-04, MCD-10 and MCD-16) at 3.5, 12.1 and 18.2 km distances, respectively downstream were calculated as losing sections. Total groundwater flux between MCD-14 and MCD-06 (19.3 km) of the main stream stretch ranged between 3,084 and 2,20,122 m^3/day, with an average of 70,710 m^3/day during August (Figure 21) that reflected between 0.3 and 29% of total stream discharge during same period of time. Maximum groundwater flux was estimated at MCD-23, between 4.6 and 7.9 km, and minimum flux was calculated at MCD-18, between 17.8 and 18.4 km of the stream stretch.

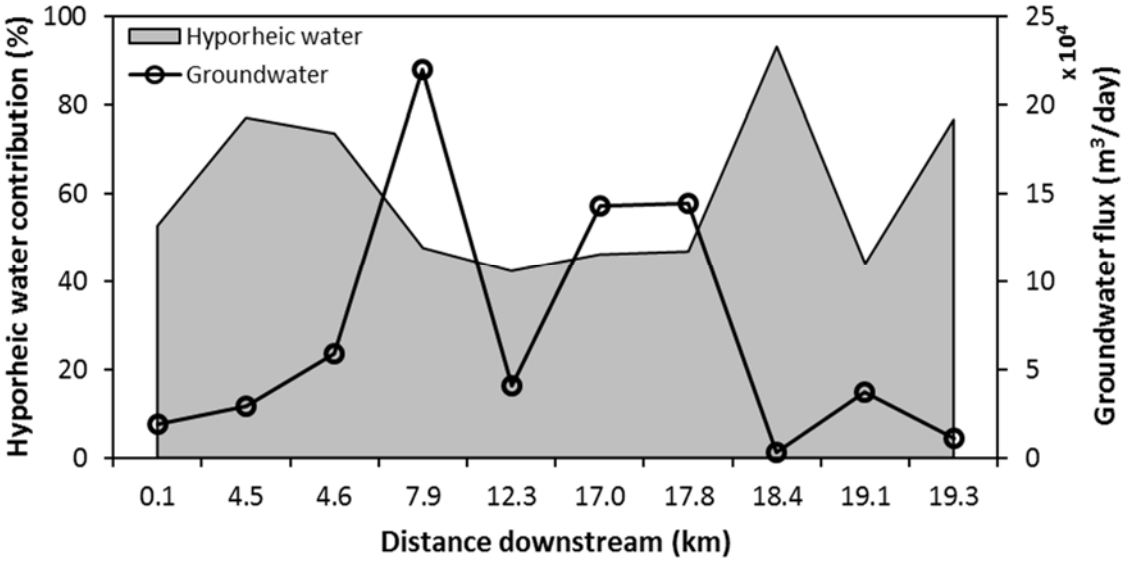

Figure 21. Groundwater flux (m^3/day) estimates including the percentage contribution from hyporheic zone for sampled sections of the McDonald Creek obtained from ^{222}Rn mass balance calculations.

Hyporheic ^{222}Rn flux for each stream section of the McDonald Creek was calculated using Equation 17. Due to cool average water temperature of the stream samples (13.9^{o}C), I ignored the evaporation loss of ^{222}Rn for our calculations. Therefore,

I estimated the range of hyporheic contribution between 40 and 90% of the total groundwater inputs, with an average of 60% for 19.3 km stream stretch of the McDonald Creek (Figure 21). The maximum hyporheic contribution was calculated at 18.4 km and the minimum contribution was estimated at 12.3 km distances downstream of the watershed. However, the rate of exchange may vary according to season and sampling locations as a function of groundwater input and topographic slope of the location.

Discussion

Based on the ^{222}Rn data, I constructed a conceptual, hydro-geomorphological model representing the dominant features that potentially influencing groundwater interaction with streamflow in the upper McDonald Creek watershed (Figure 22). This model represents the recession flow period of the creek based on the time-constrained sampling conducted for this study. The upper section of the creek contains steep slopes with thin soils that intensifies surface runoff and soil erosion with less groundwater recharge due to low soil infiltration (Liu et al., 2000). Physical constriction of the McDonald Creek was found to be associated with anomalously high values of EC and ^{222}Rn activity (Figure 22A). This constriction was also associated with strike and dip of basement rocks oriented upstream potentially providing a direct, and a unique groundwater point of exfiltration. Several small tributary inputs originating from top of the mountains deliver meltwater directly to the main stream confirmed by our finding of little or no ^{222}Rn activity and diluted solute concentrations (Figure 22B). Constriction of the stream was followed by widening of the channel that included subsequent vertical drops featuring cascades corresponding to lower ^{222}Rn activity values (Figure 22C). This observation was the impetus for modeling ^{222}Rn degassing. The terrace-ponds (Figure

22D) were considered to be highly influenced by groundwater as meander cutoffs with higher than average ^{222}Rn activity of 9,102 Bq/m^3. Finally, near the inlet into Lake McDonald, seepage was observed during sampling from the joints of exposed limestone rocks forming the eastern stream bank with strike and dip orientation of these rocks directly into the stream (Figure 22E). This corresponded to elevated ^{222}Rn activity measured at this location.

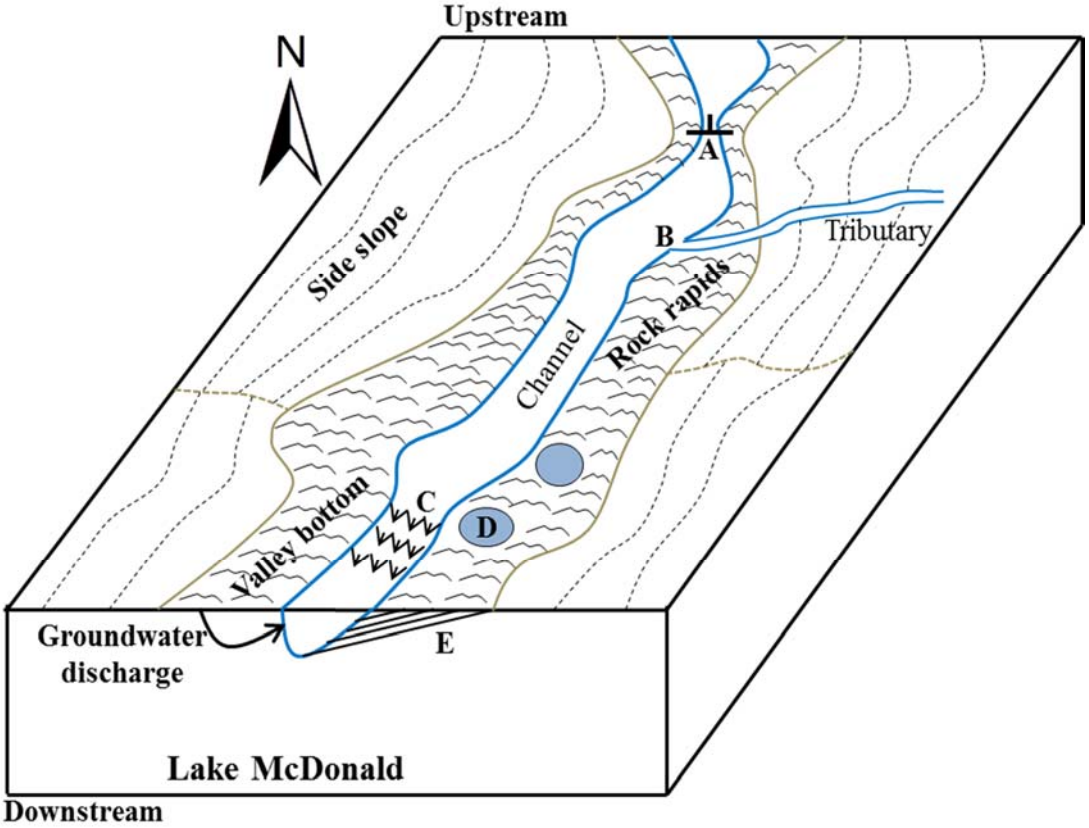

Figure 22. A conceptual representation of the upper McDonald Creek watershed with unique hydro-geomorphological features identified. The watershed is comprised steep slopes in headwater regions with a wide channel that becomes constricted coupled with upstream orientation of the strike and dip of basement rocks strata. A series of cascades are present near the inlet of Lake McDonald. (Note: A: Valley constriction with strike and dip of basement rocks strata with higher radon activities, B: Tributary input from snowmelt with no radon, C: Cascades cause loss of radon due to aeration, D: Terrace-pond with higher radon activity and E: Bedrock dip controls local seepage and increases radon).

No groundwater addition could be detected from temperature and pH data collected. The average EC values measured in tributaries was lower than the average of main stream water samples likely due to direct and rapid runoff from melting snow at the top of the mountain with low soil depth and solid bedrock (Hoy, 2012). The terrace-ponds had lower mean EC values of 66 μS/cm despite obvious groundwater contribution confirmed by high ^{222}Rn activities, potentially due to biological assimilation of humic substances enhancing the formation of neutral inorganic ion pairs in the calcium-rich water of the watershed (Cunha-Santino and Bianchini-Junior, 2004). The higher EC values measured in the spring samples is likely due to mineral dissolution within the aquifer formations with evaporite origin (Petelet-Giraud et al., 2007). Observed $\delta^{18}O$ and $\delta^{2}H$ values of water showed differential isotopic enrichment of input water sources that I attribute to early snowmelt and glacier meltwater based on data positioning relative to a regional LMWL (Kendall and McDonnell, 1998; Liu et al., 2008). Relatively lower solute concentrations were found in water samples collected from the McDonald Creek compared to other studies are likely due to dilution from meltwater that dominated stream flow at the time of sampling (Cook et al., 2003; Zhang et al., 2008; Yang et al., 2012). The dominance of Ca^{++}, Mg^{++} and SO_4^{--} reflects the general carbonate lithology of the watershed (Ross, 1959; Whipple, 1992). In overall, analysis of the solute concentrations including $\delta^{18}O$ and $\delta^{2}H$ values of the water samples were not found so informative to discern groundwater inflows compared to the ^{222}Rn mass balance estimate.

I observed large variation of ^{222}Rn activity in stream water with the range of 39-2,646 Bq/m^3 in the McDonald Creek watershed during August of 2013. This was substantially higher than the range of 110-390 Bq/m^3 measured from the Border Rivers in

Australia originated from rugged mountains (Baskaran et al., 2009) supporting the general conclusion of groundwater addition to McDonald Creek during the study period. Our finding of elevated ^{222}Rn activity at specific locations (Figure 19) indicated the potential of point-source inputs of groundwater discharge to the stream (Rogers, 1958). For example, the peak stream water value of 2,646 Bq/m^3 at 7.9 km (MCD-23/Figure 22A) coincident of maximum EC (121 μS/cm) and Cl^- (0.4 mg/L) supported this conclusion (Cook et al., 2003). Upstream of this site, I observed large alluvial deposits underlying the stream bottom replaced by solid rock and narrowing of the stream channel at the sampling point. Alluvial groundwater was likely forced out at the constriction providing a point injection of hyporheic water associated with the higher ^{222}Rn activity. In addition, the solid rock formation that formed this constriction is composed of the contact between Grinnell and Empire Formations with strike and dip of the contact of these units geologically oriented upstream potentially enhancing deep return flow groundwater addition to the stream with seepage transmitted through these layered sedimentary rocks, although as a countercurrent (Whipple, 1992). Previous studies using ^{222}Rn to assess groundwater contribution to streams have not generally considered geologic and geomorphic features as important features affecting localized exfiltration (e.g. Stellato et al., 2008; Guida et al., 2013; Knee and Jordan, 2013; Yu et al., 2013). Our study demonstrates why geology "matters" when considering surface-groundwater interactions where subsurface flow is severely confined.

Within the cascades located in the watershed (Figure 22C), I found potentially higher molecular diffusion of ^{222}Rn from the stream water supported by zero values found for background ^{222}Rn activity (Table 9). Maximum estimated loss of 427 Bq/m^3

between MCD-17 and MCD-16 along 400 m distance of the channel was likely enhanced by thinning of the boundary layer associated with shallow, fast-moving water of the cascades. The maximum loss rate calculated from these cascades was lower than 3,791 Bq/m^3 estimated by Wu et al. (2004) that was likely due to water for a longer distance (42 km) along the Heihe River, China. However, lower diffusion value of 370 Bq/m^3 was estimated by Hofmann (2011) along 25 km distance of a low gradient river in Australia. Lower ^{222}Rn molecular diffusivity values predicted for cascades of the McDonald Creek were a function of cooler water temperatures (Peng et al., 1974). I confirmed this in which I found that the diurnal change in ^{222}Rn activities at MCD-12 was significantly inversely proportional with water temperature ($P<0.05$) (Figure 20). Warmer water temperature elevates ^{222}Rn molecular diffusion decreasing the solubility of ^{222}Rn in water [(Peng et al., 1974; Clever, 1979 (c.f. Satomi and Kruger, 1982)]. In contrast, I found ^{222}Rn activity increased for MCD-06 with increase in temperature, though not significantly. This result was likely due to groundwater input from bank-side seepage into the stream (Figure 22E) observed during sample collection. Because sampling for this study was carried out only for 4 days (6 samples from single day for diurnal variation analysis), I note these results as being important factors to consider for both point sampling of ^{222}Rn activity. More sampling is required to assess the temperature effects on ^{222}Rn activity patterns and if they are temporally persistent. Sampling in different months throughout the year also necessitates for conclusive separation of seasonal influence in ^{222}Rn activities over the watershed. Because temperature may affect the calculation of ^{222}Rn diffusion, it also affects mass balance estimates of groundwater contribution at different times of day and year.

Assuming small temperature variation effect for the time period, my calculations showed that most sections of the McDonald Creek are gaining ($I>0$ $m^3/m/day$) except MCD-04, MCD-10 and MCD-16 at 3.5, 12.1 and 18.2 km distances downstream, respectively. For site MCD-23 where the peak stream ^{222}Rn activity value was measured (Figure 22A), the estimated groundwater discharge of 2,20,122 m^3/day corresponded with 29% of the total stream discharge during our sampling period. This high percentage again highlights on the potential for geomorphic features controlling groundwater exfiltration into surface waters. At 19.3 km distance below the cascade region of the watershed groundwater exfiltration was calculated to be 3,084 m^3/day, or 0.3% of the total stream discharge, based on the site ^{222}Rn activity value. The range of these estimates may reflect uncertainties attributed in estimating the degassing coefficient value (k_v), hyporheic flux estimates (F_h), and the variability of groundwater ^{222}Rn concentration (C_{gw}). Among these, C_{gw} shows the highest sensitivity to ^{222}Rn (Cartwright et al., 2011); therefore, more data are required for better representation of local groundwater ^{222}Rn concentration throughout the watershed. Similarly, hyporheic exchange also increases ^{222}Rn activities in stream water where ^{222}Rn concentration in groundwater is naturally low (Lamontagne and Cook, 2007; Cartwright et al., 2011; Cook, 2012). I estimated 60% of total groundwater inputs from hyporheic contribution indicating that the alluvial of the headwater basin is likely significant temporary storage reservoir for both deep-flow water from the basin in gaining portions of the stream as well as infiltrated stream water in losing portions of the stream. The surprising variability in exfiltration and hyporheic proportionality of groundwater for such a relatively small reach indicate complexity in interpreting basin-scale hydrologic budgets based on over-simplified conceptual flow

paths. I acknowledge the limitations of the data collected and the need for better data on hyporheic zone exchange rates to help constrain estimation of groundwater inputs for the McDonald Creek.

Integrated values from the mass balance model showed that 5.9% of the total stream discharge within the upper McDonald Creek was contributed by groundwater sources during August of 2013 and the remaining portion was derived from meltwater. This value was smaller than the 14% predicted from simulation of a monsoon dominated Himalaya Mountain system (Neupane et al., 2013). However, watershed point estimates ranged between 0.3 and 29.0%, demonstrating that groundwater contribution to stream flow may be variable based on channel's hydro-geomorphological features. For the McDonald Creek watershed, larger than expected proportion of streamflow was sustained by surface runoff, primarily from melting residual snowpack at high elevation in the watershed. These results suggest that low groundwater contribution coupled with less snowfall and earlier melting associated with continued climate change may potentially reduce baseflow in this mountain headwater system (Fagre et al., 1997; White et al., 1998).

CHAPTER FOUR

Predicting Monsoonal-driven Stream Discharge and Sediment Yield in Himalaya Mountain Basins with Changing Climate and Deforestation

Introduction

The accessibility of clean water, as an essential ecosystem service, is a crucial component for sustainable management of a watershed system (Mark and Dickinson, 2008). This has become more challenging due to changing climate and land-management practice, specifically in the Himalaya Mountains where elevation ranges from 60 m above mean sea level to more than 8,000 m within a north-south distance of about 197 km (Hannah et al., 2004). This extreme elevation range combined with potential climate and land use change affects stream discharge in this unique mountain headwater system (Ma et al., 2010). For example, monsoon precipitation accounts for 80% of total input to this mountain range (Sharma, 1993) that may increase the risk of hydrological-related disasters such as flood and landslide in steep meandering channels. This risk is further enhanced by exposed rocks without vegetation cover located at higher altitude that increases surface runoff and sediment yield (Summerfield and Hulton, 1994; Ludwig and Probst, 1998). These events reduce the water supply and hydro-electricity generation as transported sediment lowers storage capacity of downstream reservoirs (Monirul and Mirza, 2003).

The South-Asian monsoon precipitation initiates from south-eastern part of the Himalayan range and weakens towards north-western part so its contribution is substantial in eastern Himalayan region with glacier expansion during summer months

(Asahi and Watanabe, 2004; Bookhagen et al., 2005). In contrast, the western regions are predominantly influenced by westerly winds causing snowfall at higher elevation with glacier advance during winter months (Barros et al., 2006). These climatic differences result for higher snowmelt contribution (up to 50%) to the total annual stream discharge of far western Himalayan basins compared to eastern basins (~25%) (Bookhagen and Burbank, 2010). Therefore, these basins are likely to show different responses to continued climate change that potentially differentiate meltwater contribution to discharge of the rivers.

Land use, a major global research issue (Foley et al., 2005), also affects surface runoff, stream discharge, and sediment transportation due to change in rainfall interception, evapotranspiration, and surface soil hydraulic conductivity (He et al., 2008; Germer et al., 2009; Scheffler et al., 2011; Munoz-Villers and McDonnell, 2013; Yan et al., 2013). Managing seasonal flood and river water quality due to changes in evapotranspiration from different land-cover types has become a major challenge, though with little change in annual discharge value (Guo et al., 2008). In Nepal, high population growth has resulted in rapid land use change (Ives, 1987; Rai and Sharma 1998). Seasonal hydrologic changes directly influence crop production of high mountain regions (Kaltenborn et al., 2010). Land use change caused by natural and human-induced modifications also substantially influence downstream water availability and sediment supply to streams (Chalise and Khanal, 1997; Trimble, 1999; Van Rompaey et al., 2002). For example, in the Nepalese Himalaya Mountains higher soil erosion in Siwalik Hills has increased deposition of sediment onto the fertile Terai plains converting fertile agricultural land into large areas of relatively barren soil (Nayak, 1996; Ghimire et al.,

2013). Deforestation has become a major problem after government's resettlement program that destroyed a total 103,968 ha of forests in Siwalik Hills and Terai plains from 1950's to the mid-1980's (MPFS, 1988). The loss of forest cover has been mostly due to excessive fuelwood extraction, intensive livestock grazing, and expansion of agricultural land area. Land use change effects, specifically associated with deforestation, also have created social and political problems due to changes in water supply to lowland areas (Walker, 2003).

Hydrological models are commonly used to study the effect of land management on the hydrological cycle, mainly focused on surface runoff processes (Karvonen et al., 1999; Felix et al., 2002). These models may include representation of hydrological processes and associated water quality issues including sediment loading of surface water (Luo et al., 2008). The Soil and Water Assessment Tool (SWAT) is a quasi-distributed hydrological model that has been used to estimate climate change effect on stream discharge and groundwater recharge of mountain basins (Stonefelt et al., 2000; Eckhardt and Ulbrich, 2003; Gassman et al., 2007; Song and Zhang, 2012; Neupane et al., 2013). Some studies have also used SWAT for assessing land use/management change effect on watershed hydrologic responses including surface runoff and sediment yield (Fohrer et al., 2001; Tripathi et al., 2005). However, only few studies are focused on the Himalaya Mountains for predicting future hydrologic response in changing climate coupled with land use modification. The major objectives of this study are: (1) to assess the inherent different climate influences on water budgets of two Himalaya Mountain basins representing the east and west margins of Nepal and (2) to assess potential climate

change, land use change and combined climate and land use change effect on future water availability of these important basins through simulation modeling.

Materials and Methods

Study Site

For this study, I chose two Himalayan drainages located at eastern and western margins of Nepal including the Tamor River Watershed (TRW) and Seti River Watershed (SRW), respectively (Figure 23). The Tamor River originates from Kanchanjunga Mountain and has a total catchment area of 6,111 km^2. The Seti River originates from Api and Saipal mountains with total catchment area of 7,379 km^2. These rivers are major headwater reaches that eventually feed the Ganges River. The elevation for the Tamor basin ranges from 139 to 8,422 m above mean sea level (amsl). For the Seti basin, elevation ranges from 327 to 7,043 m amsl. Geologically, the basins are composed of Paleozoic-Mesozoic Tethyan Sediment Series, with metamorphic gneisses, migmatites and Proterozoic sediments that form a fractured basement aquifer system that may significantly influence groundwater contribution to stream discharge of the basins (Anderman et al., 2012). The dominant soils of both basins, derived from the WaterBase project (http://waterbase.org/download_data.html), are Cambisols and Leptosols. Cambisols are moderately developed soils distributed at lower elevation with higher vegetation productivity and Leptosols are shallow soils primarily distributed in the upper mountainous regions with steep slopes.

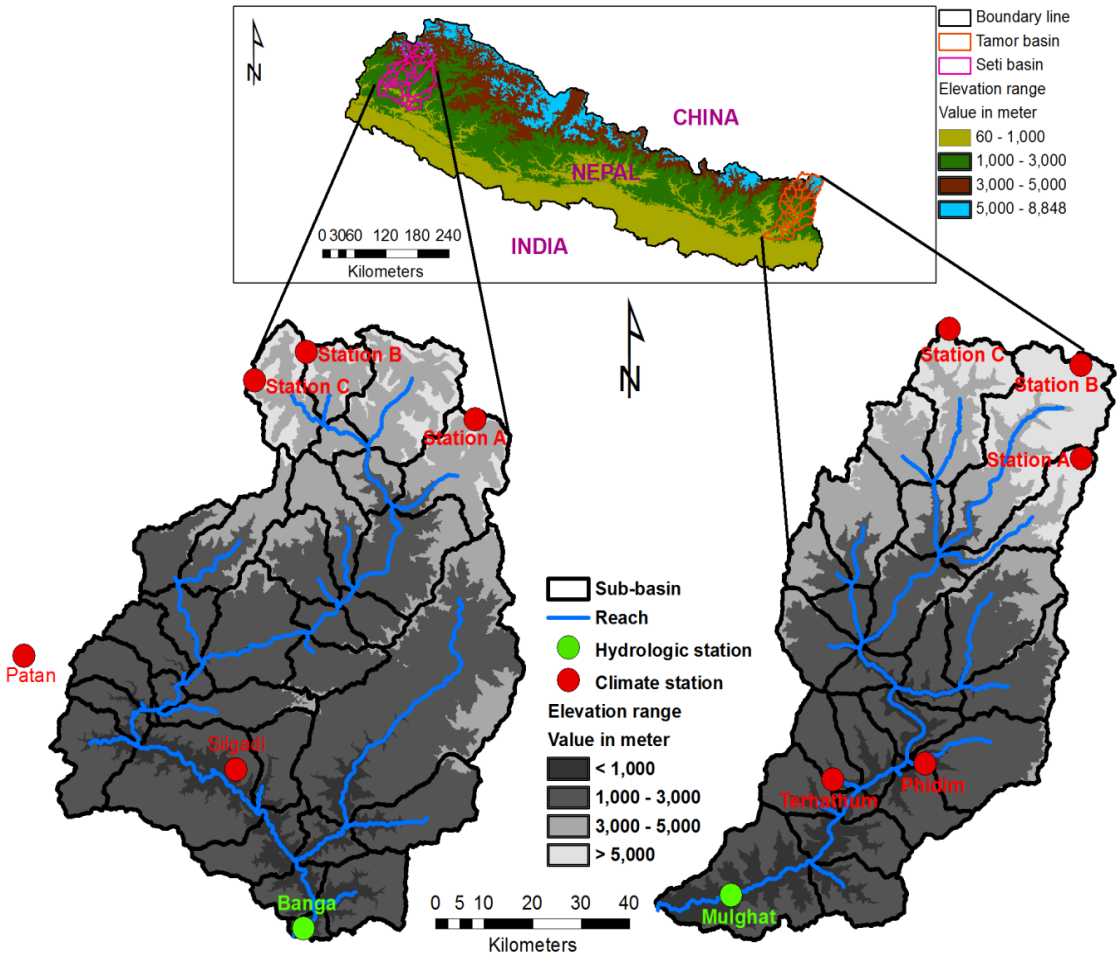

Figure 23. The Tamor and Seti river watersheds located at eastern and western margins of Nepal, respectively with the hydro-meteorological stations used in this study.

Nepal has three distinct climatic zones that varies from sub-tropical in southern valleys and foot slopes to alpine in the high mountains and is broadly based on elevation including: sub-tropical (<1800 m), temperature (1800-4000 m), and alpine (>4000 m) (Polunin and Stainton, 2000). However, the sub-tropical zone of western Himalayan region is limited to elevation of < 1400 m due to extreme colder winter months. At lower elevations, hot summers have daily temperature of 40^{o}C with total annual rainfall ranging from 1,500 to 2,000 mm (Ichiyanagi et al., 2007; Neupane et al., 2013). Cold and dry conditions are common at higher elevations with the average temperature and

precipitation values of 11°C and 257 mm, respectively (Pohle, 1991). While Nepalese watersheds are highly influenced by monsoonal precipitation, water budgets are mainly influenced by snowfall at higher elevations (Sharma, 1993).

Modeling Approach

The study simulated runoff yield using ArcGIS interface of the SWAT (version 2009) (http://swat.tamu.edu/software/arcswat/) which is a river basin model developed for the U.S. Department of Agriculture (USDA) by Blackland Research Center in Texas (Arnold et al., 1998; Neitsch et al., 2009). The hydrological component of SWAT is based on the Equation 1. I used the commonly applied runoff curve number method to estimate surface runoff in the basins (Loague and Freeze, 1985). Potential evapotranspiration (PET) was estimated using Penmann-Monteith procedure (Monteith, 1965) which is based on the energy balance components. The net water yield (WYLD in mm) to the stream channel was estimated using the Equation 3.

Snowmelt was computed by SWAT using a mass balance approach. First, the amount of snowmelt (mm of H_2O/day) was estimated by using the Equation 4. To characterize glacier processes in the basins, a classical degree-day model (Singh et al., 2006) was used as explained in Neupane et al. (2013). However, the degree-day factor for glacier melt data in this study was calculated by the following equation (Neitsch et al., 2009).

$$d = \frac{b_{gmlt,6} + b_{gmlt,12}}{2} + \frac{b_{gmlt,6} - b_{gmlt,12}}{2} . sin\left[\frac{2\pi}{365}(t - 81)\right] \quad (18)$$

where $b_{gmlt,6}$ is the melt factor for June 21st (mm H_2O day^{-1}°C), $b_{gmlt,12}$ is melt factor for December 21st (mm H_2O day^{-1}°C), and t is the day of year.

For this study, soil interflow was computed by the kinematic storage model (Sloan and Moore, 1984) that accounts for soil hydrological conductance, soil moisture, and slope. The baseflow was calculated by the following equation (Arnold et al., 1998; Neitsch et al., 2009).

$$Q_{gw,i} = Q_{gw,i-1} exp(-\alpha_{gw} \Delta t) + w_{rchrg} [1 - exp(-\alpha_{gw} \Delta t)] \quad (19)$$

where $Q_{gw,i}$ is the groundwater flow into the main channel on day i (mm), $Q_{gw,i-1}$ is the groundwater flow into the main channel on day i-1, α_{gw} is the baseflow recession constant, Δt is the time step (1 day), and w_{rchrg} is the amount of recharge entering the aquifer on day i.

Input Data

Model inputs for SWAT include topography, soil, vegetation, weather/climate, land management, and stream discharge. The accuracy of model output is highly influenced by the spatial and temporal resolution of input data used. Therefore, I used a 30 × 30 m resolution Global digital elevation model (DEM) obtained from the Advanced Spaceborne Thermal Emission and Reflection Radiometer (http://gdem.ersdac.jspacesystems.or.jp/search.jsp) for delineating sub-basin and also for defining topographic attributes such as area and slope with minimum drainage area threshold value of 130 km^2. For this process, I used ArcSWAT that automatically delineates sub-basins using grid-based DEM data. From the basin delineation process, the Tamor and Seti basins were divided into 27 and 33 sub-basins, respectively. Finally, I defined elevation bands in each sub-basin for about 500 m change in elevation to better

represent orographic precipitation patterns with snow accumulation and melt processes in these steep mountain basins (Fontaine et al., 2002).

Land use data for both basins were derived through spectral classification of Landsat 5 Thematic Mapper (TM) satellite images (http://glovis.usgs.gov/). The TM data for Tamor basin were derived from the Path/Row of 139/41 and 140/41 acquired from the year of 2009. For Seti basin, these data were derived from the Path/Row of 144/39 and 144/40 obtained from the same year. To minimize scene brightness differences between the two datasets associated primarily with solar irradiance angles, a histogram matching procedure was applied using Imagine software (ERDAS Inc. 2013). Next, the data were corrected for topographic-induced brightness differences using the topographic normalization algorithm (Equation 20) in the Imagine software where radiometric distortion of the images was normalized assuming them as a flat surface.

$$BV_{normal\ \lambda} = BV_{observed\ \lambda}/cos\ i \qquad (20)$$

where $BV_{normal\ \lambda}$ is the normalized brightness value, $BV_{observed\ \lambda}$ is the observed brightness value, and cos i is the cosine of incidence angle. The cosine of incidence angle was computed by the following equation.

$$\cos i = \cos(90 - \theta_s)\, cos\ \theta_n + \sin(90 - \theta_s)\, sin\ \theta_n \cos(\Phi_s - \Phi_n) \qquad (21)$$

where θ_s is elevation of the sun, θ_n is slope of the surface, Φ_s is azimuth of the sun, and Φ_n is aspect of the surface. The solar elevation and solar azimuth data were obtained from the header file of the images. To classify land use of the basins, I first performed an unsupervised classification using the Imagine software on the corrected TM data with 50 nominal classes representing different spectral features of the basins. These classes were interpreted by comparing class values with a coarse scale land use map derived from the

WaterBase project. This classification resulted in 10 different land use classes including forest-evergreen, forest-deciduous, forest-mixed, grassland, rice, corn, snow/ice, tundra, rock, and human settlement (Figure 24).

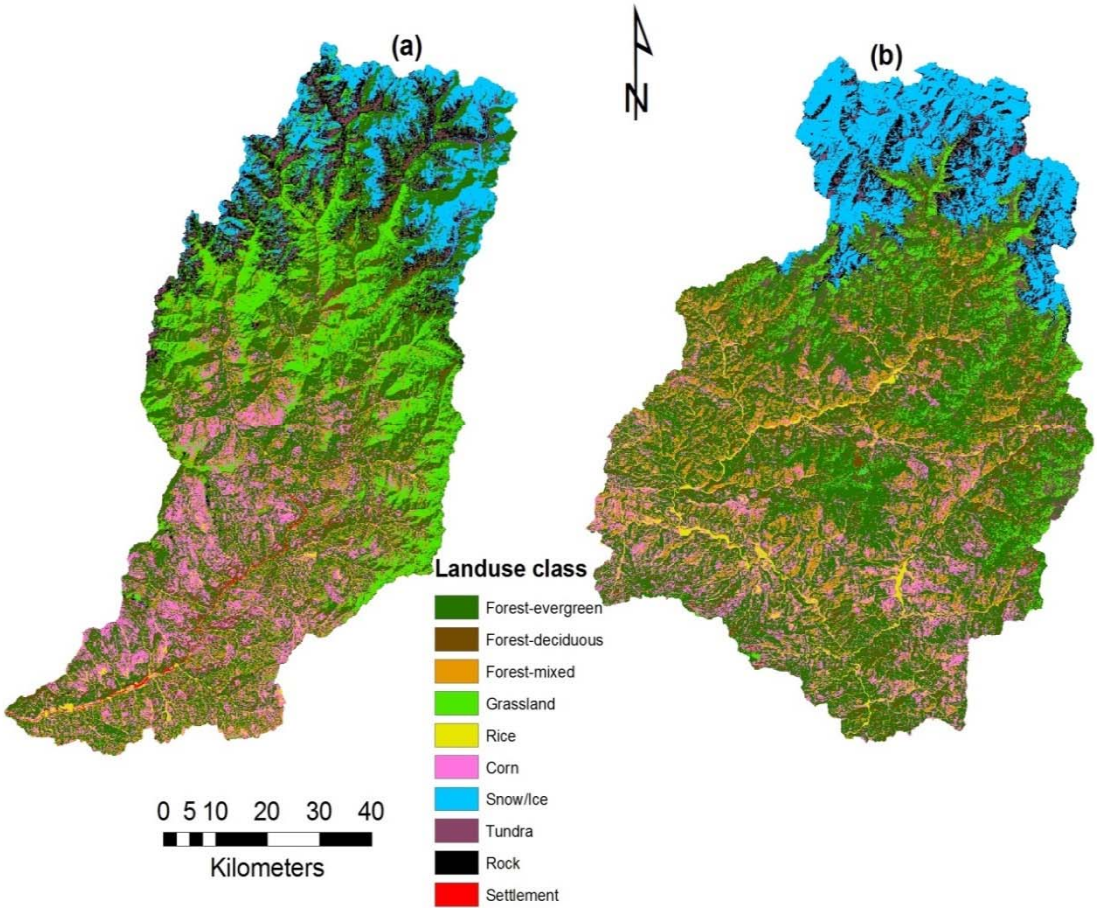

Figure 24. Land use class of the basins derived from Landsat 5 (TM) satellite data: (a) Tamor basin and (b) Seti basin.

Soil data with a resolution of 400 × 400 m were obtained from the WaterBase project. I developed a user's soil database required for the SWAT model based on the FAO/UNESCO Soil Map of the World (Batjes, 1997) that linked to the units of digital soil map through soil mapping unit codes using ArcGIS (version 10.0 ESRI Inc.) software. Attributes were assigned to each type of soil including depth, saturated

hydraulic conductivity and content of clay, silt, and sand (FAO/UNESCO, 2003). To derive soil depth data at 30 × 30 m resolution, I used topographic integration (Zheng et al., 1996) that were classified into shallow soil layer (<30 cm from surface) and deep soil layer (>30 cm from surface) to use for simulation modeling. The topographic saturation index (TSI) (Beven and Kirkby, 1979) was used as a proxy for correcting topography of the basins to calculate point soil depth based on maximum soil depth value obtained from FAO/UNESCO soil data. The soil characteristics were then combined with land use and slope to determine hydrologic response units (HRUs) for each sub-basin. Finally, to account most of the attributes from the basins, I defined 563 and 640 HRUs for Tamor and Seti basins, respectively using a minimum area threshold value of 5% for each land use, soil and slope categories.

Meteorological Data

Required meteorological inputs for SWAT include daily precipitation, maximum and minimum temperature, relative humidity, solar radiation, and wind speed. For this study, I used 31 years (1979-2009) of data obtained from the department of hydrology and meteorology (DHM), Nepal for two weather stations from each basin with recorded values of precipitation, maximum and minimum temperature, and relative humidity that included: (a) Terhathum and Phidim from the Tamor basin, and (b) Patan and Silgadi from the Seti basin (Table 10). Solar radiation for each station was estimated for the entire data record by applying the mountain climate simulator (MT-CLIM) (http://www.ntsg.umt.edu/project/mtclim) that uses daily temperature and precipitation data as model inputs. Due to lack of long-term wind measurement from the basins, five

years (2001-2005) data from Kagbeni station (28.84° N, 83.78° E, elevation: 2,838 m) were used as representative data for Terhathum station and 15 years (1994-2008) data from Surkhet station (28.88° N, 81.25° E, elevation: 950 m) were used as representative winds for Phidim, Patan, and Silgadi stations. To account for glacier melt data, three stations from each basin (Table 10) were used to simulate mean daily air temperature applying the MT-CLIM model for the period of 1981 to 1990 using measured data from the Phidim and Silgadi stations for the Tamor and Seti basins, respectively and incorporated with the degree-day model. Temperature and precipitation lapse rates required by the SWAT to distribute daily meteorological variables by elevation bands within each sub-basin were derived from a previous study conducted in central Himalaya Mountains of Nepal (Neupane et al., 2013).

Table 10. The hydro-meteorological stations with their spatial locations used in this study for hydrological simulations

Station	Type	Latitude (°)	Longitude (°)	Elevation (m)	Slope (°)	Aspect (°)
Mulghat	Hydrology	26.93	87.32	276	3.39	219.29
Banga	Hydrology	28.97	81.14	328	34.15	243.75
Terhathum	Meteorology	27.13	87.55	1,633	28.66	37.56
Phidim	Meteorology	27.15	87.75	1,205	24.12	315
Patan	Meteorology	29.46	80.53	1,266	-	-
Silgadi	Meteorology	29.26	80.98	1,360	31.14	201.43
Station A (TRW)	Meteorology	27.69	88.12	6,367	24.5	149.21
Station B (TRW)	Meteorology	27.86	88.13	6,214	42.42	208.9
Station C (TRW)	Meteorology	27.94	87.85	5,869	28.00	156.44
Station A (SRW)	Meteorology	29.88	81.49	6,477	50.97	240.23
Station B (SRW)	Meteorology	30.00	81.13	5,993	43.5	136.77
Station C (SRW)	Meteorology	29.95	81.02	6,112	42.15	177.09

Note: TRW for Tamor River Watershed and SRW for Seti River Watershed

Management Operations

For both basins, corn and rice were considered the major cultivated crop types. For planting, land units were considered to be terraced, a common land-management

practice in Nepal (Carson, 1990). The primary fertilizer for growing corn and rice was set to cattle-based fresh manure with an application rate of 42 and 71 kg/ha, respectively (Pandey et al., 2009). Traditional ploughing was used for redistributing nutrients to the upper soil layers through tillage operations. For all management operations including fertilization, tillage, planting and harvesting, I adopted the potential heat unit value (number of heat units required to bring a plant to maturity) for corn and rice farming in the basins (Neitsch et al., 2009) (Table 11).

Table 11. Management operations adopted in the basins for corn and rice cultivation including the total heat units required for plant maturity (PHU) and the total base zero heat units (PHU_0). The data were generated using 24 years (1979-2002) of daily measured air temperature data from Phidim and Silgadi stations as described in SWAT documentation: (a) Phidim station and (b) Silgadi station.

Date (a)	Operation	Base Zero Heat Units Accumulated	Plant Heat Units Accumulated	Fraction of PHU_0 (PHU_0 = 8,024)	Fraction of PHU (PHU= 993 & 1,465)
January 10, 1979	Terracing	-	-	-	-
January 13	Fertilizer application	186	-	0.02	-
January 15	Tillage operation	214	-	0.03	-
January 20	Planting corn (PHU = 993)	286	0	0.04	-
May 30	Harvest & Kill	3,027	1,443	-	1.45
July 5	Tillage operation	3,981	-	0.50	-
July 10	Planting rice (PHU = 1,465)	4,114	0	0.51	-
August 10	Fertilizer application	4,933	-	0.61	-
October 20	Harvest & Kill	6,714	1,597	-	1.09

Date (b)	Operation	Base Zero Heat Units Accumulated	Plant Heat Units Accumulated	Fraction of PHU_0 (PHU_0 = 7,731)	Fraction of PHU (PHU= 911 & 1,391)
January 10, 1979	Terracing	-	-	-	-
January 13	Fertilizer application	175	-	0.02	-
January 15	Tillage operation	202	-	0.03	-
January 20	Planting corn (PHU = 911)	270	0	0.03	-
May 30	Harvest & Kill	2,906	1,338	-	1.47
July 5	Tillage operation	3,832	-	0.50	-
July 10	Planting rice (PHU = 1,391)	3,960	0	0.51	-
August 10	Fertilizer application	4,755	-	0.62	-
October 20	Harvest & Kill	6,479	1,514	-	1.09

Model Calibration and Confirmation

Before calibrating the model, simulations for the period of 1981 to 1990 were compared with measured stream discharge data using SWAT default parameter values referred as the pre-calibration simulation. Subsequent simulations were organized by first establishing a calibration (1979-1990) and confirmation periods (1991-1995). For these two periods, I used daily stream discharge data from the gauging stations at Mulghat and Banga for Tamor and Seti basins, respectively. For calibration, the initial 2 years of simulated outputs were disregarded as a warm-up period that allows the model to cycle multiple times to minimize the effect of user estimated parameter values (Zhang et al., 2007). Also, to assess the effect of orographic precipitation and glacier melt processes in the basins, calibration and confirmation simulations were run in two different scenarios: (1) band-no glac: elevation bands were used and glacier melt data were not used and (2) band-glac: both elevation band and glacier melt data were used. These calibration outputs were considered as the baseline data to compare with potential climate and land use change simulations described later. For each analysis, simulated stream discharge data were compared to the measured values on a daily basis and the model performance was evaluated using Nash-Sutcliffe efficiency (NSE) (Equation 7) and Percent Bias (PBIAS) (Equation 6) indices (Moriasi et al., 2007). The NSE indicates how well the plot of measured versus simulated data fits the line with higher NSE values associated with higher accuracy of model outputs. The PBIAS measures an average tendency of the simulated data to be larger or smaller than their measured counterparts, with lower PBIAS values indicating the higher accuracy of model simulations.

The outputs obtained from model calibration and confirmation simulations were also evaluated using goodness of fit statistics including root mean square error (RMSE) (expressed in m^3/s throughout the paper) (Equation 22) and coefficient of determination (r^2).

$$RMSE = \sqrt{\frac{1}{N}\sum_{i=1}^{N}(Q_i^{'} - Q_i)^2} \qquad (22)$$

where Q_i' is the simulated discharge (m^3/s) at time step i and Q_i is the observed discharge (m^3/s). Microsoft Excel was used to compute the correlation coefficient of determination (r^2) with the values > 0.5 considered acceptable (Santhi et al., 2001). Although I used both daily and monthly stream discharge data during calibration and confirmation periods, only monthly data were used for potential climate and land use change simulations as described later.

Sensitivity of SWAT Parameters

To assess SWAT parameters potentially influencing hydrological processes in our study basins, I performed a sensitivity analysis based on focal group of model parameters that were identified from previous studies (e.g., Fontaine et al., 2002; Muleta and Nicklow, 2005; Rostamian et al., 2008; Neupane et al., 2013). Optimal input parameter values were derived from manual calibration procedure as explained in Neupane et al. (2013), and the relative sensitivity of each parameter was computed as in the Equation 8. The sensitivity analysis was performed comparing 10 years (1981-1990) of daily measured stream discharge data with model simulation outputs. Uncertainties of model simulated stream discharge values were also evaluated using standardized residual error analysis (White and Running, 1994).

Climate and Land Use Change Scenarios

For this study, I derived the average outputs of temperature and precipitation changes estimated for the Special Report on Emission Scenarios (SRES) including low (B1), medium (A1B), and high (A2) emission scenarios from 16 global circulation models (GCMs) (http://www.climatewizard.org/) for 2080s. To estimate climate change effects on watershed hydrology including basin precipitation, stream discharge, and sediment yield in different scenarios, the mean monthly temperature and precipitation data derived from GCMs were incorporated with the baseline SWAT database. Then, SWAT simulations were run for the period of 2080 to 2089 at monthly basis; however, I ignored the initial two years data for analysis as model warm-up period.

Land use change effect on watershed hydrological processes were carried out in three potential scenarios. The effects of three potential land use scenarios on SWAT simulation modeling were evaluated and include: (a) Scenario-I: assumed that the forested land (deciduous and mixed forests) from lower elevation (<2,500 m) and lower slope (<25^{o}) was converted into agricultural land (corn field in this study), (b) Scenario-II: assumed deforestation at lower elevation (<3,000 m) and slope (<30^{o}) to convert into grassland, and (c) Scenario-III: assumed the forested land, agricultural land and grassland with low elevation (<3,500 m) and slope (<10^{o}) were used for human settlement (Table 12). These scenarios resulted in new land used maps (Figure 25) based on the satellite-derived land use and topographic data. The land use data derived for each scenario were incorporated into the SWAT model for determination of new HRU's for each sub-basin, with the same set of parameters that was used during calibration period. For estimation of land use change effects on watershed hydrology, model simulations were run as in

climate change scenarios (explained earlier). Finally, I also estimated the influence of future climate on stream discharge and sediment yield of the basins coupled with potential land use scenarios. However, simulation outputs obtained from all these scenarios were compared with the baseline simulation data using the Equation 9.

Table 12. Three potential land use scenarios developed for the basins based on topographic attributes including elevation and slope.

Scenario	Description
Scenario-I	Deciduous and mixed forests from lower elevation (<2,500 m) and lower slope (<25^{o}) were converted into agricultural land
Scenario-II	Forested land from lower elevation (<3,000 m) and slope (<30^{o}) was converted into grassland
Scenario-III	Forested land, agricultural land, and grassland from lower elevation (<3,500 m) and slope (<10$^{o)}$ were converted into human settlement area

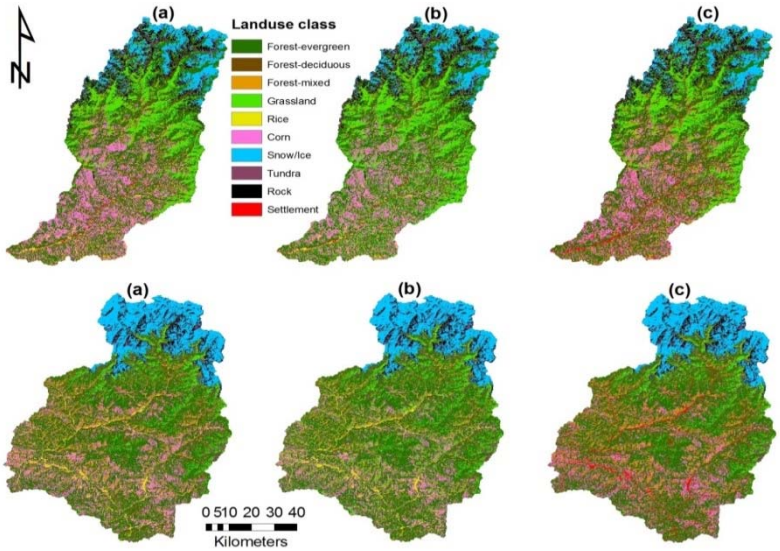

Figure 25. Potential land use scenarios for the basins (upper figures for the Tamor basin and lower figures for the Seti basin): (a) after expanding agricultural land as Scenario-I, (b) after destroying forested land as Scenario-II, and (c) after expanding settlement area as Scenario-III.

Historical Data Analysis of Precipitation and Stream Discharge

Figure 26 shows mean monthly precipitation and stream discharge values for the Tamor (eastern) and Seti (western) basins. Analysis of 24 years (1979-2002) of precipitation data obtained from DHM, Nepal clearly indicated that higher amount of precipitation in both basins occurs during summer months, mainly from June to September. Winter months are dry with little precipitation. The minimum November precipitation of the Tamor basin is 12 mm and the maximum July precipitation reaches up to 350 mm. Precipitation values of 9 and 304 mm during the same months, respectively were found for the Seti basin. Due to weaker summer monsoonal period in the Seti basin, the Seti River has lower peak flows compared to the Tamor River (Hannah et al., 2004).

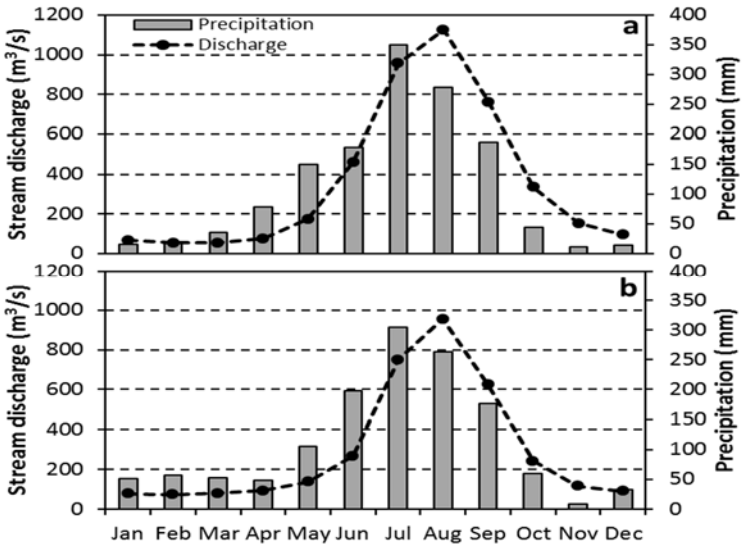

Figure 26. Mean monthly precipitation and stream discharge of the Tamor and Seti basins of Nepal (data have been averaged for the period from 1979 to 2002): (a) Tamor basin and (b) Seti basin.

Corresponding to higher summer monsoonal precipitation, stream discharge was also measured higher during same period of time with maximum discharge values of 1,126 and 956 m^3/s for the Tamor and Seti basins, respectively. Analysis of 24 years (1979-2002) of stream discharge data showed that the mean monthly discharge of 359 m^3/s was measured for the Tamor basin that was higher than 292 m^3/s observed for the Seti basin. The minimum March stream discharge of the Tamor basin is 53 m^3/s that is lower than 73 m^3/s observed on February for the Seti basin.

In Nepal, hydrological seasons are mainly of three different types: (a) dry pre-monsoon season (March-May); (b) rainy monsoon season (June-September); and post-monsoon season (October-February) with little rain. These seasons directly affect water availability and agricultural production in the basins. For example, pre-monsoon is the primary season for corn production whereas rainy monsoon season highly influence rice production in the basins. This complex precipitation distribution in these mountain basins is due to combined effects of summer monsoon and steep terrain (Kansakar et al., 2004; Shrestha et al., 2000). Seasonal analysis of precipitation and stream discharge data indicated that 73% of total precipitation in the Tamor basin occurred during monsoon season that corresponded with 77% of total stream discharge in the same season (Figure 27). These values were higher than 69% of total precipitation corresponding to 60% of total stream discharge for the Seti basin. During winter months, the basins are influenced by westerly winds causing snowfall at higher elevations; however, it weakens west-to-east. However, due to higher post-monsoonal precipitation in the Seti basin, I analyzed a higher stream discharge contribution of 30% of the Seti River in the same season.

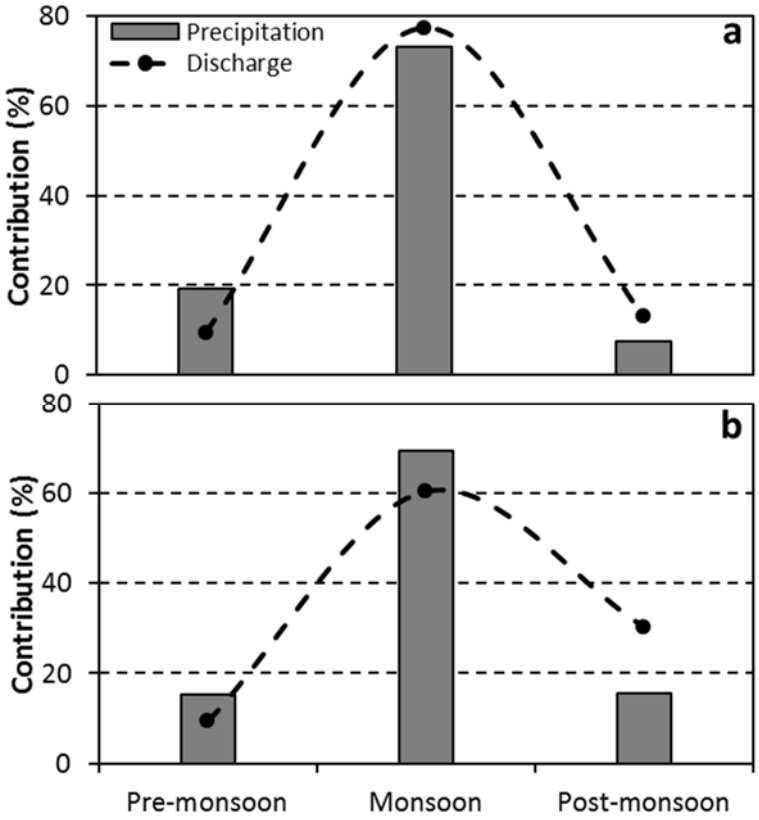

Figure 27. Precipitation and stream discharge contribution on seasonal basis for eastern and western basins of Nepal (The data have been averaged over the period from 1979 to 2002): (a) Tamor basin and (b) Seti basin.

Model Calibration and Confirmation Analysis

Identification of key parameters with precise values is an important step for calibration of a model (Ma et al., 2000). The results of the model calibration and confirmation analyses with their statistical values are presented in Table 13. During pre-calibration period, the model simulation outputs showed low correspondence for PBIAS, NSE, r^2 and RMSE with the values of 46.5, 0.16, 0.34, and 350, respectively on daily simulations for the Tamor basin, and the Seti basin had the values of 23.8, -0.28, 0.34, and 460 for these statistics, respectively. Introducing the elevation bands with rice and corn cropping in the basins, I got higher correlation between measured and simulated

values with PBIAS = 4, NSE = 0.65, r^2 = 0.65 and RMSE = 227 for daily simulations of the Tamor basin. The values of these statistics were 4.8, 0.68, 0.68 and 232, respectively for the Seti basin. These higher correlations showed the importance of orographic precipitation in the basins. However, the model showed better performance in monthly simulations with PBIAS = 2.5, NSE = 0.82, r^2 = 0.83 and RMSE = 138 with addition of glacier melt data for the Tamor basin. The values for these statistics were 2.6, 0.86, 0.87 and 127, respectively for the Seti basin.

Table 13. Model performance statistics for pre-calibration, calibration, and confirmation simulations in both daily and monthly time periods for the basins (no band-no glac: elevation bands were not used and glacier melt data were not used; band-no glac: elevation bands were used and glacier melt data were not used; band-glac: both elevation band and glacier melt data were used): (a) Tamor basin and (b) Seti basin.

(a)

Statistics	**Pre-calibration**		**Calibration**				**Confirmation**			
	no band-no glac		band-no glac		band-glac		band-no glac		band-glac	
	Daily	Monthly	Daily	Monthly	Daily	Monthly	Daily	Monthly	Daily	Monthly
PBIAS	46.5	46.5	4.0	4.0	2.5	2.5	1.4	1.4	-0.9	-0.9
NSE	0.16	0.44	0.65	0.82	0.65	0.82	0.72	0.89	0.73	0.89
r^2	0.34	0.76	0.65	0.83	0.65	0.83	0.73	0.89	0.73	0.89
RMSE	350	245	227	140	226	138	187	109	187	107

(b)

Statistics	**Pre-calibration**		**Calibration**				**Confirmation**			
	no band-no glac		band-no glac		band-glac		band-no glac		band-glac	
	Daily	Monthly	Daily	Monthly	Daily	Monthly	Daily	Monthly	Daily	Monthly
PBIAS	23.8	23.8	4.8	4.8	2.6	2.6	0.2	1.8	-4.3	-2.5
NSE	-0.28	0.68	0.68	0.85	0.68	0.86	0.56	0.80	0.56	0.81
r^2	0.34	0.76	0.68	0.86	0.68	0.87	0.58	0.80	0.59	0.81
RMSE	460	192	232	131	230	127	202	120	201	117

Similar to the calibration period, confirmation analysis also followed the higher correlation of simulated stream discharge *vs* measured values with PBIAS = -0.9, NSE = 0.73, r^2 = 0.73 and RMSE = 187 at daily simulation for the Tamor basin with addition of glacier melt data that shows the importance of glacier melt contribution to estimate stream discharge of the basin. The model showed better performance in monthly simulations with the values of -0.9, 0.89, 0.89 and 107 for these statistics, respectively. For the Seti basin, I analyzed these statistical values as -4.3, 0.56, 0.59 and 201, respectively at daily simulation. However, the values were -2.5, 0.81, 0.81 and 117, respectively at monthly simulation for the basin. During confirmation period, I analyzed negative PBIAS values that indicate the model underestimation bias for both daily and monthly simulations. After model calibration, simulated mean daily stream discharge of 299 m^3/s corresponded well with the measured value of 306 m^3/s for the Tamor basin, and for the Seti basin, simulated value of 303 m^3/s corresponded with the measured value of 311 m^3/s.

Using 10 years (1981-1990) of the model simulation outputs, I estimated a loss of 148 mm (about 8%) of water from total inputs for the Tamor basin and the value increased to 21% for the Seti basin, potentially attributed to the transmission of large amount of surface water to the deep groundwater reservoirs primarily due to intense faults and fractures, characteristics of the Himalaya Mountains (Negi et al., 2007; Searle et al., 2008) that indicates higher water flux into these systems. These losses were substantially higher than in the Kali Gandaki Watershed (4% of the total input) located in central part of Nepal (Neupane et al., 2013). I estimated a 50% of total annual stream discharge of the Tamor basin was contributed by rain (Figure 28) that was lower than 58%

predicted for the Seti basin. These outputs demonstrated the dominant role of monsoonal precipitation in yearly water budget of the basins. Snowmelt, glacier melt, and groundwater contribution were estimated as 3, 25, and 22%, respectively for the Tamor basin. However, snowmelt contribution was substantially higher with the value of 6% for the Seti basin that might be due to major influence of westerly winds to the western Himalaya Mountains causing snowfall at higher elevations (Bookhagen and Burbank, 2010) that corresponded to 44% higher amount of snowfall in the basin. Higher groundwater contribution to the stream discharge of these basins that I estimated is also supported by Anderman et al. (2012) that shows the flow of water through the fractured basement rocks as approximately six times the annual contribution from glacier and snowmelt in the Himalaya Mountains. These estimations suggest that existing higher meltwater contribution to the stream discharge is largely influenced by continued climate change coupled with less snowfall and earlier melting (Fagre et al., 1997; White et al., 1998; Neupane et al., 2013). In SWAT, the unconfined shallow aquifer is the primary groundwater source (Neitsch et al., 2009), so it represents a crucial hydrological component for complex mountain basins (Luo et al., 2012). The separation of baseflow component during pre-calibration period indicated that about 31% of total annual flow was contributed by the baseflow component for the Tamor basin (Figure 29) that was higher than the value of 26% calculated for the Seti basin; however, major baseflow contribution to the discharge was observed during winter months.

A visual comparison of the hydrographs (Figure 30) obtained using the SWAT default parameter values indicated that the stream discharge during winter months was consistently underestimated by the model at daily and monthly simulations for the basins.

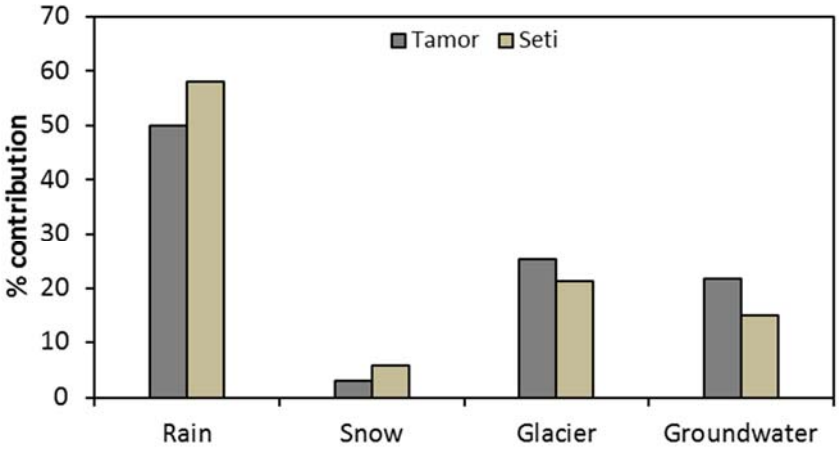

Figure 28. Mean yearly stream discharge contribution of the Tamor and Seti basins by different source waters estimated from model simulation outputs (the data have been averaged from the year of 1981 to 1990).

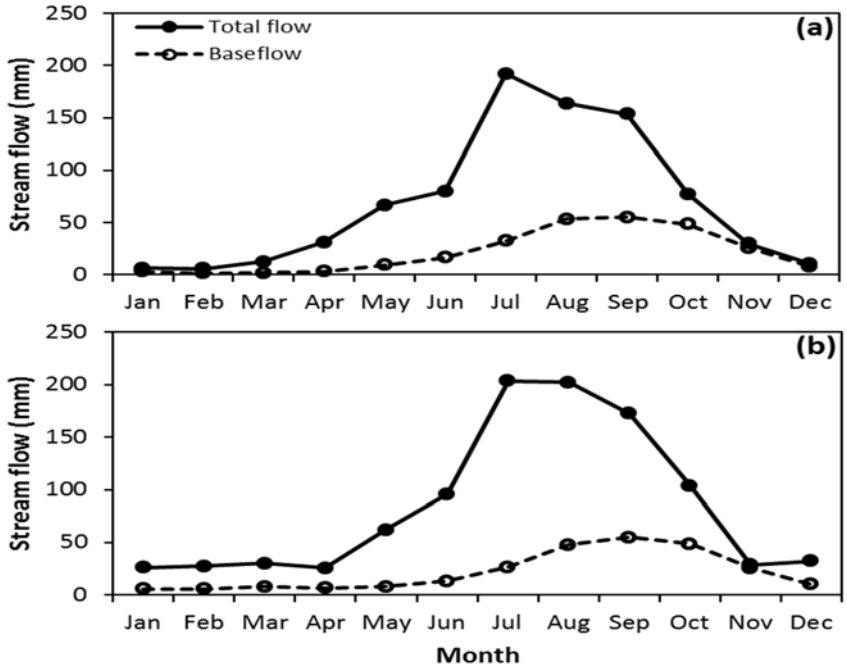

Figure 29. Comparison of total stream flow with the baseflow component (the data is averaged over the period from 1981 to 1990): (a) Tamor basin and (b) Seti basin.

Overestimation of modeled peak flows was observed during monsoon season for daily simulations. However, calibration and confirmation of the model substantially improved

the fit of modeled vs. observed daily stream discharge values (Figure 31) with the inclusion of elevation bands and glacier melt data. I showed that the Tamor and Seti SWAT models simulated the stream discharge with reasonable accuracy; however, they were not able to capture some of the summer peak flows for daily simulations that might be attributed to accuracy in measured precipitation and stream discharge data, especially during high flow seasons. This was supported by the findings of Rossi et al. (2009) who indicated more pronounced errors of stream discharge values at extreme low and high flow seasons influenced by recording and rating errors, respectively.

Sensitivity Analysis

The parameters influencing hydrological processes of the basins in order of their sensitivity rank are shown in Table 14 (the first is most sensitive). From 20 parameters tested, 18 were found to affect accuracy of stream discharge of the basins. However differed in their rank, identified sensitive parameters were almost same for both basins. I estimated the TLAPS and PLAPS, which govern the extreme orographic effects of complex mountains influencing the amount of precipitation (Minder et al., 2010) that determine the stream discharge, as the most sensitive parameters for accuracy of stream discharge in the basins. However, higher negative TLAPS value of -6.2^{o}C/Km (out of the given range) for the Seti basin compared to the Tamor basin (-5.1^{o}C/Km) might be the indication of higher influence of moisture-bearing westerly winds to Seti basin that weakens towards eastern part of the Himalaya Mountains (Owen et al., 2008; Puranik and Karekar, 2009; Bookhagen and Burbank, 2010).

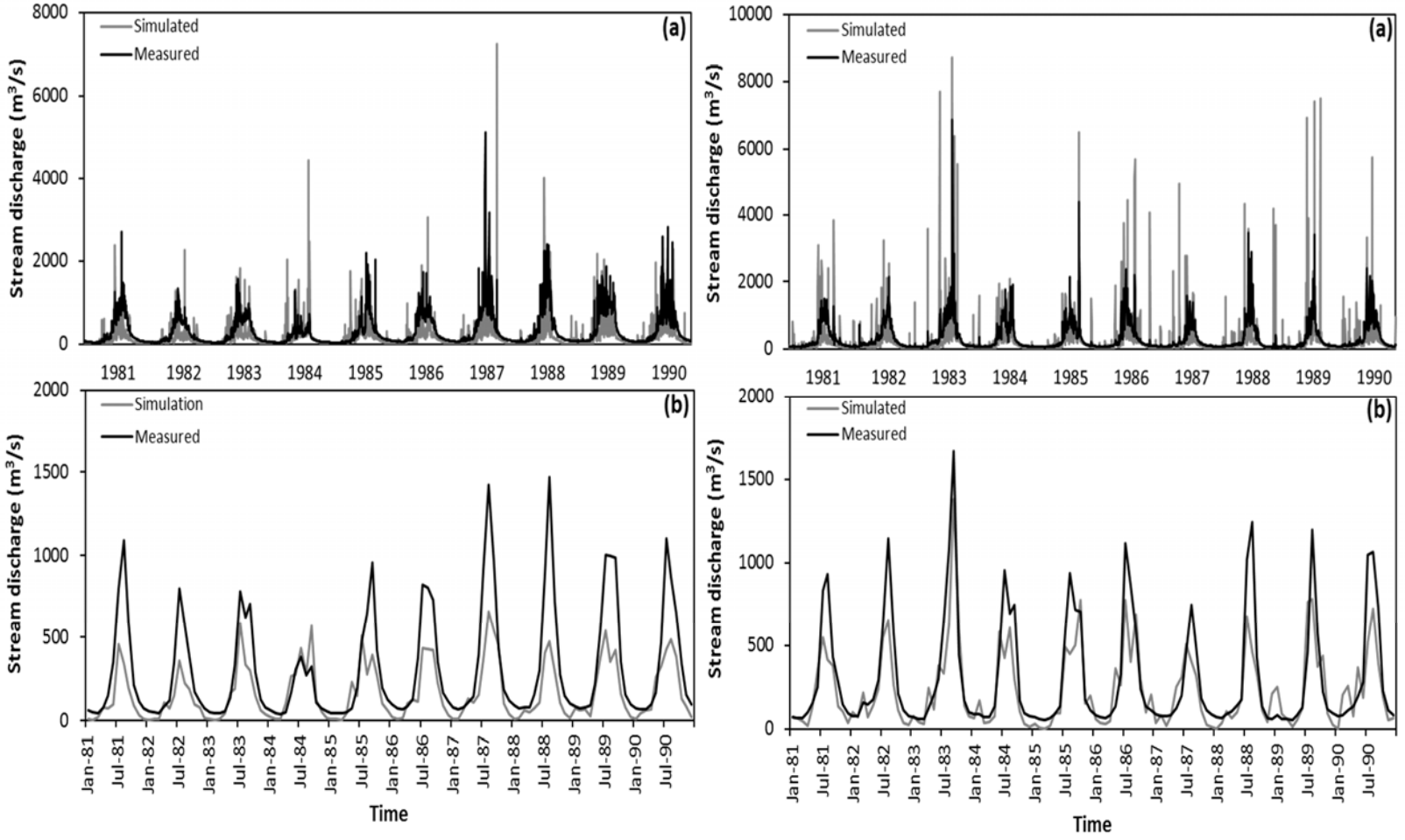

Figure 30. Pre-calibration hydrographs obtained from model simulations (left graphs for the Tamor basin and right graphs for the Seti basin): (a) daily and (b) monthly periods.

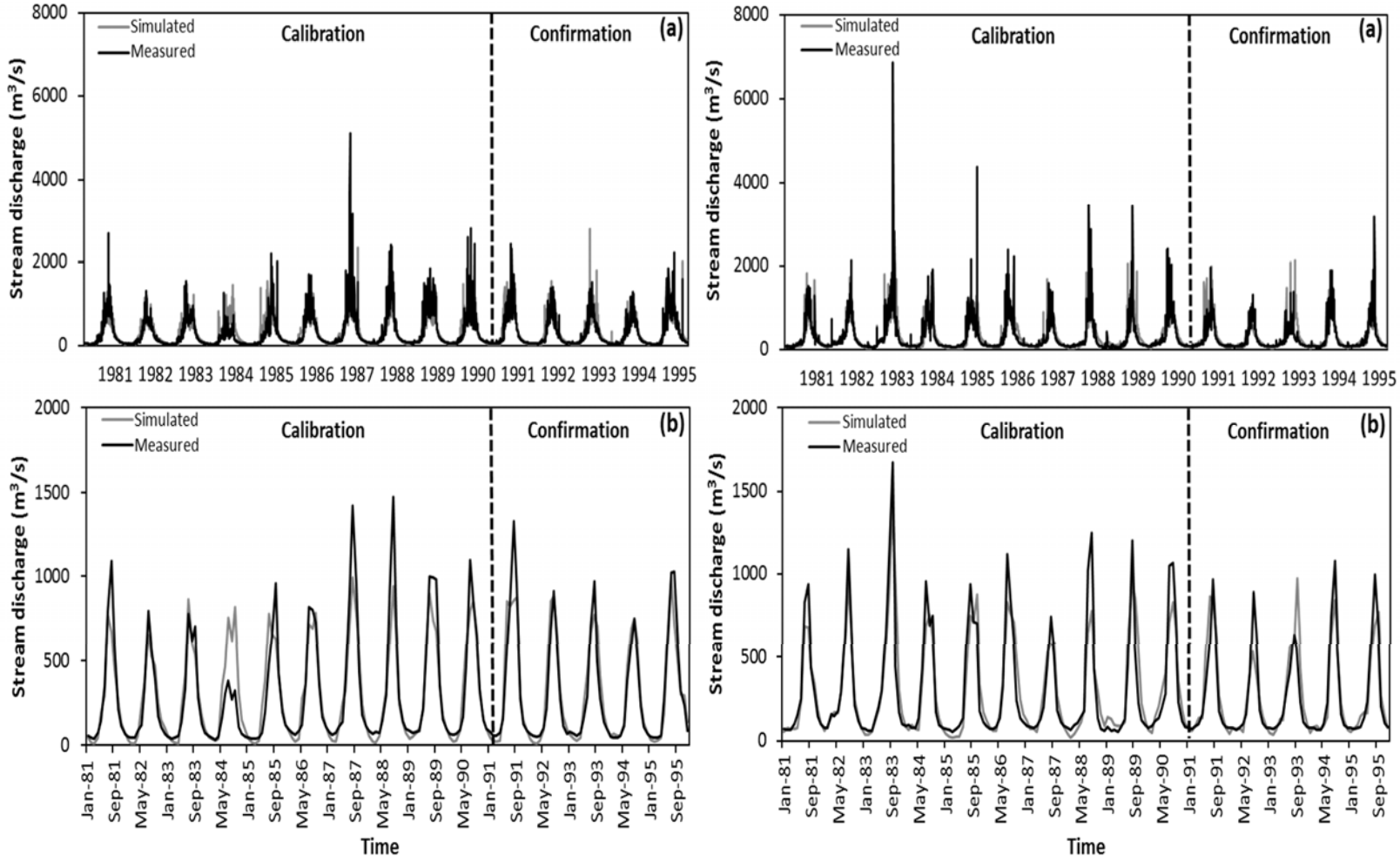

Figure 31. Hydrographs obtained during model calibration and confirmation periods (left graphs for the Tamor basin and right graphs of the Seti basin): (a) daily and (b) monthly time periods

Table 14. Sensitivity results with the ranking of key SWAT parameters for stream discharge in Tamor and Seti basins including the range of parameter values adopted from Muleta and Nicklow (2005), Rostamian et al. (2008) and Neupane et al. (2013).

Parameter	**Description**	**Range**	**Optimal value**		**S_r**		**Rank**	
			Tamor	Seti	Tamor	Seti	Tamor	Seti
[a]TLAPS	Temperature Lapse Rate (^{o}C/Km)	(-5.8) - (-4)	-5.1	-6.2	0.556179	0.167313	1	2
PLAPS	Precipitation Lapse Rate (mm H_2O/Km)	368 - 2,629	700	510	0.373324	0.393225	2	1
REVAPMN	Threshold depth of water in the shallow aquifer for revap (mm H_2O)	0 - 100	40	28	0.172975	0.029025	3	6
GWQMN	Threshold depth of water in the shallow aquifer required for return flow to occur (mm H_2O)	0 - 100	35	41	0.170522	0.043751	4	5
ESCO	Soil evaporation compensation factor	0.001 - 1	0.95	0.16	0.132555	0.004741	5	9
SMFMX	Maximum melt rate for snow during the year (mm/^{o}C-day)	1.4 - 7.5	7.5	7	0.043788	0.018087	6	7
GW_REVAP	Groundwater "revap" coefficient	0.02 - 0.2	0.14	0.2	0.008327	0.068731	7	4
SMFMN	Minimum melt rate for snow during the year (mm/^{o}C-day)	1.4 - 7.5	5	5	0.005884	0.000053	8	13
[a]TIMP	Snow pack temperature lag factor	0.5 - 1	0.05	0.05	0.005682	0.003713	9	10
RCHRG_DP	Deep aquifer percolation fraction	0.01 - 0.75	0.01	0.24	0.005062	0.134512	10	3
ALPHA_BF	Baseflow alpha factor (days)	0.001 - 1	0.70	0.75	0.004546	0.000027	11	14
GW_DELAY	Groundwater delay time (days)	0.001 - 100	20	5	0.003689	0.006319	12	8
[a]CH_K2	Effective hydraulic conductivity in main channel alluvium (mm/hr)	0 - 150	200	280	0.000923	0.000947	13	11
ALPHA_BNK	Baseflow alpha factor for bank storage (days)	0.05 - 1	0.12	0.11	0.000454	0.000017	14	15
EPCO	Plant uptake compensation factor	0.001 - 1	0.02	0.02	0.000121	0.000185	15	12
CH_N2	Manning's n value for the main channel	0.01 - 0.15	0.06	0.06	0.000051	0.000010	16	16
SURLAG	Surface runoff lag time (days)	0.001 - 15	12	10	0.000003	0.000002	17	18
SMTMP	Snow melt base temperature (^{o}C)	(-2) - 20	5	5	0.000000	0.000000	NS	NS
SFTMP	Snowfall temperature (^{o}C)	(-10) - 5	1	1	0.000000	0.000000	NS	NS
OV_N	Manning's n value for overland flow	0 - 0.80	0.5	0.5	0.000000	0.000004	NS	17

Note: [a]calibrated baseline value of this parameter is out of the given range.

Next to lapse rates, groundwater flow parameters such as REVAPMN, RCHRG_DP, GWQMN, and GW_REVAP were identified as sensitive parameters. Also, ESCO, SMFMX, SMFMN, GW_DELAY, TIMP, ALPHA_BF, CH_K2, EPCO, ALPHA_BNK, CH_N2, and SURLAG were found to affect the stream discharge of the basins. For both basins, I analyzed the minimal TIMP value of 0.05, lower than the minimum value of 0.5 given by Muleta and Nicklow (2005), that might be the indication of extreme lower snow temperature, specifically to the Himalaya Mountains (Fontaine et al., 2002). I estimated the maximum CH_K2 values of 200 and 280 mm/hr for the Tamor and Seti basins, respectively, higher than the maximum range suggested by Rostamian et al. (2008). These higher CH_K2 values might be the reflection of large sized gravel and sand to the stream bed of the Himalaya Mountain Rivers that augments water transmission to deeper groundwater system (Scanlon et al., 2002). This is further supported by structural discontinuities with the faults and fractures, typical of the Himalaya Mountains (Negi et al., 2007; Anderman et al., 2012). Model simulation uncertainties analyzed for one year daily stream discharge values from calibration period (Figure 32) confirmed that the model estimations had significant over and underestimation values, specifically during peak flow seasons, with better results during low flow seasons.

Potential GCM-derived Changes in Temperature and Precipitation of the Basins

The future climate conditions for the Terhathum, Phidim, Patan, and Silgadi stations were determined using the average of GCM-derived scenarios obtained from 16 different models for 2080s (Table 15). Analysis of temperature change showed an

obvious increase in temperature in all the stations. For the Terhathum and Phidim stations, the annual average temperatures were higher than current values that ranged from 2.5 to 4.1^{o}C with the maximum temperature projected for the SRES-A2 scenario. These predictions were lower than the range of 2.7 to 4.4^{o}C and 2.6 to 4.4^{o}C for the Patan and Silgadi stations, respectively. Therefore, higher predicted temperatures of these stations were likely to affect future water availability and rate of agricultural production in the basins. I estimated overall warming in all the scenarios, with maximum influence to the SRES-A2 scenario. The temperature change was projected to be higher during winter months and lower during summer months, with the value range between +4.8 and +2.0^{o}C, respectively for the Terhathum and Phidim stations. The values ranged from +5.2 to 2.2^{o}C for the Pathan station and from +5.1 to 2.2^{o}C for the Silgadi station.

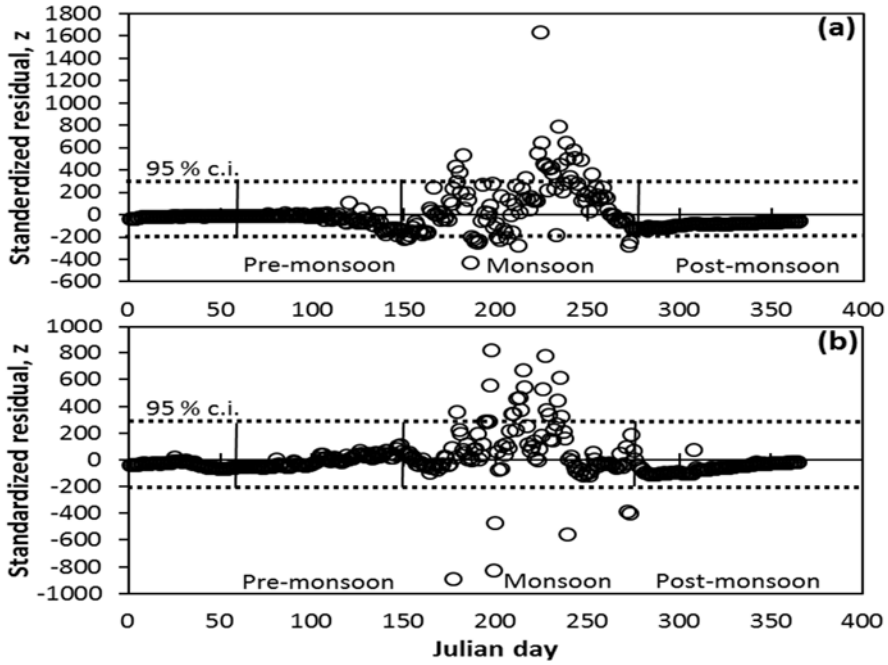

Figure 32. Uncertainty analysis performed for the model simulation outputs versus measured stream discharge: (a) Tamor basin and (b) Seti basin.

Table 15. Various scenarios for the Terhathum, Phidim, Patan and Silgadi meteorological stations obtained from CGM outputs to use for future hydrologic assessment of the basins: (a) annual and monthly average temperature change (°C) and (b) annual and monthly cumulative precipitation change (%).

(a)	Terhathum station												
Scenario	Month												
	1	2	3	4	5	6	7	8	9	10	11	12	Annual
SRES-B1	2.9	2.9	2.9	2.8	2.6	2.1	2.0	2.0	2.1	2.3	2.4	2.6	2.5
SRES-A1B	4.2	4.3	4.1	4.2	3.7	3.0	3.0	3.0	3.1	3.4	3.6	3.8	3.6
SRES-A2	4.7	4.7	4.7	4.8	4.1	3.3	3.3	3.4	3.4	3.8	4.0	4.5	4.1
	Phidim station												
SRES-B1	2.9	2.9	2.9	2.9	2.6	2.1	2.0	2.0	2.1	2.3	2.4	2.6	2.5
SRES-A1B	4.3	4.3	4.1	4.2	3.7	3.0	3.0	3.0	3.1	3.4	3.6	3.8	3.6
SRES-A2	4.8	4.7	4.7	4.8	4.2	3.3	3.3	3.4	3.4	3.8	4.0	4.5	4.1
	Patan station												
SRES-B1	3.1	3.0	3.2	3.0	2.7	2.6	2.3	2.2	2.3	2.4	2.4	2.9	2.7
SRES-A1B	4.5	4.6	4.4	4.3	4.0	3.7	3.3	3.3	3.5	3.5	3.7	4.2	3.9
SRES-A2	5.2	5.0	5.2	4.9	4.6	4.1	3.6	3.7	3.9	4.1	4.2	4.9	4.4
	Silgadi station												
SRES-B1	3.0	3.0	3.1	2.9	2.7	2.6	2.3	2.2	2.3	2.4	2.4	2.9	2.6
SRES-A1B	4.5	4.6	4.3	4.3	4.0	3.7	3.3	3.3	3.5	3.5	3.7	4.2	3.9
SRES-A2	5.1	5.0	5.1	4.9	4.6	4.2	3.6	3.7	3.9	4.1	4.2	4.9	4.4

(b)	Terhathum station												
Scenario	Month												
	1	2	3	4	5	6	7	8	9	10	11	12	Annual
SRES-B1	-15	-6	-1	5	8	11	8	13	10	25	-3	0	5
SRES-A1B	-18	-10	1	-4	19	22	14	18	22	33	2	5	9
SRES-A2	-16	-14	-1	2	15	28	16	25	23	26	5	-6	9
	Phidim station												
SRES-B1	-15	-6	-1	5	7	11	8	13	10	25	-3	0	5
SRES-A1B	-18	-10	1	-4	17	22	14	18	22	33	2	5	8
SRES-A2	-16	-14	-1	2	13	28	16	25	23	26	5	-6	8
	Patan station												
SRES-B1	-4	-11	-20	-14	-2	4	3	7	16	9	-4	-9	-2
SRES-A1B	-14	-9	-24	-23	-2	13	7	7	28	39	-10	-13	0
SRES-A2	-11	-25	-21	-22	-1	16	7	6	26	28	-3	-8	-1
	Silgadi station												
SRES-B1	-5	-10	-18	-13	-1	4	5	8	19	8	-4	-9	-1
SRES-A1B	-15	-9	-21	-22	-2	16	9	9	29	36	-9	-12	1
SRES-A2	-11	-22	-20	-19	0	18	9	8	28	26	-2	-8	0

The annual accumulated precipitation change ranged from +5 to +9% for the Terhathum station and from +5 to +8% for the Phidim station. For the Patan station, the range was between -2 and 0% and it was between -1 and +1% for the Silgadi station. Under the same climate change scenarios, future precipitation increased for the Tamor basin compared to the current values but it decreased for the Seti basin. Therefore, higher projected temperature combined with less precipitation in the Seti basin might directly reduce the future water availability, primarily during low-flow seasons. Mostly, precipitation was projected to be higher during summer months and lower during winter

months with the value range between +33 and -18%, respectively for the Terhathum and Phidim stations. The value ranged between +39 and -25% for the Patan station and from +36 to -22% for the Silgadi station. Regarding both temperature and precipitation, the changes were clear; however, precipitation showed much uncertainty that might be due to various climate-driven variables influenced by the extreme topography of the Himalaya Mountains (Beniston, 2003).

Effects of Climate Change

I estimated the hydrologic responses in both annual and seasonal basis at the main basin outlets in three different GCM-derived scenarios. My simulation outputs showed that the precipitation distribution in the basins was higher in all scenarios compared to the baseline data with maximum increase of 9% in the SRES-A2 for the Tamor basin (Figure 33). This estimation was higher than the value of 7% predicted in the SRES-A1B for the Seti basin. These precipitation changes corresponded with similar changes in stream discharge with the values of 13 and 8% in these scenarios for the Tamor and Seti rivers, respectively. Similar increase of stream discharge with the value of 6% was estimated for the Kali Gandaki River in these scenarios (Neupane et al., 2013). For both basins, sediment yield to the main channel was estimated to be higher in all GCM scenarios than that of baseline simulation. For the Tamor basin, maximum increase in sediment yield with the value of 54% was estimated in the SRES-B1 scenario. This was lower than the value of 63% estimated in the SRES-A1B scenario for the Seti basin that corresponded with maximum precipitation and stream discharge increase of 7 and 8%, respectively in the same scenario. Steep mountain channels have significant control on channel dynamics

and morphology that influence streamflow velocity and sediment transportation (Hassan et al., 2005). Therefore, these estimations might be important for the Himalaya Mountain basins since they are primarily affected by summer monsoonal precipitation that governs the downstream agricultural production and hydropower generation (NEA, 1996).

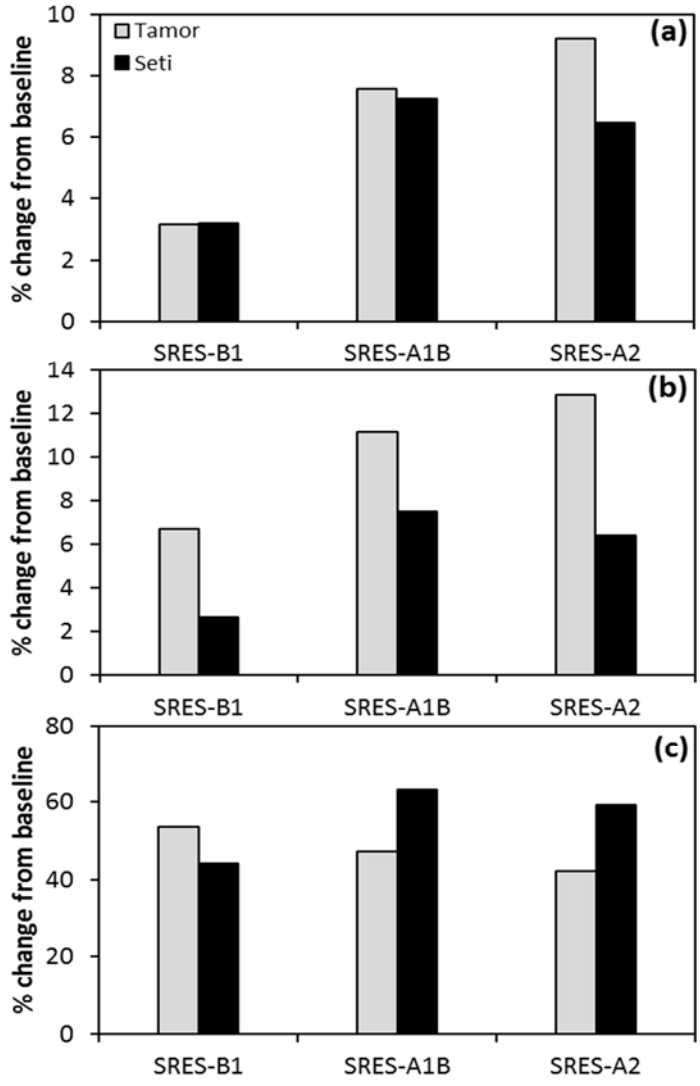

Figure 33. Mean annual changes of (a) precipitation, (b) stream discharge and (c) sediment yield for the Tamor and Seti basins from baseline in different GCM scenarios.

Seasonally, the baseline precipitation contributions of 26, 65 and 9% were estimated for pre-monsoon, monsoon, and post-monsoon seasons, respectively for the Tamor basin (Figure 34). The contribution increased during monsoon season in all the scenarios with maximum value of 69% in the SRES-A2 scenario. Contrary to that, contribution decreased during post-monsoon season with minimum contribution value of 7% in the same scenario. For the Seti basin, the baseline contribution values were 22, 65, and 13% during pre-monsoon, monsoon, and post-monsoon seasons, respectively. The monsoonal contribution was higher in all the scenarios with maximum value of 69% in the SRES-A2 scenario. Similar changes in stream discharge with the maximum contribution values of 72 and 68% were predicted during monsoon season for the Tamor and Seti basins, respectively in the SRES-A2 scenario. Simulation outputs indicated that the summer monsoonal period with all GCM-derived scenarios are likely to be the worst scenarios for these mountain basins in future as they are prone to hydrological-related disasters such as flood and landslide, specifically during peak flow seasons. Potential changes in seasonality of stream discharge was also supported by the findings of Singh and Bengtsson (2004) and Neupane et al. (2013), that is likely to affect the downstream irrigation and hydropower generation.

Effects of Land Use Change

Potential land use change effect on stream discharge and sediment yield was shown by comparing monthly simulation outputs of three potential land use scenarios with the baseline data (Figure 35). Our analysis showed that the stream discharge decreased in all scenarios for both basins with maximum decrease of 4.4% in

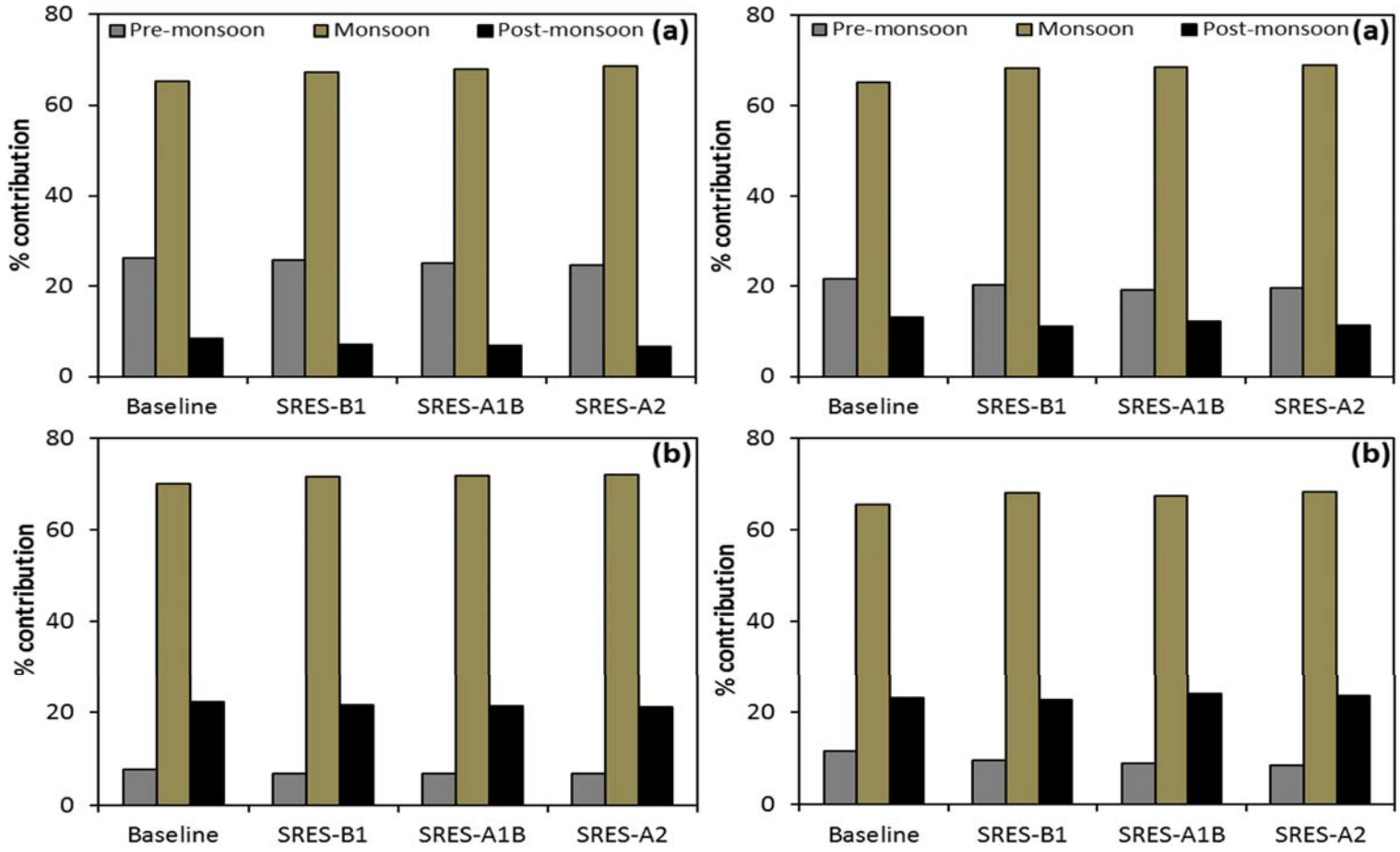

Figure 34. Potential seasonal precipitation and stream discharge contribution of the basins for different GCM scenarios (left graphs for the Tamor basin and right graphs for the Seti basin): (a) precipitation and (b) stream discharge (pre-monsoon: March-May, monsoon: June-September, and post-monsoon: October-February)

Scenario-II for the Tamor River and minimum decrease of 0.3% in Scenario-III for the Seti River with corresponding changes of -2.9 and +0.5% precipitation in these scenarios, respectively. Despite minimal decrease in precipitation and stream discharge of the Tamor basin, sediment yield was substantially higher in all land use scenarios with maximum increase of 65% in Scenario-I that might be attributed to deforestation increasing sediment flux of complex mountain terrain (Lu et al., 2003). However, I analyzed minimal changes for the Seti basin with 1% increase in Scenario-I whereas 2 and 4% decrease in Scenario-II and Scenario-III, respectively. In this study, I estimated a substantial loss of input water from the systems potentially stored in deep groundwater reservoirs not accounted by the SWAT model. This is also supported by the prevalent faults and fractures of these mountain terrains for prompt transmission of surface water to deep groundwater system (Searle et al., 2008; Anderman et al., 2012). These findings might be accounted for similar potential change of stream discharge outputs even in different land use scenarios.

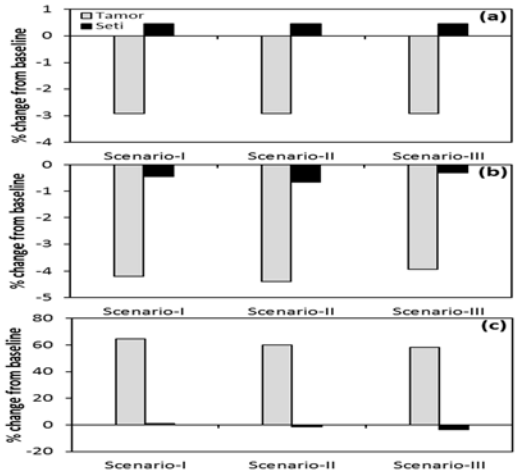

Figure 35. Mean annual changes of (a) precipitation, (b) stream discharge, and (c) sediment yield from baseline simulation in potential land use scenarios for the Tamor and Seti basins.

Combined Effects of Climate and Land Use Changes

The combined effects of potential climate change and land use modification on stream discharge and sediment yield of the basins are presented in Figure 36. However decrease of the stream discharge values compared to the baseline in potential land use scenarios, I estimated a substantial increase when combined these scenarios with potential GCM-derived scenarios. This is because, regarding to the coupled effects of potential climate change and land use modification, the decrease in magnitude of the stream discharge caused by land use change will be offset by climate change and the magnitude will be further enhanced in climate change scenarios if higher in land use scenarios (Ma et al., 2009). The maximum stream discharge increase of 12% was analyzed for the Tamor basin in the SRES-A2 that changed by -3.9% in land use scenario. For the Seti basin, the maximum increase of 7.7% was estimated in the SRES-A1B which had minimal decrease of 0.3% in land use scenario. Similarly, the amount of sediment yield was intensified in combined scenarios for the Tamor basin with the maximum increase of 124% in the SRES-B1 that was increased only by 65% in land use scenario. For the Seti basin, maximum increase with the value of 33% was estimated in the SRES-A1B that was changed by +1% in land use scenario. Finally, potential land use scenarios coupled with GCM-derived scenarios intensified both stream discharge and sediment yield with substantial increase to the Tamor basin that potentially enhance the risk of flood and landslide in the basin, and ultimately downstream reservoir sedimentation affecting the irrigation and hydropower generation.

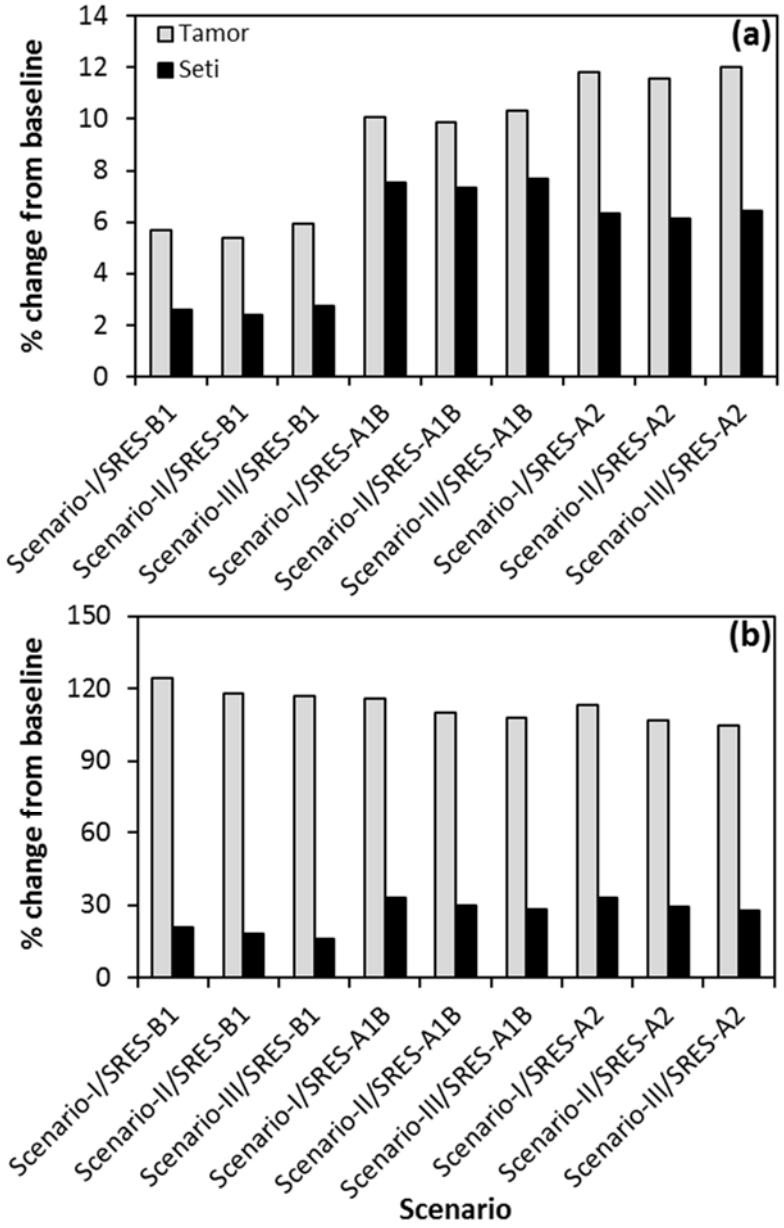

Figure 36. Mean annual changes of (a) stream discharge and (b) sediment yield in combined scenarios of climate change and land use modification for the Tamor and Seti basins.

Recently, there have been both national and transnational conflicts in sharing of water resource as its demand increases due to high population pressure. This is particularly serious in between Nepal and India as the downstream water demand

increases during low flow seasons for agricultural production and hydropower generation in both countries, specifically in large river basins including the Koshi, Gandaki, Karnali, Bagmati and Mahakali Rivers (Sharma and Shakya, 2006). Also, severe flood events occur during high flow monsoon season that destroy property and lives downstream of the basins. Therefore, the scale of impact on future water resources due to potential climate change and land use modification needs to be assessed for sustainable management strategies.

CHAPTER FIVE

Conclusions

In this study, the effects of potential climate on some watershed hydrological processes were assessed based on projected climate change conditions developed by GCM simulations within SWAT. The model accurately represented stream discharge of the KGW from Himalaya Mountain system through detailed data incorporation. Evaluation criteria statistics showed that the model was able to simulate the daily and monthly stream discharge reasonably well. However, the model showed better performance in monthly simulations with the inclusion of elevation bands and estimated glacier melt data for the basin. Sensitivity results showed the lapse rates which cause changes in mountain orography with changing temperature and precipitation are most influential to change stream discharge of the basin. This is expected to be important since it could add more uncertainties in predicting watershed hydrological processes using GCM outputs with no consideration of physical factors influencing lapse rates for complex mountain systems. Simulation outputs indicated the rainfall as most influential source water for stream discharge of the basin. Snowmelt was estimated with higher contribution during pre-monsoon season, presumably indicating the importance of seasonal snowmelt during that period. Estimation of higher groundwater contribution to the stream discharge during post-monsoon season might be due to excess surface waters for groundwater recharge caused during monsoonal precipitation. However, glaciers have

higher mean yearly stream discharge contribution than snow and groundwater with substantial contribution of 34% during monsoon season.

The projected annual temperature and precipitation changes showed that the climate in KGW will generally become warmer in all the scenarios and wetter in most of the scenarios. Annually, the stream discharge change is predicted to be within ±40% with relative precipitation change of ±37%. In summary, reasonable lapse rate estimation with the inclusion of snow and glacier melt data for complex mountain system would result for better representation of watershed hydrological processes. Stream discharge of the KGW would experience substantial change in A2 scenario of the GCM outputs. Due to uncertainties in climate change scenarios and GCM outputs, there is also uncertainty in future stream discharge simulation. However, projected simulations showed potential increase of the stream discharge during monsoon and post-monsoon seasons and decrease during pre-monsoon season influencing the seasonal water availability which might be crucial for management of future water resources in the basin.

I analyzed the environmental tracers that helped to better assess the model simulation outputs and also for estimation of future groundwater contribution to the stream discharge of mountain basins. Examination of multiple groundwater tracers showed that only ^{222}Rn provided significant information to estimate groundwater contribution to stream discharge of the McDonald Creek using a mass balance approach. The small range of water $\delta^{18}O$ and $\delta^{2}H$ values and lack of discernible trend in solute chemistry analysis supported our general conclusion that the stream water was dominated by surface meltwater in the watershed. The large variation in ^{222}Rn activities coupled with finding the maximum ^{222}Rn activity, that also coincided with maximum EC and Cl^-

values, measured at 7.9 km prompted examination of the role of geology affecting groundwater exfiltration in this complex mountain basin. Cascades in the stream were also found to potentially result in loss of ^{222}Rn from the stream water due to molecular diffusion. From ^{222}Rn data, I estimated a 5.9% of groundwater inputs to the total stream discharge with the remaining portions from meltwater in the watershed. About 60% of the total groundwater input was assessed to be gained from hyporheic zone of the stream channel. However, further sampling of the local groundwater and alluvium is required to accurately model groundwater exchange.

I estimated the effects of potential climate change and land use modifications on available stream discharge and sediment yield of the Tamor and Seti basins using a complex physically based distributed hydrological model, the SWAT. Simulation outputs indicated higher stream discharge in all GCM-derived scenarios for both basins with corresponding increase in precipitation. Seasonally, the maximum stream discharge contribution of 70 and 66% were estimated during monsoon season for the Tamor and Seti basins, respectively in the baseline scenario that increased to 72 and 68%, respectively in the SRES-A2 scenario. However, the contribution decreased in both pre-monsoon and post-monsoon seasons (except minimal increase in post-monsoon season for the Seti basin). These changes might affect the seasonal water availability downstream influencing crop production and hydroelectricity generation, specifically during low flow seasons. Similarly, sediment yield also increased substantially in all GCM scenarios for both basins with maximum increase of 63% in the SRES-A1B for the Seti River. The maximum increase in sediment yield with the value of 65% was estimated in Scenario-I for the Tamor River but it increased to only 1% for the Seti River

in the same scenario indicating the Seti River less prone to future sedimentation problems in land use scenarios compared to the Tamor basin. Despite substantial changes in stream discharge with GCM-derived scenarios, I estimated minimal changes between land use scenarios, potentially due to buffering of the systems caused by structural discontinuities with intense faults and fractures of mountain terrains for higher water transmission to groundwater reservoirs. However, in combined scenarios, both the stream discharge and sediment yield were higher for the basins with substantial increase of 124% in sediment yield for the Tamor River. Therefore, understanding the effects of both climate change and land use modification on the stream discharge and sediment yield might be crucial for national and transnational water management implications.

REFERENCES

Adam JC, Hamlet AF, Lettenmaier DP. 2009. Implications of global climate change for snowmelt hydrology in the twenty-first century. Hydrological Processes 23: 962-972.

Akhtar M, Ahmad N, Booij MJ. 2008. The impact of climate change on the water resources of Hindukush Karakorum-Himalaya region under different glacier coverage scenarios. Journal of Hydrology 355: 148- 163.

Andermann C, Longuevergne L, Bonnet S, Crave A, Davy P, Gloaguen R. 2012. Impact of transient groundwater storage on the discharge of Himalayan rivers. Nature Geoscience 5: 127-132.

Arnold JG, Muttiah RS, Srinivasan R, Allen PM. 2000. Regional estimation of base flow and groundwater recharge in the Upper Mississippi river basin. Journal of Hydrology 227: 21-40.

Arnold JG, Srinivasan R, Muttiah RS, Williams JR. 1998. Large area hydrologic modeling and assessment Part I: Model development. Journal of the American Water Resources Association 34: 73-89.

Asahi K, Watanabe T. 2004. Paleoclimate of the Nepal Himalayas during the Last Glacial: Reconstructing from glacial equilibrium-line altitude. Himalayan Journal of Sciences 2: 100-101.

Awasthi KD, Sitaula BK, Singh BR, Bajacharaya RM. 2002. Land-use change in two Nepalese watersheds: GIS and geomorphometric analysis. Land Degradation & Development 13: 495-513.

Barnett TP, Adam JC, Lettenmaier DP. 2005. Potential impacts of a warming climate on water availability in snow-dominated regions. Nature 438: 303-309.

Barros AP, Chiao S, Lang TJ, Burbank D, Putkonen J. 2006. From weather to climate-Seasonal and interannual variability of storms and implications for erosion processes in the Himalaya. Geological Society of America 398: 17-38.

Baskaran S, Ransley T, Brodie RS, Baker P. 2009. Investing groundwater-river interactions using environmental tracers. Australian Journal of Earth Sciences 56: 13-19.

Batjes NH. 1997. A world dataset of derived soil properties by FAO-UNESCO soil unit for global modeling. Soil Use and Management 13: 9-16.

Bengtsson L, Westerstrom G. 1992. Urban snowmelt and runoff in northern Sweden. Hydrological Sciences Journal 37: 263-275.

Beniston M. 2003. Climate change in mountain regions: a review of possible impacts. Climate Change 59: 5-31.

Beven, K.J., Kirkby, M.J., 1979. A physically based, variable contributing area model of basin hydrology. Hydrological Sciences-Bulletin-des Sciences Hydrologiques 24, 43-69.

Bookhagen B, Burbank DW. 2010. Toward a complete Himalayan hydrological budget: Spatiotemporal distribution of snowmelt and rainfall and their impact on river discharge. Journal of Geophysical Research 115: doi:10.1029/2009JF001426.

Bookhagen B, Thiede RC, Strecker MR. 2005. Late Quaternary intensified monsoon phases control landscape evolution in the northwest Himalaya. Geology 33: 149-152.

Brodie RS, Sundaram B, Tottenham R, Hostetler S, Ransley T. 2007. An adaptive management framework for connected groundwater-surface water resources in Australia. Bureau of Rural Sciences, Canberra, Australia.

Broecker WS, Peng TH. 1982. Tracers in the Sea. Columbia University, Palisades, NY, pp 689.

Burnett WC, Peterson RN, Santos IR, Hicks RW. 2010. Use of automated radon measurements for rapid assessment of groundwater flow into Florida streams. Journal of Hydrology 380: 298-304.

Carson B. 1990. Terracing re-examined in the light of recent findings in Nepal and Indonesia. Research Needs and Applications to Reduce Erosion and Sedimentation in Tropical Steeplands (Proceedings of the Fiji Symposium): IAHS-AISH Publ. No.192.

Cartwright I, Hofmann H, Sirianos MA, Weaver TR, Simmons CT. 2011. Geochemical and 222Rn constraints on baseflow to the Murray River, Australia, and timescales for the decay of low-salinity groundwater lenses. Journal of Hydrology 405: 333-343.

Chalise SR, Khanal NR. 1997. Erosion processes and their implications in sustainable management of watersheds in Nepal Himalayas. Regional Hydrology: Concepts and Models for Sustainable Water Resource Management. IAHS Publ. no. 246.

Clever HL. 1979. Krypton, Xenon and Radon-Gas Solubilities. Solubility Data Series 2: Pergamon Press, New York.

Collins DN, Hasnain SI. 1995. Runoff and sediment transport form glacierized basins ate the Himalayan scale. Effects of scale of interpretation and management of sediment and water quality (Proceedings of Boulder Symposium, July 1995). IAHS Publication 226: 17-25.

Cook PG, Favreau G, Dighton JC, Tickell S. 2003. Determining natural groundwater influx to a tropical river using radon, chlorofluorocarbons and ionic environmental tracers. Journal of Hydrology 277: 74-88.

Cook PG, Lamontagne S, Berhane D, Clark JF. 2006. Quantifying groundwater discharge to Cockburn River, southeastern Australia, using dissolved gas tracers 222Rn and SF6. Water Resources Research 42: W10411, doi:10.1029/2006WR004921.

Cook PG. 2012. Estimating groundwater discharge to rivers from river chemistry surveys. Hydrological Processes DOI: 10.1002/hyp.9493.

Corbett DR, Burnett WC, Cable PH, Clark SB. 1997. Radon tracing of groundwater input into Par Pond, Savannah River Site. Journal of Hydrology 203: 209-227.

Covino TP, McGlynn BL. 2007. Stream gains and losses across a mountain-to-valley transition: Impacts on watershed hydrology and stream water chemistry. Water Resources Research 43: W10431, doi:10.1029/2006WR005544.

Cruz RV, Harasawa H, Lal M, Wu S, Anokhin Y, Punsalmaa B, Honda Y, Jafari M, Li C, Huu Ninh N. 2007: Asia. Climate Change 2007: Impacts, Adaptation and Vulnerability. Contribution of Working Group II to the Fourth Assessment Report of the Intergovernmental Panel on Climate Change, Parry ML, Canziani OF, Palutikof JP, Van der Linden PJ and Hanson CE, Eds., Cambridge University Press, Cambridge, UK, 469-506.

Cunha-Santino MB, Bianchini-Junior I. 2004. Humic substances mineralization: the variation pH, electrical conductivity and optical density. Acta Limnologica Brasiliensia 16: 63-75.

Cyranoski D. 2005. The long-range forecast. Nature 438: 275-276.

Danckwerts PV. 1951. Significance of Liquid-Film Coefficients in Gas Absorption. Industrial and Engineering Chemistry 43: 1460-1467.

Downing DJ, Gardner RH, Hoffman FO. 1985. An Examination of Response-Surface Methodologies for Uncertainty Analysis in Assessment Models. American Statistical Association and the American Society for Quality Control 27: 151-163.

Dyurgerov M. 2003. Mountain and subpolar glaciers show an increase in sensitivity to climate warming and intensification of the water cycle. Journal of Hydrology 282: 164–176.

Eckhardt K, Ulbrich U. 2003. Potential impacts of climate change on groundwater recharge and streamflow in a central European low mountain range. Journal of Hydrology 284: 244-252.

Ellins KK, Roman-Mas A, Lee R. 1990. Using 222Rn to examine groundwater/surface discharge interaction in the Rio Grande de Manati, Puerto Rico. Journal of Hydrology 115: 319-341.

Elsinger RJ, Moore WS. 1983. Gas exchange in the Pee Dee River based on 222Rn evasion. Geophysical Research Letters 10: 443-446.

Fagre DB, Comanor PL, White JD, Hauer FR, Running SW. 1997. Watershed responses to climate change at Glacier National Park. Journal of the American Water Resources Association 33: 755-765.

FAO. 1998. Developing participatory and integrated watershed management, Community Forestry Case Study Series, 13, Rome.

FAO/UNESCO. 2003. Digital Soil Map of the World and Derived Soil Properties. Rev. 1. (CD Rom) (Source: http://www. fao.org/catalog/what_new-e.htm).

Felix N, Scherrer S, Weiler M. 2002. A process based assessment of the potential to reduce flood runoff by land use change. Journal of Hydrology 267: 74-79.

Finklin AI. 1986. A Climatic Handbook for Glacier National Park-with Data for Waterton Lakes National Park. USDA Forest Service General Technical Report INT-204.

Fohrer N, Haverkamp S, Eckhardt K, Frede HG. 2001. Hydrologic response to land use changes on the catchment scale. Physics and Chemistry of the Earth 26: 577-582.

Foley JA, DeFries R, Asner GP, Barford C, Bonan G, Carpenter SR, Chapin ST, Coe MT, Daily GC, Gibbs HK, Helkowski JH, Holloway T, Howard EA, Kucharik CJ, Monfreda C, Patz JA, Prentice IC, Ramankutty N, Snyder PK. 2005. Global Consequences of Land Use. Science 309: 570-574.

Fontaine TA, Cruickshank TS, Arnold JG, Hotchkiss RH. 2002. Development of a snowfall-snowmelt routine for mountainous terrain for the soil and water assessment tool (SWAT). Journal of Hydrology 262: 209-223.

Francos A, Elorza FJ, Bouraoui F, Bidoglio G, Galbiati, L. 2003. Sensitivity analysis of distributed environmental simulation models: understanding the model behaviour in hydrological studies at the catchment scale. Reliability Engineering and System Safety 79: 205-218.

Fujita K, Thompson LG, Ageta Y, Yasunari T, Kajikawa Y, Sakai A, Takeuchi N. 2006. Thirty-year history of glacier melting in the Nepal Himalayas. Journal of Geophysical Research 111: D03109, doi:10.1029/2005JD005894.

Gardner RH, Huff DD, O'Neill RV, Mankin JB, Carney J, Jones J. 1980. Application of Error Analysis to a Marsh Hydrology Model. Water Resources Research 16: 659-664.

Gassman PW, Reyes MR, Green CH, Arnold JG. 2007. The soil and water assessment tool: historical development, applications and future research directions. Transactions of the American Society of Agricultural and Biological Engineers 50: 1211-1250.

Gautam R, Christina Hsu N, Lau WKM, Yasunari TJ. 2013. Satellite observations of desert dust-induced Himalayan snow darkening. Geophysical Research Letters 40: 988-993.

Genereux D, Pringle C. 1997. Chemical mixing model of streamflow generation at La Selva Biological Station, Costa Rica. Journal of Hydrology 199: 319-330.

Genereux D. 2004. Comparison of naturally-occurring chloride and oxygen-18 as tracers of interbasin groundwater transfer in lowland rainforest, Costa Rica. Journal of Hydrology 295: 17-27.

Genereux DP, Hemond HF. 1992. Determination of Gas Exchange Rate Constants for a Small Stream on Walker Branch Watershed, Tennessee. Water Resources Research 28: 2365-2374.

Germer S, Neill C, Vetter T, Chaves J, Krusche AV, Elsenbeer H. 2009. Implications of long-term land-use change for the hydrology and solute budgets of small catchments in Amazonia. Journal of Hydrology 364: 349-363.

Ghimire SK, Higaki D, Bhattarai TP. 2013. Estimation of Soil Erosion Rates and Eroded Sediment in a Degraded Catchment of the Siwalik Hills, Nepal. Land 2: 370-391.

Gibson JJ, Edwards TWD, Birks SJ, St Amour NA, Buhay WM, McEachern P, Wolfe BB, Peters DL. 2005. Progress in isotope tracer hydrology in Canada. Hydrological Processes 19: 303-327.

Gleick PH. 1996. Water Resources. In Encyclopedia of Climate and Weather, ed. by Schneider SH, Oxford University Press, New York 2: 817-823.

Gonfiantini R, Stichler W, Rozanski K. 1995. Standards and intercomparison materials distributed by the International Atomic Energy Agency for stable isotope measurements, in: Reference and Intercomparison Materials for Stable Isotopes of Light Elements, TECDOC-825. IAEA, Vienna, pp.13-29.

Gooseff MN. 2010. Defining hyporheic zones-Advancing in our conceptual and operational definitions of where stream water and groundwater meet. Geography Compass 4: 945-955.

Grabs WE, Pokhrel AP. 1993. Establishment of a Measuring Service for Snow and Glacier Hydrology in Nepal-Conceptual and Operational Aspects. Snow and Glacier Hydrology. IAHS Publ. no. 218, 1993.

Guida M, Guida D, Guadagnuolo D, Cuomo A, Siervo V. 2013. Using Radon-222 as a Naturally Occurring Tracer to investigate the streamflow-groundwater interactions in a typical Mediterranean fluvial-karst landscape: the interdisciplinary case study of the Bussento river (Campania region, Southern Italy). Wseas Transactions on Systems 12: 85-104.

Guo H, Hu Q, Jiang T. 2008. Annual and seasonal streamflow responses to climate and land-cover changes in the Poyang Lake basin, China. Journal of Hydrology 355: 106-122.

Hannah DM, Kansakar SR, Gerrard J, Rees G. 2004. Linking river flow and precipitation regimes for Himalayan basins of Nepal: assessing hydroclimatological variability and implications of climate change. Hydrology: Science & Practice for the 21st Century 1: 36-45.

Hassan MA, Church M, Lisle TE, Brardinoni F, Benda L, Grant GE. 2005. Sediment transport and channel morphology of small, forested streams. Journal of the American water Resources Association 41: 853-876.

He H, Zhou J, Zhang W. 2008. Modelling the impacts of environmental changes on hydrological regimes in the Hei River Watershed, China. Global and Planetary Change 61: 175-193.

Hofmann H. 2011. Understanding connectivity within groundwater systems and between groundwater and rivers. Ph.D. Thesis. School of Geosciences, Monash University, Australia.

Hoy C. 2012. A hydrologic characterization of three headwater mountain wetlands in eastern Kentucky, USA. Theses and Dissertations--Forestry. Paper 5.

Ichiyanagi K, Yamanaka MD, Muraji Y, Vaidya BK. 2007. Precipitation in Nepal between 1987 and 1996. International Journal of Climatology 27: 1753-1762.

ICIMOD. 2008. The case of the Hindu Kush-Himalayas: ICIMOD's Position on Climate Change and Mountain Systems. Mountain Research and Development 28: 328-331.

Immerzeel WW, Droogers P, De Jong SM, Bierkens MFP. 2009. Large-scale monitoring of snow cover and runoff simulation in Himalayan river basins using remote sensing. Remote Sensing of Environment 113: 40-49.

Immerzeel WW, Van Beek LPH, Bierkens MFP. 2010. Climate Change Will Affect the Asian Water Towers. Science 328: 1382-1385.

Immerzeel WW, Van Beek LPH, Konz M, Shrestha AB, Bierkens MFP. 2012. Hydrological response to climate change in a glacierized catchment in the Himalayas. Climate Change 110: 721-736.

Ives JD. 1987. The theory of Himalayan environmental degradation: its validity and application challenged by recent research. Mountain Research and Development 7: 189-199.

Jansson P, Hock R, Schneider T. 2003. The concept of glacier storage: a review. Journal of Hydrology 282: 116–129.

Kaltenborn BP, Nellemann C, Vistnes II. 2010. High mountain glaciers and climate change – Challenges to human livelihoods and adaptation. United Nations Environment Programme, GRID-Arendal, Norway.

Kansakar SR, Hannah DM, Gerrard J, Rees G. 2004. Spatial pattern in the precipitation regime of Nepal. International Journal of Climatology 24: 1645-1659.

Karvonen T, Koivusalo H, Jauhiainen M, Palko J, Weppling K. 1999. A hydrological model for predicting runoff from different land use areas. Journal of Hydrology 217: 253-265.

Kaser G, GroBhauser M, Marzeion B. 2010. Contribution potential of glaciers to water availability in different climate regimes. Proceedings of the National Academy of Sciences of the United States of America 107: 20223-20227.

Kattan Z. 2008. Estimation of evaporation and irrigation return flow in arid zones using stable isotope ratios and chloride mass-balance analysis: Case of the Euphrates River, Syria. Journal of Arid Environments 72: 730-747.

Kendall C, Coplen TB. 2001. Distribution of oxygen-18 and deuterium in river waters across the United States. Hydrological Process 15: 1363-1393.

Kendall C, McDonnell JJ. 1998. Isotope tracers in catchment hydrology. Elsevier, Amsterdam.

Kiffney PM, Greene CM, Hall JE, Davies JR. 2006. Tributary streams create spatial discontinuities in habitat, biological productivity, and diversity in mainstem rivers. Canadian Journal of Fisheries and Aquatic Science 63: 2518-2530.

Knee KL, Jordan TE. 2013. Spatial Distribution of Dissolved Radon in the Choptank River and Its Tributaries: Implications for Groundwater Discharge and Nitrate Inputs. Estuaries and Coasts 36: 1237-1252.

Knight J, Harrison S. 2009. Sediments and future climate. Nature Geoscience 2: 230.

Kundzewicz ZW, Mata LJ, Arnell NW, Döll P, Kabat P, Jiménez B, Miller KA, Oki T, Sen Z, Shiklomanov IA. 2007. Freshwater resources and their management. Climate Change 2007: Impacts, Adaptation and Vulnerability. Contribution of Working Group II to the Fourth Assessment Report of the Intergovernmental Panel on Climate Change, Parry ML, Canziani OF, Palutikof JP, Van der Linden PJ, Hanson CE (Eds.). Cambridge University Press, Cambridge, UK, 173-210.

Kuras PK, Weiler M, Alila Y. 2008. The spatiotemporal variability of runoff generation and groundwater dynamics in a snow-dominated catchment. Journal of Hydrology 352: 50-66.

Lambs L, Balakrishna K, Brunet F, Probst JL. 2005. Oxygen and hydrogen isotopic composition of major Indian rivers: a first global assessment. Hydrological Processes 19: 3345-3355.

Lamontagne S, Cook PG. 2007. Estimation of hyporheic water residence time in situ using 222Rn disequilibrium. Limnology and Oceanography: Methods 5: 407-416.

Lenhart T, Eckhardt K, Fohrer N, Frede HG. 2002. Comparison of two different approaches of sensitivity analysis. Physics and Chemistry of the Earth 27: 645-654.

Lewis WK, Whitman WC. 1924. Principles of gas absorption. Industrial and Engineering Chemistry 16: 1215-1220.

Liu BY, Nearing MA, Risse LM. 2000. Slope gradient effects on soil loss for steep slopes. Transactions of the American Society of Agricultural Engineers 37: 1835-1840.

Liu S, Sun W, Shen Y, Li G. 2003. Glacier changes since the Little Ice Age maximum in the western Qilian Shan, northwest China, and consequences of glacier runoff for water supply. Journal of Glaciology 49: 117-124.

Liu Y, An S, Xu Z, Fan N, Cui J, Wang Z, Liu S, Pan J, Lin G. 2008. Spatio-temporal variation of stable isotopes of river waters, water source identification and water security in the Heishui Valley (China) during the dry-season. Hydrogeology Journal 16: 311-319.

Loague KM, Freeze RA. 1985. A Comparison of Rainfall-Runoff Modeling Techniques on Small Upland Catchments. Water Resources Research 21: 229-248.

Loheide II SP, Gorelick SM. 2006. Quantifying Stream-Aquifer Interactions through the Analysis of Remotely Sensed Thermographic Profiles and In Situ Temperature Histories. Environmental Science and Technology 40: 3336-3341.

Lu XX, Ashmore P, Wang JF. 2003. Seasonal Water Discharge and Sediment Load Changes in the Upper Yangtze, China. Mountain Research and Development 23: 56-64.

Lu XX. 2005. Spatial variability and temporal change of water discharge and sediment flux in the lower Jinsha tributary: impact of environmental changes. River Research and Applications 21: 229-243.

Ludwig W, Probst JL. 1998. River sediment discharge to the oceans: present-day controls and global budgets. American Journal of Science 298: 265-295.

Luo Y, Arnold J, Allen P, Chen X. 2012. Baseflow simulation using SWAT model in an inland river basin in Tianshan Mountains, Northwest China. Hydrology and Earth System Sciences 16: 1259-1267.

Luo Y, Zhang X, Liu X, Ficklin D, Zhang M. 2008. Dynamic modeling of organophosphate pesticide load in surface water in the northern San Joaquin Valley watershed of California. Environmental Pollution 156: 1171-1181.

Ma L, Ascough II JC, Ahuja LR, Shaffer MJ, Hanson JD, Rojas KW. 2000. Root zone water quality model sensitivity analysis using Monte Carlo simulations. American Society of Agricultural Engineers 43: 883-895.

Ma X, Xu J, Luo Y, Aggarwal SP, Li J. 2009. Response of hydrological processes to land-cover and climate changes in Kejie watershed, south-west China. Hydrological Processes 23: 1179-1191.

Ma X, Xu J, Noordwijk MV. 2010. Sensitivity of streamflow from a Himalayan catchment to plausible changes in land cover and climate. Hydrological Processes 24: 1379-1390.

Manning AH, Solomon DK. 2003. Using noble gases to investigate mountain-front recharge. Journal of Hydrology 275: 194-207.

Mark AF, Dickinson KJM. 2008. Maximizing water yield with indigenous non-forest vegetation: a New Zealand perspective. Frontiers in Ecology and the Environment 6: 25-34.

McCarthy KA, McFarland WD., Wilkinson JM, White LD. 1992. The dynamic relationship between ground water and the Columbia River: using deuterium and oxygen-18 as tracers. Journal of Hydrology 135: 1-12.

Minder JR, Mote PW, Lundquist JD. 2010. Surface temperature lapse rates over complex terrain: Lessons from the Cascade Mountains. Journal of Geophysical Research 115: D14122, doi:10.1029/2009JD013493.

Monirul M, Mirza Q. 1997. The runoff sensitivity of the Ganges River basin to climate change and its implication. Journal of Environmental Hydrology 5: 1–13.

Monirul M, Mirza Q. 2003. Climate change and extreme weather events: can developing countries adapt? Climate Policy 3: 233-248.

Monteith JL. 1965. Evaporation and environment. Symposia of the Society for Experimental Biology 19: 205-234.

Moriasi DN, Arnold JG, Van Liew MW, Binger RL, Harmel RD, Veith TL. 2007. Model evaluation guidelines for systematic quantification of accuracy in watershed simulations. American Society of Agricultural and Biological Engineers 50: 885-900.

Mote PW, Hamlet AF, Salathe E. 2008. Has spring snowpack declined in the Washington Cascades? Hydrology and Earth System Sciences 12: 193-206.

MPFS, 1988. Master Plan for Forestry Sector Nepal. Ministry of Forest and Soil Conservation, Kathmandu, Nepal.

Muleta MK, Nicklow JW. 2005. Sensitivity and uncertainty analysis coupled with automatic calibration for a distributed watershed model. Journal of Hydrology 306: 127-145.

Mullinger NJ, Binley AM, Pates JM, Crook NP. 2007. Radon in Chalk streams: Spatial and temporal variation of groundwater sources in the Pang and Lambourn catchments, UK. Journal of Hydrology 339: 172-182.

Munoz-Villers LE, McDonnell JJ. 2013. Land use change effects on runoff generation in a humid tropical montane cloud forest region. Hydrology and Earth System Sciences 17: 3543-3560.

Nayak JN. 1996. Sediment management of the Kosi River basin in Nepal. Erosion and Sediment Yield: Global and Regional Perspectives. IAHS Publ. no. 236.

NEA (Nepal Electricity Authority). 1996. Summary Environmental Impact Assessment for the Kali Gandaki "A" Hydroelectricity Project in Nepal.

Negi GCS, Joshi V, Nayal M, Sati M. 2007. Geo-Hydrological Studies for Augmentation of Spring Discharge in the Western Himalaya. Final Technical Report. Ministry of Water Resources, New Delhi.

Neitsch SL, Arnold JG, Kiniry JR, Williams JR. 2005. Soil and Water Assessment Tool-Theoretical Documentation (Version 2005). Temple, Texas: Grassland, Soil and Water Research Laboratory, Agricultural Research Service, Blackland Research Center, Texas Agricultural Experiment Station.

Neitsch SL, Arnold JG, Kiniry JR, Williams JR. 2009. Soil and Water Assessment Tool: Theoretical Documentation, version 2009.

Neupane RP, Yao J, White JD. 2013. Estimating the effects of climate change on the intensification of monsoonal-driven stream discharge in a Himalayan watershed. Hydrological Processes: DOI: 10.1002/hyp.10115.

Ojiambo BS, Poreda RJ, Lyons WB. 2001. Ground water/surface water interactions in Lake Naivasha, Kenya, using delta 18O, delta D, and 3H/3He age-dating. Ground Water 39: 526-533.

Owen LA, Caffee MW, Finkel RC, Seong YB. 2008. Quaternary glaciation of the Himalayan-Tibetan orogen. Journal of Quaternary Science 23: 513-531.

Pandey PR, Pandey H, Nakagawa M. 2009. Assessment of rice and maize based cropping systems for rural livelihood improvement in Nepal. The Journal of Agriculture and Environment 10: 57-64.

Peng TH, Takahashi T, Broecker WS. 1974. Surface Radon Measurements in the North Pacific Ocean Station Papa. Journal of Geophysical Research 79: 1772-1780.

Petelet-Giraud E, Negrel Ph, Gourcy L, Schmidt C, Schirmer M. 2007. Geochemical and isotopic constraints on groundwater-surface water interactions in a highly anthropized site. The Wolfen/Bitterfeld megasite (Mulde subcatchment, Germany). Environmental Pollution 148: 707-717.

Pohle P. 1991. Geographical Research on the History of the Cultural Landscape of Southern Mustang. The Land Use Map of Kagbeni as a Basis. Geographical Research, Nepal.

Polunin O, Stainton A. 2000. Flowers of the Himalaya. Oxford University Press, New York USA.

Puranik DM, Karekar RN. 2009. Western disturbances seen with AMSU-B and infrared sensors. Earth System Science 118: 27-39.

Rai SC, Sharma E. 1998. Comparative assessment of runoff characteristics under different land use patterns within a Himalayan watershed. Hydrological Processes 12: 2235-2248.

Rautio A, Korkka-Niemi K. 2011. Characterization of groundwater-lake water interactions at Pyhajarvi, a lake in SW Finland. Boreal Environment Research 16: 363-380.

Rawat JS, Rawat MS. 1994. Accelerated erosion and denudation in the Nana Kosi watershed, Central Himalaya, India. Part I: sediment load. Mountain Research and Development 14: 25-38.

Ritchie JT. 1972. Model for predicting evaporation from a row crop with incomplete cover. Water Resources Research 8: 1204-1213.

Rodgers P, Soulsby C, Petry J, Malcolm I, Gibbins C, Dunn S. 2004. Groundwater-surface-water interactions in a braided river: a tracer-based assessment. Hydrological Processes 18: 1315-1332.

Rogers AS. 1958. Physical behavior and geologic control of radon in mountain streams. U.S. Geological Survey Bulletin 1052-E, pp 187.

Ross CP. 1959. Geology of Glacier National Park and the Flathead region Northwestern Montana. Geological Survey Professional Paper 296; 125.

Rossi CG, Srinivasan R, Jirayoot K, Duc TL, Souvannabouth P, Binh N, Gassman PW. 2009. Hydrologic evaluation of the lower Mekong river basin with the Soil and Water Assessment Tool model. International Agricultural Engineering Journal 18: 1-13.

Rostamian R, Jaleh A, Afyuni M, Mousavi SF, Heidarpour M, Jalalian A, Abbaspour KC. 2008. Application of a SWAT model for estimating runoff and sediment in two mountainous basins in central Iran. Hydrological Sciences Journal 53: 977-988.

Santhi C, Arnold JG, Williams JR, Dugas WA, Srinivasan R, Hauck LM. 2001. Validation of the SWAT model on a large river basin with point and nonpoint sources. Journal of the American Water Resources Association 37: 1169-1188.

Satomi K, Kruger P. 1982. Radon emanation mechanism from finely ground rocks. Stanford Geothermal Program Interdisciplinary Research in Engineering and Earth Sciences, Stanford University, California.

Scanlon BR, Healy RW, Cook PG. 2002. Choosing appropriate techniques for quantifying groundwater recharge. Hydrogeology Journal 10: 18-39.

Scheffler R, Neill C, Krusche AV, Elsenbeer H. 2011. Soil hydraulic response to land-use change associated with the recent soybean expansion at the Amazon agricultural frontier. Agriculture, Ecosystems and Environment 144: 281-289.

Searle MP, Law RD, Godin L, Larson KP, Streule MJ, Cottle JM, Jessup MJ. 2008. Defining the Himalayan Main Central Thrust in Nepal. Journal of the Geological Society, London 165: 523-534.

Sharma KP, Moore III B, Vorosmarty CJ. 2000. Anthropogenic, climatic, and hydrologic trends in the Kosi Basin, Himalaya. Climatic Change 47: 141-165.

Sharma KP. 1993. Role of Meltwater in Major River Systems of Nepal. Snow and Glacier Hydrology (Proceedings of the Kathmandu Symposium), 113-122.

Sharma PD, Goel AK, Minhas RS. 1991. Water and sediment yields into the Satluj river from the high Himalaya. Mountain Research and Development 11: 87-100.

Sharma RH, Shakya NM. 2006. Hydrological changes and its impact on water resources of Bagmati watershed, Nepal. Journal of Hydrology 327: 315-322.

Shrestha AB, Wake CP, Dibb JE, Mayewski PA. 2000. Precipitation fluctuations in the Nepal Himalaya and its vicinity and relationship with some large scale climatological parameters. International Journal of Climatology 20: 317-327.

Shrestha KL. 2005. Global Change Impact Assessment for Himalayan Mountain Regions for Environmental Management and Sustainable Development. Global Environmental Research 9: 69-81.

Singh P, Arora M, Goel NK. 2006. Effect of climate change on runoff of a glacierized Himalayan basin. Hydrological Processes 20: 1979-1992.

Singh P, Bengtsson L. 2004. Hydrological sensitivity of a large Himalayan basin to climate change. Hydrological Processes 18: 2363-2385.

Singh P, Jain SK. 2002. Snow and glacier melt in the Satluj River at Bhakra Dam in the western Himalayan region. Hydrological Sciences Journal 47: 93-106.

Singh P, Kumar N. 1997. Impact assessment of climate change on the hydrological response of a snow and glacier melt runoff dominated Himalayan River. Journal of Hydrology 193: 316–350.

Sloan PG, Moore ID. 1984. Modeling Subsurface Stormflow on Steeply Sloping Forested Watersheds. Water Resources Research 20: 1815-1822.

Smerdon BD, Allen DM, Grasby SE, Berg MA. 2009. An approach for predicting groundwater recharge in mountainous watersheds. Journal of Hydrology 365: 156-172.

Song L, Zhang J. 2012. Hydrological Response to Climate Change in Beijiang River Basin Based on the SWAT Model. Procedia Engineering 28: 241-245.

Song X, Liu X, Xia J, Yu J, Tang C. 2006. A study of interaction between surface water and groundwater using environmental isotope in Huaisha River basin. Science in China Series D: Earth Sciences 49: 1299-1310.

Soto AU, Madrid-Aris M. 1994. Roughness coefficient in mountain rivers. American Society of Civil Engineering 1: 1-8.

Stellato L, Petrella E, Terrasi F, Belloni P, Belli M, Sansone U, Celico F. 2008. Some limitations in using 222Rn to assess river-groundwater interactions: the case of Castel di Sangro alluvial plain (central Italy). Hydrogeology Journal 16: 701-712.

Stenborg T. 1969. Studies of the internal drainage of glaciers. Geografiska Annaler 51: 13-41.

Stonefelt MD, Fontaine TA, Hotchkiss RH. 2000. Impacts of climate change on water yield in the upper Wind River basin. Journal of the American Water Resources Association 36: 321-336.

Summerfield MA, Hulton NJ. 1994. Natural controls of fluvial denudation rates in major world drainage basins. Journal of Geophysical Research 99: 13,871-13,883.

Thayyen RJ, Gergan JT. 2010. Role of glaciers in watershed hydrology: a preliminary study of a “Himalayan catchment”. The Cryosphere 4: 115-128.

Thomas A. 2000. Climatic changes in yield index and soil water deficit trends in China. Agricultural and Forest Meteorology 102: 71-81.

Thornton PE, Thornton MM, Mayer BW, Wilhelmi N, Wei Y, Cook RB. 2012. Daymet: Daily surface weather on a 1 km grid for North America, 1980-2011. Acquired online (http://daymet.ornl.gov/) on June of 2013 from Oak Ridge National Laboratory Distributed Active Archive Center, Oak Ridge, Tennessee, U.S.A. doi:10.3334/ORNLDAAC/Daymet_V2.

Tiwari PC. 2000. Land-use changes in Himalaya and their impact on the plains ecosystem: need for sustainable land use. Land Use Policy 17: 101-111.

Trimble SW. 1999. Decreased Rates of Alluvial Sediment Storage in the Coon Creek Basin, Wisconsin, 1975-93. Science 285: 1244-1246.

Tripathi MP, Panda RK, Raghuwanshi NS. 2005. Development of effective management plan for critical subwatersheds using SWAT model. Hydrological Processes 19: 809-826.

Unland NP, Cartwright I, Andersen MS, Rau GC, Reed J, Gilfedder BS, Atkinson AP, Hofmann H. 2013. Investigating the spatio-temporal variability in groundwater and surface water interactions: a multi-technique approach. Hydrology and Earth System Sciences 17: 3437-3453.

USDA. 1986. Urban hydrology for small watersheds. Technical Release 55. Engineering Division, Soil Conservation Service, US Department of Agriculture.

Van Liew MW, Veith TL, Bosch DD, Arnold JG. 2007. Suitability of SWAT for the Conservation Effects Assessment Project: Comparison on USDA Agricultural Research Service Watersheds. Journal of Hydrologic Engineering 12: 173-189.

Van Rompaey AJJ, Govers G, Puttemans C. 2002. Modeling land use changes and their impact on soil erosion and sediment supply to rivers. Earth Surface Processes and Landforms 27: 481-494.

Vanacker V, Molina A, Govers G, Poesen J, Deckers J. 2007. Spatial variation of suspended sediment concentrations in a tropical Andean river system: The Paute River, southern Ecuador. Geomorpholgoy 87: 53-67.

Walker A. 2003. Agricultural Transformation and the Politics of Hydrology in Northern Thailand. Development and Change 34: 941-964.

Wang X, Melesse AM. 2005. Evaluation of the SWAT Model's Snowmelt Hydrology in a Northwestern Minnesota Watershed. American Society of Agricultural Engineers 48: 1-18.

Whipple JW. 1992. Geologic map of Glacier National Park, Montana. Base from U.S. Geological Survey.

White JD, Running SW, Thornton PE, Keane RE, Ryan KC, Fagre DB, Key CH. 1998. Assessing simulated ecosystem processes for climate variability research at Glacier National Park, USA. Ecological Applications 8: 805-823.

White JD, Running SW. 1994. Testing scale dependent assumptions in regional ecosystem simulations. Journal of Vegetation Science 5: 687-702.

Winter TC, Buso DC, Shattuck PC, Harte PT, Vroblesky DA, Goode DJ. 2008. The effect of terrace geology on ground-water movement and on the interaction of ground water and surface water on a mountainside near Mirror Lake, New Hampshire, USA. Hydrological Processes 22: 21-32.

Winter TC, Harvey JW, Franke OL, Alley WM. 1998. Ground Water and Surface Water A Single Resource. U.S. Geological Survey Circular 1139, Denver.

Winter TC. 2001. The concept of hydrologic landscapes. Journal of the American Water Resources Association 37: 335-349.

Wu Y, Wen X, Zhang Y. 2004. Analysis of the exchange of groundwater and river water by using Radon-222 in the middle Heihe Basin of northwestern China. Environmental Geology 45: 647-653.

Xu J, Grumbine RE, Shrestha A, Eriksson M, Yang X, Wang Y, Wilkes A. 2009. The Melting Himalayas: Cascading Effects of Climate Change on Water, Biodiversity, and Livelihoods. Conservation Biology 23: 520-530.

Yan B, Fang NF, Zhang PC, Shi ZH. 2013. Impacts of land use change on watershed streamflow and sediment yield: An assessment using hydrologic modelling and partial least squares regression. Journal of Hydrology 484: 26-37.

Yang L, Song X, Zhang Y, Han D, Zhang B, Long D. 2012. Characterizing interactions between surface water and groundwater in the Jialu River basin using major ion chemistry and stable isotopes. Hydrology and Earth System Sciences 9: 5955-5981.

Yu MCL, Cartwright I, Braden JL, de Bree ST. 2013. Examining the spatial and temporal variation of groundwater inflows to a valley-to-floodplain river using 222Rn, geochemistry and river discharge: the Ovens River, southeast Australia. Hydrology and Earth System Sciences 17: 4907-4924.

Yue Z, Lu XX, Ying H, Yunmei Z. 2004. Anthropogenic Impacts on the Sediment Flux in the Dry-hot Valleys of Southwest China-an Example of the Longchuan River. Journal of Mountain Science 1: 239-249.

Zhang Q, Kang S, Wang F, Li C, Xu Y. 2008. Major Ion Geochemistry of Nam Co Lake and its Sources, Tibetan Plateau. Aquatic Geochemistry 14: 321-336.

Zhang X, Srinivasan R, Hao F. 2007. Predicting hydrologic response to climate change in the Luohe River Basin using the SWAT model. American Society of Agricultural and Biological Engineers 50: 901-910.

Zheng D, Hunt ER, Running SW. 1996. Comparison of available soil water capacity estimated from topography and soil series information. Landscape Ecology 11: 3-14.